An Electrophysiological Study Of Voluntary Movement and Spinal Cord Injury

Thesis by

Luke Stuart Urban

In Partial Fulfillment of the Requirements for

the degree of

Doctor of Philosophy

CALIFORNIA INSTITUTE OF TECHNOLOGY

Pasadena, California

2018

(Defended March 23rd, 2018)

Luke Stuart Urban

ORCID: 0000-0001-7695-7405

ACKNOWLEDGEMENTS

I would first like to thank my thesis adviser, Professor Joel Burdick, for his support and guidance throughout my graduate studies. This work has been an incredible experience, and I have developed a deep passion for it. I would like to thank Professor Reggie Edgerton (UCLA) for opening his lab to me and teaching me about the spinal cord. I would like to thank Professor Richard Andersen for the experience of working with nonhuman primates and for teaching me about the parietal cortex. I would like to thank Professor Patricia Phelps (UCLA) for welcoming me in her lab and teaching me about anatomy and histology.

I would like to thank Professor Pietro Perona and Professor Yaser Abu-Mostafa for serving on my thesis committee, Professor Yu-Chong Tai for serving on my candidacy committee, and Professor Doris Tsao and Professor David Anderson for serving on my qualifying committee.

I would like to thank Dr. Hui Zhong and Dr. Erica Dale for their surgical work in the spinal stimulation experiments. It was amazing to see their skill in action. I would also like to thank Dr. Vassilios Christopoulos and Dr. Markus Hauschild for their guidance and mentorship. I also would like to thank Mike Thornton and Katie Ingraham for their assistance in histology and immunofluorescence. They were kind and patient as I slowly learned how to pipette. I want to thank the rest of the members of the Burdick, Edgerton, Andersen, and Phelps groups for the camaraderie over the years.

I would also like to thank Professor Nicole Rust (University of Pennsylvania) for exposing me to electrophysiology while I was a research assistant in her lab. Recording that first neuron was a life changing experience. I want to thank my Master's thesis adviser, Professor Pawan Sinha (MIT), for inspiring me through his work in Project Prakash, where he provides free cataract surgery to blind children in India and studies how they regain vision. He showed me that research can be both intellectually and personally fulfilling. And

I want to thank Professor Patrick Winston (MIT) for encouraging me to pursue research and academia while I was an undergraduate.

I also want to thank my friends for keeping me sane over these past years; you are too numerous and too beautiful to count. I also would like to thank my family for keeping me grounded; I tried my best.

In particular, I want to thank my dad. He instilled in me a love of math and science, and he taught me how to problem solve. None of this was possible without him. Also, it should be noted that in high school my father advised me against taking calculus, so I could focus more on sports.

ABSTRACT

Voluntary movement is generated from the interaction between neurons in our brain and the neurons in our spinal cord that engage our muscles. A spinal cord injury destroys the connection between these two regions, but parts of their underlying neural circuits survive. A new class of treatment (the brain-machine interface) takes advantage of this fact by either a) recording neural activity from the brain and predicting the intended movement (neural prosthetics) or b) stimulating neural activity in the spinal cord to facilitate muscle activity (spinal stimulation). This thesis covers new research studying the brain-machine interface and its application for spinal injury.

First, the electrical properties of the microelectrode (the main tool of the brain-machine interface) are studied during deep brain recording and stimulation. This work shows that the insulation coating the electrode forms a capacitor with the surrounding neural tissue. This capacitance causes large spikes of voltage in the surrounding tissue during deep brain stimulation, which will cause electrical artifacts in neural recordings and may damage the surrounding neurons. This work also shows that a coaxially shielded electrode will block this effect.

Second, the activity of neurons in the parietal cortex is studied during hand movements, which has applications for neural prosthetics. Prior work suggests that the parietal cortex encodes a state-estimator [1], which combines sensory feedback with the internal efference copy to predict the state of the hand. To test this idea, we used a visual lag to misalign sensory feedback from the efference copy. The expectation was that a state-estimator would unknowingly combine the delayed visual feedback with the current efference information, resulting in incorrect predictions of the hand. Our results show a drop in correlation between neural activity in the parietal cortex and hand movement during a visual lag, supporting the idea that the parietal cortex encodes a state-estimator. This correlation gradually recovers over time, showing that parietal cortex is adaptive to sensory delays.

Third, while the intention of spinal stimulation was to interact locally with neural circuits in the spinal cord, results from the clinic show that electrical stimulation of the lumbosacral enlargement enables paraplegic patients to regain voluntary movement of their

legs [2]. This means that spinal stimulation facilitates communication across an injury site. To further study this effect, we developed a new behavioral task in the rodent. Rats were trained to kick their right hindlimb in response to an auditory cue. The animals then received a spinal injury that caused paraplegia. After injury, the animals recovered the behavior (they could kick in response to the cue), but only during spinal stimulation. Their recovered behavior was slower and more stereotyped than their pre-injury response. Administering quipazine to these rodents disrupted their ability to respond to the cue, suggesting that serotonin plays an important role in the recovered pathway. This work proves that the new behavioral task is a successful tool for studying the recovery of voluntary movement.

Future work will combine cortical recordings with this behavioral task in the rodent to study plasticity in the nervous system and improve treatment of spinal cord injuries.

[1] Mulliken, Grant H., Sam Musallam, and Richard A. Andersen. "Forward estimation of movement state in posterior parietal cortex." *Proceedings of the National Academy of Sciences*105.24 (2008): 8170-8177.

[2] Harkema, Susan, et al. "Effect of epidural stimulation of the lumbosacral spinal cord on voluntary movement, standing, and assisted stepping after motor complete paraplegia: a case study." *The Lancet* 377.9781 (2011): 1938-1947.

PREFACE

Animal testing is a sensitive topic. The following experiments were conducted on two rhesus macaque monkeys and twelve Sprague Dawley rats. While great care was taken to mitigate pain and suffering, the realities of animal testing are undeniable. These animals underwent surgical procedures and experimentation that were against their direct benefit.

It is an ugly fact that millions of people in this world suffer from injury and disease. If we do nothing, they and their families will continue to suffer. The experiments described in this thesis study how our nervous system generates movement. The goal of this research is to develop treatments for people suffering from spinal cord injury, with applications also in stroke, Parkinson's, ALS, and other motor disorders.

The rhesus macaque monkeys (Marduk and Razor) have since been retired from laboratory work, and will spend the rest of their days at an animal sanctuary. The Sprague Dawley rats (1, 2, 3, 4, 5, 6, 6^{2nd}, 8, 9, 10, 11, 12) were not so fortunate — after their experiment, they were euthanized.

I would like to thank my co-workers, my advisors, the independent vet staff employed at both Caltech and UCLA, the university approval boards composed of faculty and local community members, and the federal agencies involved in animal testing oversight.

This work has been a privilege and was done with the absolute best of intentions.

‘Drink deep, or taste not’

-Dr. Seth Brundle

TABLE OF CONTENTS

LIST OF ILLUSTRATIONS AND/OR TABLES

Chapter 1: Introduction

SPINAL CORD INJURY AND THE BRAIN-MACHINE INTERFACE

Figure 1.1: 'Capitol Crawl' protesters demanding the passage of the Americans with Disabilities Act (1990). Photo Credit: Tom Olin/Disability History Museum

1.1 – Overview

Spinal cord injuries are a debilitating condition affecting over 5 million people worldwide (300,000 in the US alone) [1]. These injuries profoundly impact the lives of both patients and families (**Figure 1.1**). Life expectancy for those suffering from spinal injury is significantly lower than the average population, and has failed to improve since the 1980's [2]. The lifetime costs of a spinal injury can also total into the millions of dollars [3]. Over the past decade, a new class of treatments for paralysis has been developed, utilizing the **brain-machine interface**. These treatments use electrodes to record and stimulate neural activity in an effort

to restore mobility for both paraplegic and tetraplegic humans. In **neural prosthetics**, electrodes record brain activity from tetraplegic patients, and computer algorithms decode the patient's intended movements, enabling the patient to control a robotic limb [4,5,6]. In **spinal stimulation**, electrodes apply brief pulses of electrical current to reactivate neural tissue affected by a spinal injury, enabling paraplegic patients to stand on their own legs and even regain voluntary movement [7,8]. These treatments rely on a fundamental understanding of how our nervous system generates movement, and of the interaction between neuron and electrode.

This thesis covers three new research projects focused on the brain-machine interface and its application for spinal cord injury:

1. Capacitive Coupling In Deep Brain Electrodes (*brain-machine interface*)
2. State-Estimation In The Posterior Parietal Cortex (*neural prosthetics*)
3. Voluntary Movement After Spinal Injury (*spinal stimulation*)

The next sections provide background material for each of these thesis topics.

1.2 – Brain-Machine Interface

1.2.1 – Background

The fundamental component of the brain-machine interface is the electrode. Developed in the 1950's, the electrode consists of a metal wire coated in a thin layer of insulation [9,10,11]. The metal tip of the electrode is exposed and can interact with the electrical properties of nearby neurons [12]. Voltage can be measured from the electrode to record neural activity, or voltage can be applied to the electrode to stimulate neural activity [13]. While new optical methods are in development [14,15], the metal electrode remains the standard tool for studying the brain. In neural prosthetics, high-density arrays of electrodes [16], such as the Utah array [17,18] (**Figure 1.2a**), record activity from large populations of neurons on the surface of the brain. In spinal stimulation, electrodes are implanted in the epidural space between the spinal cord and the vertebra, and evoke neural activity

by electrically stimulating through the membranes encasing the spinal cord [8] (**Figure 1.2b**). In addition to interacting with the surface of the nervous system, there are also devices that penetrate deep into neural tissue. For patients with severe Parkinson's, electrodes are surgically implanted deep into the brain, and brief pulses of electrical current are used to reduce tremors associated with the disease [19,20,21] (**Figure 1.2c**). For patients with severe epilepsy, deep-brain electrodes are implanted in multiple brain areas and neural activity is recorded to locate the origin of the seizures to guide surgical intervention [22,23,24]. These electrodes can be used for acute studies, lasting hours, or chronic implantations, lasting years [25,26]. As the application of the brain-machine interface grows, it is important to reexamine the electrode in its modern context.

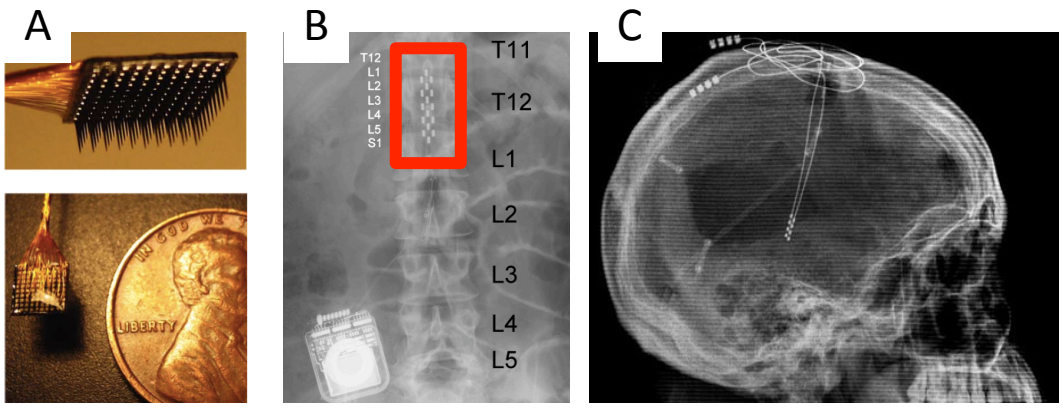

Figure 1.2: Examples of electrode technologies. A) Utah array [18] B) X-Ray of epidural electrode (boxed in red) [8] C) X-Ray of deep-brain electrodes (Cleveland Clinic)

1.2.2 – *Research: Capacitive Coupling of Deep-Brain Electrodes*

When an electrode is inserted multiple centimeters into the brain, the shank of the electrode is embedded in neural tissue that is both electrically active and electrically sensitive. The thin layer of insulation coating the electrode will act as a capacitor, coupling the voltage on the electrode to the voltage in the surrounding tissue. This capacitive coupling has the potential to corrupt neural recordings and cause unconstrained and unexpected neural stimulation. To study this effect, the surrounding neural tissue was incorporated into the circuit models of deep brain

recording and stimulation. Capacitive coupling during neural recordings was modeled using the telegrapher's equations. Capacitive coupling during neural stimulation was modeled using a simplified circuit and a multiphysics computational model. The effect of capacitive coupling was also studied for a coaxially shielded electrode.

Results show that the insulation acts as a megahertz high-pass filter during deep brain stimulation. The sharp discontinuities found in standard stimulation waveforms (rectangular waves and decaying exponentials [13]) contain frequencies above this megahertz threshold that will pass through the insulation, evoking spikes of voltage in the surrounding tissue. While a coaxial electrode will block this effect, capacitive coupling presents a problem for safety protocols used during neural stimulation.

Standard safety guidelines require biphasic stimulation, where all current pushed down the electrode is pulled out [13]. This assumes that current can only flow in and out through the tip of the electrode. Capacitive coupling breaks this assumption. Current can be pushed through the tip of the electrode, but extracted from the insulation, creating a charge imbalance that can degrade the electrode and damage neural tissue. To prevent this charge imbalance, the stimulation waveform used to inject current should be identical to the waveform used to extract current. While capacitive coupling impacts deep brain stimulation, it will not affect deep brain recordings, as the insulation effectively filters out the surrounding neural activity.

1.3 – Neural Prosthetics

1.3.1 – Background

In 2003, a young man was shot in East Los Angeles [27]. The bullet damaged his C3 vertebra, paralyzing him below the neck. In 2014, he volunteered for a neural prosthetics study conducted by Caltech scientists at the Rancho Los Amigos

National Rehabilitation Center [6]. A portion of his skull was removed, and electrode arrays were implanted over the posterior region of his parietal cortex. His skull was replaced and a percutaneous connector was fixed to his skull. After the patient recovered from surgery, researchers used this connector to record activity from individual neurons in his parietal cortex. The patient could modulate the activity of these neurons by thinking about moving his hand. By understanding the relationship between neural activity and his intended movement, researchers were able to predict the patient's desired action. This prediction was used to control a robotic limb, enabling the patient to perform basic tasks, such as drinking a beer (**Figure 1.3a**).

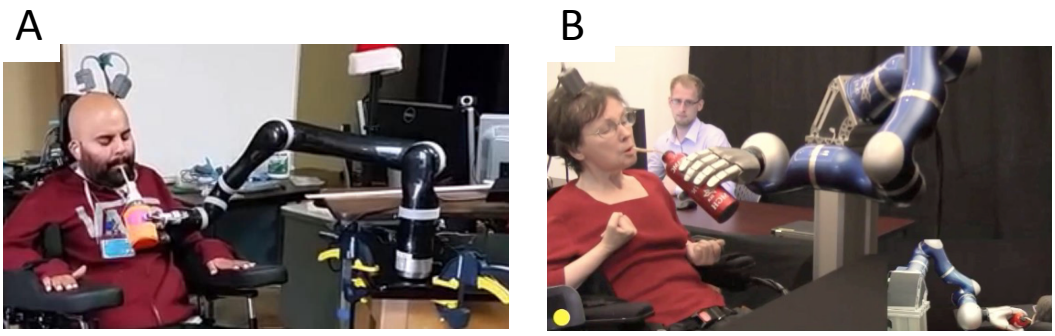

Figure 1.3: Examples of neural prosthetics. Tetraplegic patients control a robotic arm using intracortical electrodes implanted in either A) the parietal cortex [6] or B) the motor cortex [5]

This treatment is founded on a series of animal studies conducted over the last century. In 1890, Hitzig and Fritsch found that electrically stimulating a specific area of a dog's brain (now known as motor cortex) caused the dog's muscles to twitch, and that the exact location of stimulation dictated which muscle group contracted [28]. Evarts expanded on this idea in the 1960's by showing that neurons from this brain area in a rhesus macaque monkey modulate their firing rates (i.e., the number of action potentials per second) as the monkey moves its hand [29]. Georgopoulos in the 1980's used this modulation to predict the movement of the animal's hand from its neural activity [30]. Schwartz converted this prediction into

a control signal, enabling rhesus macaque monkeys to move a robotic limb using only their brain activity [31]. This quickly led to human implantations, performed first by Donohue and the BrainGate group in 2004[5], where a tetraplegic patient was able to control the movement of a robotic limb (**Figure 1.3b**).

These early studies focused exclusively on neurons in the motor cortex, which have close anatomical connections with the muscles (neurons in primary motor cortex directly synapse onto the motor neurons that innervate the muscles). Recent studies in the Andersen group, working in rhesus macaque monkeys, showed that neurons in the posterior parietal cortex also encode movement [32]. This result was surprising since the parietal cortex was traditionally thought to encode cognitive signals [33], such as goal location [34] or behavioral state [35]. While this newly discovered movement signal has led to successful human trials [6] (**Figure 1.3a**), the exact role of parietal neurons in movement is unclear.

1.3.2 – Research: State-Estimation in the Posterior Parietal Cortex

Previous studies suggest that the parietal cortex acts as a state-estimator, which combines sensory feedback with an internal efference copy of the motor command to predict the state of the hand [36]. To test this idea, two nonhuman primates were trained to perform reaching tasks in a virtual reality environment. The animal's hand position was displayed either in real-time or with an artificial visual lag. The idea was that a visual lag would misalign the sensory feedback from the efference copy. A state-estimator in the parietal cortex would unknowingly combine these mismatched signals, resulting in poor predictions of the state of the limb. Both animals were implanted with a high-density electrode array in the posterior parietal cortex, and one animal had a second electrode array implanted in motor cortex. Neural activity from the arrays was used to predict the velocity of the hand during movement.

Both animals showed that neurons in the posterior parietal cortex can predict the state of the hand during real-time hand reaches. When the visual lag is introduced, the predictive strength of the parietal cortex drops. Over time, the parietal cortex adjusts to the sensory delay, and the predictive strength returns. This adjustment coincides with a change in the animal's behavior (the animals slow down during fine hand movements). This drop and recovery is not seen in motor cortex. These results agree with our hypothesis that parietal cortex acts as a state-estimator, but also shows that the parietal cortex is adaptive to sensory disturbances. This resilience makes the parietal cortex an ideal brain area for neural prosthetics.

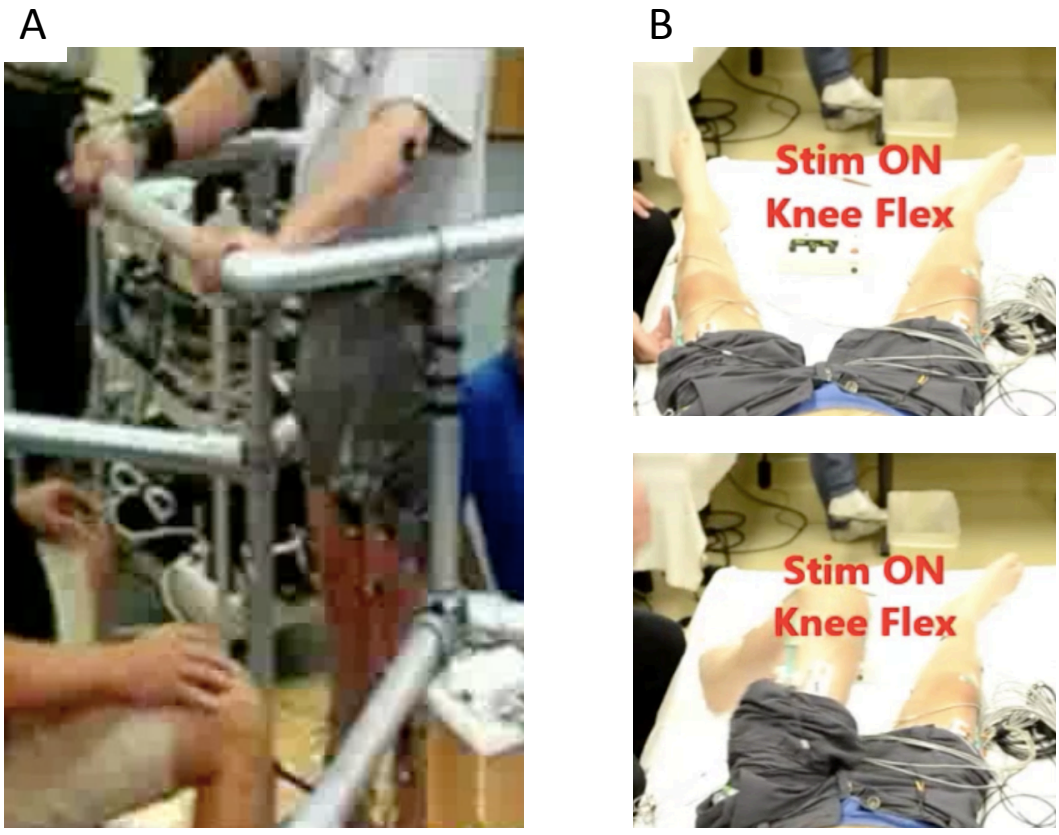

Figure 1.4: Spinal stimulation A) Example of paraplegic patient supporting his own body weight during standing while receiving epidural stimulation [8] B) Example of paraplegic patient voluntarily moving his left leg while receiving transcutaneous electrical stimulation of his lumbosacral enlargement [7]

1.4 – Spinal Stimulation

1.4.1 – Background

The first patient was a young man who had been in a car accident. His T7 vertebra had been crushed, leaving him paralyzed below his armpits. He was diagnosed with a complete spinal injury (ASIA-A — no motor function, no sensory feedback). He volunteered for a joint study involving Caltech, UCLA, and the University of Louisville [8]. After a year of physical therapy failed to improve his condition, an array of electrodes was surgically implanted into the epidural space between his spinal cord and his vertebra, positioned over his lumbosacral enlargement. This enlargement of the spinal cord contains both the neurons that innervate the legs and a sensory feedback loop that stabilizes muscle activity during standing and walking. Researchers applied electrical current in a steady 30-Hz stimulation pattern across the patient's lumbosacral enlargement to reactivate this postural control circuit, and the patient was able to stand on his own legs again (**Figure 1.4a**). Remarkably, after seven months of treatment, the patient regained voluntary movement. This treatment has since been repeated with multiple patients all of who regained standing and voluntary movement of their legs [37] (**Figure 1.4b**).

Spinal stimulation is based on the idea that the spinal cord is more than a simple connection between the brain and the muscles. Reflex circuits, which consist of local connections in the spinal cord that process sensory information and produce motor responses without input from the brain, were well known at the turn of the last century. In 1899, Sherrington demonstrated such a reflex in a spinalized dog [38]. By pressing on the dog's paw, Sherrington caused either an extended limb to retract or a retracted limb to extend. This extension and flexion reflex was thought to form the basis of walking, until Brown showed in 1911 that an alternating stepping motion could arise without sensory input (i.e., without pressing on the dog's paw), and was therefore intrinsic to something in the spinal cord [39]. The mechanism responsible for this stepping behavior became known as the 'central pattern generator', and controls the coordination of muscle contractions during

walking. This central pattern generator survives after a spinal injury, but enters into a nonfunctional state. Great focus was therefore placed on reactivating the neural circuits in this central pattern generator as a treatment for spinal injury. Grilner showed in 1979 that a mixture of drugs (nialamide and L-dopa) in combination with tonic electrical stimulation could evoke stepping behavior from spinalized cats [40]. Edgerton improved on this treatment by targeting the electrical stimulation to the lumbosacral enlargement (across the L2/S1 spinal segments), which evoked stepping behavior in spinalized rodents without the need for pharmacology [41]. These results led to successful human trials, where patients regained weight bearing during standing and even voluntary movement, using either surgically implanted epidural electrodes or transcutaneous stimulating electrodes [7].

1.4.2 – Research: Recovery of Voluntary Movement in Spinalized Rodents

The recovery of voluntary movement was unexpected. Clinical trials were founded on research that had been conducted in animals with completely transected spinal cords, where there was no chance of recovery. To study the mechanism enabling the recovery of voluntary movement, we developed a new behavioral task in the rodent. Six Sprague-Dawley rats were trained to kick their right hindlimb in response to an auditory cue. The animals then received a spinal injury in the form of a simultaneous double hemisection (a left over-hemisection at spinal level T7 and a right hemisection at spinal level T10). This injury destroyed the direct projections from the brain, resulting in paraplegia, but preserved a tract of neural tissue between the injuries that could reorganize for recovery. After the injury, the rodents were treated using 40-Hz epidural stimulation across their L2 and S1 spinal levels, similar to the treatment of the humans.

Two months after injury, the rodents regained voluntary movement of their hindlimb, but only when receiving spinal stimulation. The spinalized rats could kick their leg in response to the auditory cue, but their response was slower and their muscle activity was more stereotyped than their pre-injury behavior. The animals

could perform this task within seconds of the stimulator being turned on, and their performance disappeared within seconds of the stimulator being turned off. Administering quipazine to these animals extinguished this behavior, suggesting that serotonin plays an important role in the recovered pathway. This work demonstrates a new behavioral task in the rodent that is a) simple, b) repetitive, c) stereotyped, and d) event-related. This task will serve as an important tool for studying the mechanism enabling the recovery of voluntary movement.

1.5 – Summary

The brain-machine interface is proving to be a useful tool in the treatment of paralysis for both tetraplegic and paraplegic humans. This thesis will cover new scientific research studying the brain-machine interface and its application for spinal injury. The first chapter (**brain-machine interface)** studies the insulation coating deep-brain electrodes, and its implications for capacitive coupling during neural recording and stimulation. The second chapter (**neural prosthetics**) explores the functional properties of neurons in the posterior parietal cortex, showing that they act as a state-estimator, integrating sensory and motor information to predict the movement of the hand. The third chapter (**spinal stimulation**) demonstrates a new behavioral paradigm in the rodent for studying the recovery of voluntary movement after a spinal injury. Future work will study the anatomical and functional properties of the pathway enabling voluntary movement after a spinal injury. Through this work we hope to both improve the treatment for those suffering from spinal injury as well as learn fundamental science about our nervous system.

1.6 – CITATIONS

[1] Spinal cord facts and figures at a glance. Journal of Spinal Cord Medicine, 2005. 28(1): p. 76-77.

[2] White, Non-Hispanic, and Non-Hispanic Black. "Spinal cord injury (SCI) facts and figures at a glance." *National spinal cord injury statistical center, facts and figures at a glance* (2016).

[3] National Spinal Cord Injury Statistical Center. "Facts and Figures At a Glance. Birmingham, AL: University of Alabama at Birmingham, March 2013." (2015).

[4] Collinger, Jennifer L., et al. "High-performance neuroprosthetic control by an individual with tetraplegia." *The Lancet* 381.9866 (2013): 557-564.

[5] Hochberg, Leigh R., et al. "Neuronal ensemble control of prosthetic devices by a human with tetraplegia." *Nature*442.7099 (2006): 164.

[6] Aflalo, Tyson, et al. "Decoding motor imagery from the posterior parietal cortex of a tetraplegic human." *Science*348.6237 (2015): 906-910.

[7] Gerasimenko, Yury P., et al. "Noninvasive reactivation of motor descending control after paralysis." *Journal of neurotrauma* 32.24 (2015): 1968-1980.

[8] Harkema, Susan, et al. "Effect of epidural stimulation of the lumbosacral spinal cord on voluntary movement, standing, and assisted stepping after motor complete paraplegia: a case study." *The Lancet* 377.9781 (2011): 1938-1947.

[9] Weale, Robert Alexander. "A new micro-electrode for electro-physiological work." *Nature* 167.4248 (1951): 529.

[10] Green, J. D. "A simple microelectrode for recording from the central nervous system." *Nature* 182.4640 (1958): 962.

[11] Hubel, David H. "Tungsten microelectrode for recording from single units." *Science* 125.3247 (1957): 549-550.

[12] Robinson, David A. "The electrical properties of metal microelectrodes." *Proceedings of the IEEE* 56.6 (1968): 1065-1071.

[13] Cogan, Stuart F. "Neural stimulation and recording electrodes." *Annu. Rev. Biomed. Eng.* 10 (2008): 275-309.

[14] Fenno, Lief, Ofer Yizhar, and Karl Deisseroth. "The development and application of optogenetics." *Annual review of neuroscience* 34 (2011).

[15] Stosiek, Christoph, et al. "In vivo two-photon calcium imaging of neuronal networks." *Proceedings of the National Academy of Sciences* 100.12 (2003): 7319-7324.

[16] Hoogerwerf, Arnold C., and Kensall D. Wise. "A three-dimensional microelectrode array for chronic neural recording." *IEEE Transactions on Biomedical Engineering*41.12 (1994): 1136-1146.

[17] Rousche, Patrick J., and Richard A. Normann. "Chronic recording capability of the Utah Intracortical Electrode Array in cat sensory cortex." *Journal of neuroscience methods* 82.1 (1998): 1-15.

[18] Kelly, Ryan C., et al. "Comparison of recordings from microelectrode arrays and single electrodes in the visual cortex." *Journal of Neuroscience* 27.2 (2007): 261-264.

[19] Weaver, Frances M., et al. "Bilateral deep brain stimulation vs best medical therapy for patients with advanced Parkinson disease: a randomized controlled trial." *Jama* 301.1 (2009): 63-73.

[20] Deuschl, Günther, et al. "A randomized trial of deep-brain stimulation for Parkinson's disease." *New England Journal of Medicine* 355.9 (2006): 896-908.

[21] Deep-Brain Stimulation for Parkinson's Disease Study Group. "Deep-brain stimulation of the subthalamic nucleus or the pars interna of the globus pallidus in Parkinson's disease." *New England Journal of Medicine* 345.13 (2001): 956-963.

[22] Fried, Itzhak, et al. "Cerebral microdialysis combined with single-neuron and electroencephalographic recording in neurosurgical patients." *Journal of neurosurgery* 91.4 (1999): 697-705.

[23] Chassoux, Francine, et al. "Stereoelectroencephalography in focal cortical dysplasia: a 3D approach to delineating the dysplastic cortex." *Brain* 123.8 (2000): 1733-1751.

[24] Schachter, Steven C., and Donald L. Schomer, eds. *The Comprehensive Evaluation and Treatment of Epilepsy: a practical guide*. Elsevier, 1997.

[25] Andrade, D. M., et al. "Long-term follow-up of patients with thalamic deep brain stimulation for epilepsy." *Neurology* 66.10 (2006): 1571-1573.

[26] Benabid, Alim L., et al. "Long-term suppression of tremor by chronic stimulation of the ventral intermediate thalamic nucleus." *The Lancet* 337.8738 (1991): 403-406.

[27] Sorto, Erik. Payback: Cost of Being a Gangster, Lone Wolf Editions, 2008

[28] Fritsch, G., and E. Hitzig. "Electric excitability of the cerebrum (Über die elektrische Erregbarkeit des Grosshirns)." *Epilepsy & Behavior* 15.2 (2009): 123-130.

[29] Evarts, Edward V. "Relation of pyramidal tract activity to force exerted during voluntary movement." *Journal of neurophysiology* 31.1 (1968): 14-27.

[30] Georgopoulos, Apostolos P., et al. "On the relations between the direction of two-dimensional arm movements and cell discharge in primate motor cortex." *Journal of Neuroscience*2.11 (1982): 1527-1537.

[31] Taylor, Dawn M., Stephen I. Helms Tillery, and Andrew B. Schwartz. "Direct cortical control of 3D neuroprosthetic devices." *Science* 296.5574 (2002): 1829-1832.

[32] Mulliken, Grant H., Sam Musallam, and Richard A. Andersen. "Decoding trajectories from posterior parietal cortex ensembles." *Journal of Neuroscience* 28.48 (2008): 12913-12926.

[33] Musallam, Sam, et al. "Cognitive control signals for neural prosthetics." *Science* 305.5681 (2004): 258-262.

[34] Scherberger, Hansjörg, and Richard A. Andersen. "Target selection signals for arm reaching in the posterior parietal cortex." *Journal of Neuroscience* 27.8 (2007): 2001-2012.

[35] Hwang, Eun Jung, and Richard A. Andersen. "Brain control of movement execution onset using local field potentials in posterior parietal cortex." *Journal of Neuroscience* 29.45 (2009): 14363-14370.

[36] Mulliken, Grant H., Sam Musallam, and Richard A. Andersen. "Forward estimation of movement state in posterior parietal cortex." *Proceedings of the National Academy of Sciences*105.24 (2008): 8170-8177.

[37] Angeli, Claudia A., et al. "Altering spinal cord excitability enables voluntary movements after chronic complete paralysis in humans." *Brain* 137.5 (2014): 1394-1409.

[38] Sherrington, Charles Scott. "On the innervation of antagonistic muscles. Sixth note." *Proceedings of the Royal Society of London* 66.424-433 (1900): 66-67.

[39] Brown, T. Graham. "The intrinsic factors in the act of progression in the mammal." *Proc. R. Soc. Lond. B*. Vol. 84. No. 572. The Royal Society, 1911.

[40] Grillner, S., and P. Zangger. "On the central generation of locomotion in the low spinal cat." *Experimental Brain Research* 34.2 (1979): 241-261.

[41] Ichiyama, R. M., et al. "Hindlimb stepping movements in complete spinal rats induced by epidural spinal cord stimulation." *Neuroscience letters* 383.3 (2005): 339-344.

[42] Fuchs, ALBERT F., FARREL R. Robinson, and A. N. D. R. E. A. S. Straube. "Role of the caudal fastigial nucleus in saccade generation. I. Neuronal discharge pattern." *Journal of neurophysiology* 70.5 (1993): 1723-1740.

Chapter 2: BRAIN-MACHINE INTERFACE

CAPACTIVE COUPLING IN DEEP BRAIN RECORDING AND STIMULATION

THE ELECTRODE

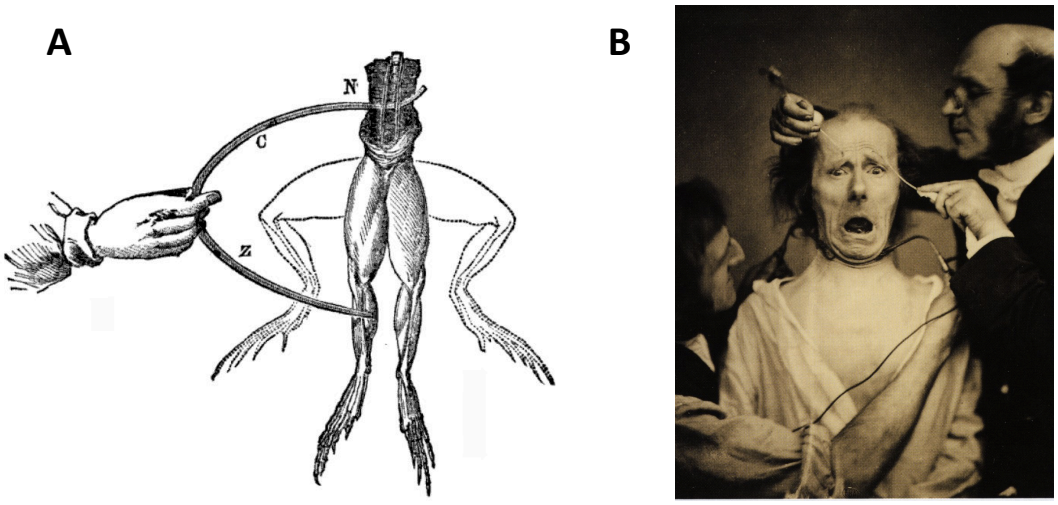

Figure 2.1: A) Diagram of Galvani's experiment [1], B) The use of electrical stimulation to evoke facial expressions by Duchenne. [3]

2.1 – Background

2.1.1 – History

The first brain-machine interface was created in 1781. Luigi Galvani touched two metal prongs to the dissected leg of a frog, and it twitched [1] (**Figure 2.1a**). Twenty years later, Alessandro Volta invented the battery to prove that this twitching was caused by electrical current flowing through the frog's leg [2]. While scientists, such as Duchenne [3], continued to experiment with electrical stimulation (**Figure 2.1b**), it wasn't until Hitzig and Fritsch, in 1870, that electrical current was systematically applied to the nervous system [4]. They found that electrically stimulating a specific location on the brain (now known as motor cortex) caused the muscles to contract. At the time, it was unclear if electricity

merely evoked this behavior, or if it was intrinsic to how the brain generates movement. To answer this question, Canton designed an electronic amplifier to record electrical activity generated by the brain [5], leading to what is now known as the electroencephalograph (EEG) [6].

2.1.2 – Micropipette

These early devices used bulky electrodes to record or stimulate from large sections of neural tissue. At the time there was debate about whether the nervous system was a continuous mass or comprised of discrete units. The anatomical work of Cajal proved the existence of neurons [7,8], and so there was a rush to build devices to interact with these small cells. Marshall Albert Barber, in 1904, was the first to develop just such a device — the micropipette [9]. He heated a hollow glass cylinder and stretched it until it formed a sharp point. The fine tip was then broken off. This produced a tapered glass tube with an opening at the tip approximately 50 microns wide. The micropipette was filled with saline, a metal electrode was inserted into the back, and the tip of the micropipette was then placed near a cell body [10]. Since ions could only flow in or out of the tip of the micropipette, any change in ion concentration in the saline inside the micropipette could be attributed to the nearby cell body. This device enabled for the first time the ability to record the electrical activity of individual cells.

2.1.3 – Microelectrode

Unfortunately, the micropipette had drawbacks when recording from neurons. First, they were fragile. Slight movements could break the tip of the micropipette, making these devices impractical for recording from behaving animals. Second, it was difficult to produce micropipettes with low impedance [11]. This caused the devices to be noisy, making it difficult to resolve the action potential of individual neurons. In the 1950's the metal microelectrode was developed to overcome these limitations [12,13,14]. Thin tungsten wires were sharpened, using electro-polishing, until their tip measured nearly half a micron (**Figure 2.2a**). The electrode was then coated in

lacquer to electrically insulate the metal wire. The viscosity of the lacquer prevented beading near the electro-polished tip, leaving the sharp tip of the electrode uninsulated. These devices could record or stimulate electrical activity in individual neurons with more robustness than the micropipette, and have proven so successful that they have become the dominant tool in electrophysiology.

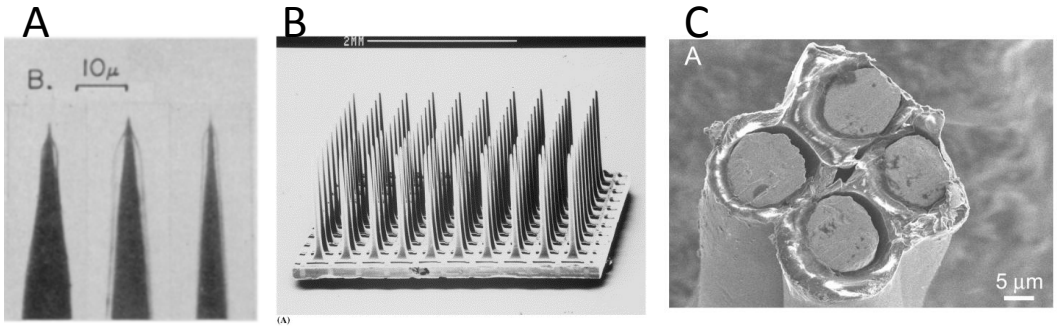

Figure 2.2: Examples of microelectrode technology: A) Single-unit electrodes [14] B) High-density electrode grid [54] C) Tetrode [55]

While there have been improvements in material choices and electrode geometries, the underlying design of the microelectrode has remained the same: a metal wire coated in insulation. High-density grids of electrodes have been created such that 100 electrodes can be inserted into a 16 mm^2 area of cortex [15] (**Fig 2.2b)**. Deep brain electrodes have been developed, which require stereotaxic techniques to be inserted deep into the brain [16]. Another device, the tetrode, consists of four microelectrodes twisted together, which are used to triangulate the spatial location of the recorded neurons [17] (**Fig 2.2c)**. In addition to the microelectrode, which interacts with individual neurons, larger macro-electrodes have shown incredible success in the clinic. In particular, the cochlear implant uses macro-electrodes to stimulate the auditory nerve to restore hearing in deaf patients [18].

Despite the success of these devices, there are a number of drawbacks to the microelectrode. The microelectrode has poor sampling resolution, allowing only a few neurons to be recorded from an area populated by thousands. Even state-of-the-

art high-density electrode arrays are only capable of recording from approximately a hundred neurons [19,20,21]. Also, microelectrodes record and stimulate neural activity indiscriminately, which prevents the study of specific neuron cell types. While there have been attempts to identify inhibitory vs. excitatory neurons based on the shape of their waveforms [22,23], this has proven limited success and will not easily extend to other genetic subtypes of neurons. Stimulation with microelectrodes also generates electrical artifacts that can swamp neural recordings [24]. This prevents the simultaneous recording and stimulation of the nervous system. The origin of these stimulation artifacts is poorly understood, and typical solutions involve processing the recordings offline with software [25].

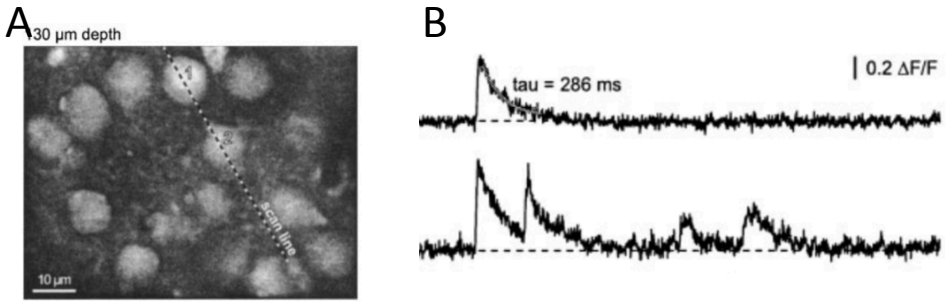

Figure 2.3: Example of calcium imaging A) Image of the calcium concentration across a neural population. [28], B)Calcium concentration as function of time from cell 1 and cell2 labeled in image A). Spikes calcium correspond to action potentials in the cells. [28]

2.1.4 – Optical methods

To overcome the limitations of the microelectrode, new optical methods are being developed. These new methods use either fluorescent markers (calcium imaging) or light sensitive proteins (optogenetics) to record or stimulate neural activity.

Calcium naturally flows in and out of a neuron during an action potential, and the concentration of calcium inside the neuron correlates directly with its membrane voltage [26,27]. The concentration of calcium inside a neuron can be monitored by using either a fluorescent dye that is coupled to calcium molecules [28] or genetically expressing a calcium-sensitive fluorescent protein [29]. The tissue can

then be scanned with a laser, and the resulting fluorescence can be imaged with a microscope, providing a 2D picture of neural activity (two-photon microscopy) [30] (**Figure 2.3)**.

In optogenetics, researchers use viral techniques to trigger or silence neural activity. This method inserts foreign DNA into the cell bodies of neurons [31], which causes the cells to produce membrane receptors with specifically designed properties. If the DNA encodes channelrhodopsin [32], shining blue light on the neuron will trigger an action potential. If the DNA encodes halorhodopsin [33], shining yellow light will suppress an action potential. Light for optogenetics is typically generated from a low-powered laser source and delivered via an optic fiber that can be inserted deep into the brain [34]. The strength of optogenetics is that it can be genetically targeted to specific types of neurons, allowing for precise interaction with neural circuits [35]. In addition to optical genetic techniques, similar methods are being developed where, instead of light, other modalities can trigger neural activity, such as ultrasound [36], heat [37], and pharmacology [38].

These new methods promise more precise control of neural circuits and an increased ability to record from neural populations. Also, since these methods operate using light, they are immune to electrical stimulation artifacts.

2.2 – Capacitive Coupling In Deep Brain Electrodes

The brain-machine interface has become a common tool for treating neurological disorders such as Parkinson's and epilepsy. For Parkinson's, microelectrodes are implanted deep into the brain and electrical stimulation is used to reduce the tremors associated with the disease [39,40,41,42]. For epilepsy, microelectrodes are implanted in multiple brain areas and neural activity is recorded to locate the origin of the seizure as a guide for surgical intervention [43]. In both cases, an electrode is inserted multiple centimeters into the brain. In this configuration, the long insulated

shank of the electrode is surrounded by neural tissue that is both electrically active and electrically sensitive.

This presents a problem for the circuit analysis of the electrode. Traditionally, the insulation surrounding the electrode is modeled as a shunting capacitor, coupling the voltage on the electrode to the ground of the amplifier or stimulator [44]. When an electrode is inserted deep in the brain, the insulation will still act as a capacitor, but will instead couple the voltage on the electrode to the voltage in surrounding tissue. This capacitive coupling allows electrical activity to cross back and forth through the insulation, which has serious implications for both deep brain recording and stimulation.

During deep brain recordings, capacitive coupling enables neurons along the insulation to influence the signal recorded by the neural amplifier. In the case of severe capacitive coupling, neural activity in the surrounding tissue could be directly recorded by the amplifier. This activity would incorrectly appear to originate from the tip of the electrode, and would cause false conclusions to be drawn from the neural recording, such as misidentifying the origin of a seizure. This misidentification could occur if the electrode unknowingly penetrates the origin of the seizure, such that the shank of the electrode is embedded in the affected neural structure, while the tip of the electrode sits in healthy tissue. When a seizure occurs, neurons along the insulation will generate coherent electrical activity, which could be picked up in the neural recording. This would give the false impression that the seizure originates at the tip of the electrode, and would direct surgical intervention to the wrong brain area.

Even in less severe cases of capacitive coupling, neural recordings can be distorted. Consider an experiment recording action potentials from deep in the brain. If neurons along the insulation can inject noise onto the electrode, and if these neurons respond to experimental parameters, the noise they inject will be experimentally

tuned. This noise could cause the neural recording to fade in and out in an experimentally biased manner, giving the false impression that the brain area is experimentally relevant. For these reasons, it is important to reexamine the electrical properties of the microelectrode during deep brain recordings.

Capacitive coupling also allows deep brain stimulation to leak across the insulation into the surrounding tissue. This leakage could trigger neural activity along the shank of the electrode, or worse — damage the tissue. Stimulation protocols prevent tissue damage by requiring that electric charge does not accumulate at the tip of the electrode [45]. This is accomplished using biphasic stimulation, where a positive stimulation pulse is paired with a negative pulse [57]. As long as the negative pulse removes the current produced by the positive pulse, charge should not accumulate.

This charge balancing assumes the shank of the electrode acts as a pipe, allowing current to flow only through the opening at its tip. Capacitive coupling breaks this assumption by allowing current to also leak across the insulation. Current could be pushed through the tip of the electrode, but pulled from the insulation. This would create a charge imbalance at both the tip of the electrode and in the surrounding tissue, degrading the metal of the electrode and damaging the nervous system.

For Parkinsonian patients, this capacitive coupling could both reduce the efficacy of deep brain stimulation by prematurely degrading the electrode and causing a build up of scar tissue, and produce unintended side effects by activating neural structures along the shank of the electrode. Since deep brain electrodes are intended to stimulate specific brain areas over a period of years to decades [56], it is important to reexamine the electrical properties of the microelectrode when used for deep brain stimulation.

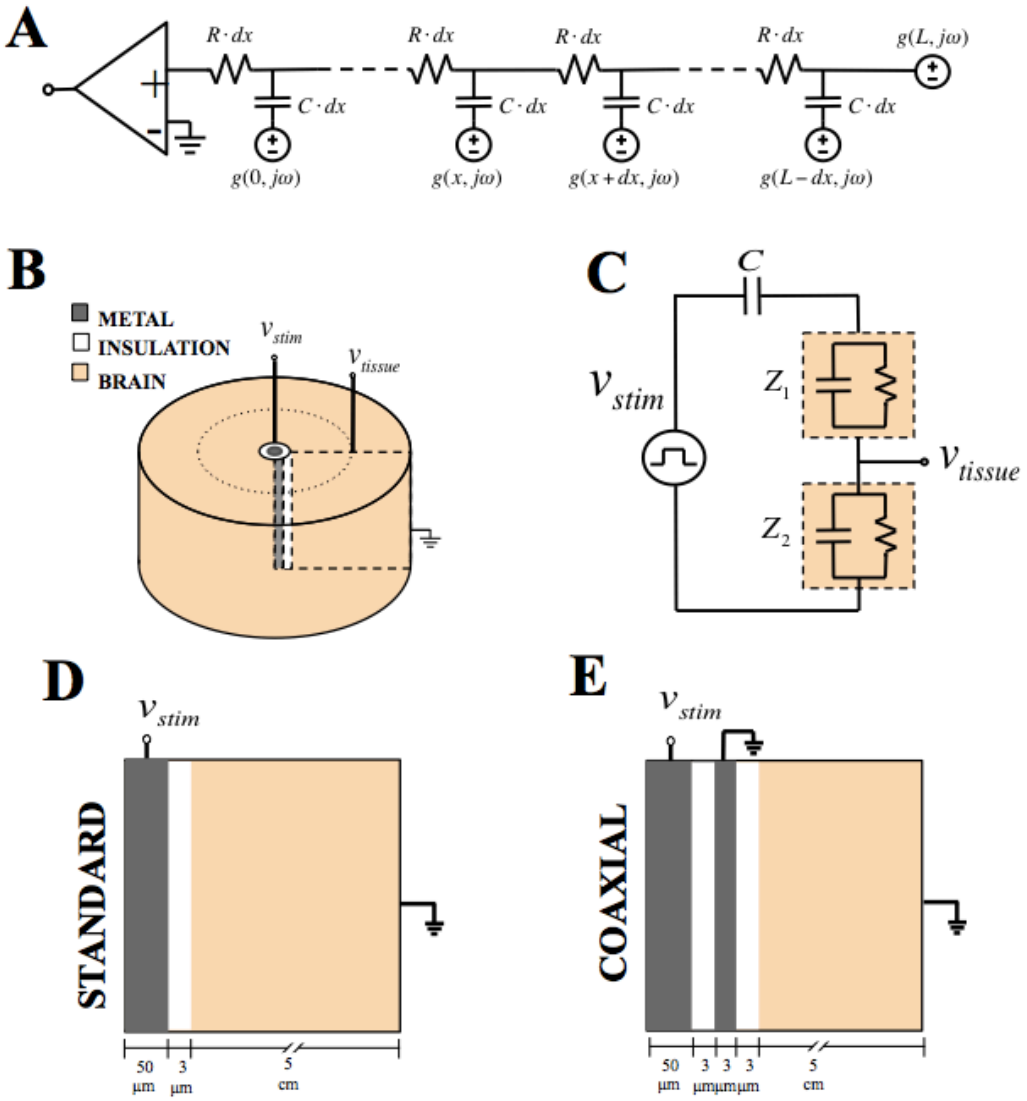

Figure 2.4: Circuit diagram for deep brain recording. The electrical activity generated by neurons surrounding the insulation of the electrode is incorporated using the telegrapher's equations. Simplified model of deep brain stimulation. The brain is modeled as a cylinder centered on the electrode. The electrode penetrates the entire length of the brain, but only contacts the tissue through the insulation. The stimulation voltage is applied to the metal core of the electrode, and the outside surface of the brain is grounded. Circuit diagram for the simplified model of deep brain stimulation. The electrode insulation is modeled as a capacitor. The neural tissue is modeled as a resistor and capacitor in parallel. The resistivity and permittivity of the brain were defined using an experimentally derived Cole-Cole model. The voltage at a desired point in the brain is defined as the voltage at a junction between two concentric cylinders of neural tissue. The first cylinder represents the neural tissue between the electrode and the desired point in the brain, and the second cylinder represents the neural tissue from the desired point to the edge of the brain. Schematic for the COMSOL model of deep brain stimulation. This represents a radial section of the simplified model of deep brain stimulation (Figure 1B). The stimulation was applied to the top edge of the electrode, and the outer surfaces of the brain were grounded. The resistivity and permittivity of the brain were defined using an experimentally derived Cole-Cole model. Schematic for the COMSOL model of deep brain stimulation using a coaxial electrode. This model mimics the standard electrode COMSOL model, except for an additional layer of metal and insulation. The top edge of the addition layer of metal is grounded.

To quantify the effect of capacitive coupling, the surrounding neural tissue was incorporated into the electrical circuit models of deep brain recording and stimulation.

2.3 – Model

2.3.1 – Deep Brain Recording

Neurons populated along the insulation will produce an electric field that varies in both time and position. The effect of this electric field was incorporated into neural recordings using the telegrapher's equation, similar to how voltage is modeled along an axon in cable theory [46]. The inductance terms in these equations were neglected due to the small diameter of the electrode, and the conductance terms were ignored due to the high resistivity of the insulation (Appendix A.1). This results in an infinite series of resistive elements coupled by capacitors to the surrounding electrical field (**Figure 2.4a**). The voltage drop across each resistive element results in the spatial derivative of the electrode voltage being proportional to the current along the electrode:

$$v(x+\delta x, j\omega) - v(x, j\omega) = R\delta x \cdot i(x, j\omega)$$
$$v_x(x, j\omega) = R \cdot i(x, j\omega).$$

The current flowing across the capacitive elements results in the spatial derivative of the current being proportional to the voltage across the insulation:

$$i_c(x, j\omega) = i(x+\delta x, j\omega) - i(x, j\omega)$$
$$i(x+\delta x, j\omega) - i(x, j\omega) = j\omega C\delta x \cdot [v(x, j\omega) - g(x, j\omega)]$$
$$i_x(x, j\omega) = j\omega C \cdot [v(x, j\omega) - g(x, j\omega)].$$

Combining these equations results in a nonhomogeneous differential equation,

$$v_{xx}(x, j\omega) - j\omega\tau \cdot v(x, j\omega) = -j\omega\tau \cdot g(x, j\omega).$$

with a time constant defined by the resistive and capacitive elements. This time constant is a function of the electrode geometry, the resistivity of the metal, and the dielectric properties of the insulation (**Table 1**).

$$C = \frac{2\pi\epsilon_0 k_i}{\ln\left(\frac{r_i}{r_m}\right)} \quad R = \frac{\rho_m}{\pi r_m^2} \qquad \tau = RC = \frac{2\ \varepsilon_0\ k_i\ \rho_m}{{r_m}^2 \ln\left(\frac{r_i}{r_m}\right)}.$$

Boundary Conditions: To solve this differential equation, mix-boundary conditions were defined using facts about neural recording systems. First, neural amplifiers are designed not to draw current from the electrode, which is accomplished by having extremely high input impedance [47]. This constrains the current at the amplifier to be zero. As stated in the model derivation, the current on the electrode is proportional to the spatial derivative of the voltage:

$$i(0, j\omega) = \frac{1}{R}\ v_x(0, j\omega) = 0$$

$$Condition\ 1: \qquad v_x(0, j\omega) = 0.$$

Second, the electrode is designed to measure the electric field at its tip. This requires the voltage at the tip of the electrode to equal the voltage in the surrounding electric field.

$$Condition\ 2: \qquad v(L, j\omega) = g(L, j\omega).$$

3.2.2 – Deep Brain Stimulation

To model capacitive coupling during deep-brain stimulation, the brain was approximated as a cylinder centered on the electrode. The electrode was defined as having a metal core, coated in a thin layer of insulation. The electrode penetrated the entire length of the brain, and only contacted the neural tissue through its insulation. The neural tissue was assumed to have homogenous electrical properties, with resistivity and permittivity defined by experimentally derived Cole-Cole models [48].

$$\epsilon(\omega) = \epsilon_\infty + \sum_{n=1}^{4} \frac{\Delta\epsilon_n}{1 + (j\omega\tau_n)^{1+\alpha_n}} + \frac{\sigma_i}{j\omega\epsilon_0}$$

$$k_b(\omega) = Real[\epsilon(w)] \qquad \sigma_b(\omega) = \omega\,\epsilon_0 \cdot Imag[\epsilon(\omega)].$$

The stimulating voltage was applied to the metal core of the electrode, and the outer surface of the brain was grounded. This grounding configuration replicates a bone screw embedded in the skull used as the stimulation reference (**Figure 2.4b**).

2.3.2.1. – Electrical Circuit

To compute the voltage at a given point in the tissue, the brain was broken into two concentric cylinders. The inner cylinder models the section of tissue from the insulation to the desired point in the brain, and the outer cylinder models the remaining portion of the brain. Due to the high conductivity of metal, the voltage was assumed to be uniform across the core of the metal electrode. This allows the stimulation model to be represented by lump circuit elements. The metal core is represented as the stimulation input, and the insulation is approximated as a capacitor. Both cylinders of neural tissue are represented as a resistor and capacitor in parallel, which models the flow of current through the tissue and the build up of surface charge. This results in a complete circuit, where the stimulation voltage is connected, through a capacitor, to a series of two parallel circuits of resistors and capacitors, with parameters taken from **Table 1**.

$$C = 2\pi L \cdot \frac{\epsilon_0 k_i}{\ln\left(\frac{r_i}{r_m}\right)}$$

$$Z_1(r, j\omega) = \frac{1}{2\pi L} \cdot \frac{\ln\left(\frac{r}{r_i}\right)}{\sigma_b(\omega) + j\omega \cdot \varepsilon_0 k_b(\omega)}$$

$$Z_2(r, j\omega) = \frac{1}{2\pi L} \cdot \frac{\ln\left(\frac{r_b}{r}\right)}{\sigma_b(\omega) + j\omega \cdot \varepsilon_0 k_b(\omega)}.$$

The voltage in the tissue was defined as the voltage at the junction between these two parallel circuits (**Figure 4C**).

$$V_{tissue}(r, j\omega) = H(r, j\omega) \cdot V_{stim}(j\omega)$$

$$H_{stim}(r, j\omega) = \frac{Z_2(r, j\omega)}{\frac{1}{j\omega C} + Z_1(r, j\omega) + Z_2(r, j\omega)}.$$

2.3.2.2 – Computational Model

A computational model of deep-brain stimulation was built using the COMSOL multi-physics software. Due to the rotational symmetry, the model was constructed from a radial slice of the stimulation model described above (**Figure 2.4d**). The top edge of the metal core was defined as the stimulation input, and the outside edges of the brain were defined as ground. A second COMSOL model was constructed to represent a coaxially shielded electrode. This coaxial electrode was identical to the standard electrode, except that it was wrapped in an additional layer of metal and insulation (**Figure 2.4e**). The top edge of this additional metal layer was grounded. This coaxial electrode differs from commercially available concentric electrodes in that the outer ring of metal does not contact neural tissue.

ε_0	Permittivity of free space	$8.8 \cdot 10^{-12} F \cdot m$
k_i	Dielectric constant of paralyene-C	3
ρ_m	Resistivity of metal	$10^{-7} \Omega \cdot m$
r_m	Radius of metal core	$50 \mu m$
r_i	Radius of insulation	$51 \mu m$
r_b	Radius of brain	$5 cm$
L	Length of electrode	$5 cm$

Table 1: Electrode parameters

2.4 – Analysis

2.4.1 – Deep Brain Recording

The complete solution for the voltage along the electrode was solved by combining the particular and homogenous solutions of the differential equation governing capacitive coupling. The particular solution was derived using the Laplace transform in the spatial domain:

$$L_x\{\, v_{xx}(x,j\omega) - \, j\omega\tau \cdot v(x,j\omega) \, = \, -j\omega\tau \cdot g(x,j\omega) \,\}$$
$$k^2 \, \mathrm{V}(k,j\omega) - j\omega\tau \cdot \mathrm{V}(k,j\omega) \, = \, -j\omega\tau \cdot G(k,j\omega)$$
$$\mathrm{V(k},j\omega) = \frac{j\omega\tau}{j\omega\tau - k^2} \cdot G(k,j\omega).$$

This shows that the insulation acts as a low-pass spatial filter of the external electric field; as the spatial-frequency (k) increases, the surrounding electrical activity is attenuated. To consider a worst-case scenario, a spatially uniform electrical field was assumed along the insulation. This is equivalent to a seizure occurring along the entire length of the electrode.

$$\mathrm{g}(x,j\omega) = g(j\omega) \qquad\qquad G(k,j\omega) = L_x\{g(j\omega)\} = \frac{g(j\omega)}{k}.$$

Given this electric field, the analytical form of the particular solution was derived using the inverse Laplace transform.

$$v_p(x,j\omega) = L_k^{-1}\left\{\frac{j\omega\tau}{j\omega\tau - k^2} \cdot G(k,j\omega)\right\} = L_k^{-1}\left\{\frac{j\omega\tau}{j\omega\tau - k^2} \cdot \frac{g(j\omega)}{k}\right\}$$
$$v_p(x,j\omega) = g(j\omega) \cdot \left[1 - \cosh\left(\sqrt{j\omega\tau} \cdot x\right)\right].$$

The homogenous solution was derived using standard techniques:

$$v_{h_{xx}}(x, j\omega) - j\omega\tau \cdot v_h(x, j\omega) = 0$$

$$v_h(x, j\omega) = C_0 e^{\sqrt{j\omega\tau}\cdot x} + C_1 e^{-\sqrt{j\omega\tau}\cdot x}.$$

The particular and homogenous solutions were combined using the boundary conditions.

$$v(x, j\omega) = v_h(x, j\omega) + v_p(x, j\omega)$$

$$v(x, j\omega) = C_0 e^{\sqrt{j\omega\tau}\cdot x} + C_1 e^{-\sqrt{j\omega\tau}\cdot x} + g(j\omega) \cdot \left[1 - \cosh\left(\sqrt{j\omega\tau} \cdot x\right)\right].$$

Boundary Condition 1:

$$\mathrm{v_x}(x, j\omega) = \sqrt{j\omega\tau} \cdot \left(C_0 e^{\sqrt{j\omega\tau}\cdot x} - C_1 e^{-\sqrt{j\omega\tau}\cdot x} - g(j\omega) \cdot \sinh\left(\sqrt{j\omega\tau} \cdot x\right)\right)$$

$$\mathrm{v_x}(0, j\omega) = \sqrt{j\omega\tau} \cdot (C_0 - C_1) = 0$$

$$C_0 = C_1.$$

Boundary Condition 2:

$$v(L, j\omega) = C_0 \cdot \left(e^{-\sqrt{j\omega\tau}\cdot L} + e^{\sqrt{j\omega\tau}\cdot L}\right) + g(j\omega) \cdot \left[1 - \cosh\left(\sqrt{j\omega\tau} L\right)\right] = g(L, j\omega)$$

$$C_0 = \frac{g(L, j\omega) + g(j\omega) \cdot \left[\cosh\left(\sqrt{j\omega\tau} \cdot L\right) - 1\right]}{e^{-\sqrt{j\omega\tau}\cdot L} + e^{\sqrt{j\omega\tau}\cdot L}}.$$

Plugging in these coefficients produces the complete solution for the voltage along an electrode immersed in a spatially uniform electric field:

$$v(x, j\omega) = g(L, j\omega) \cdot \frac{\cosh\left(\sqrt{j\omega\tau} \cdot x\right)}{\cosh\left(\sqrt{j\omega\tau} \cdot L\right)} + g(j\omega) \cdot \left[1 - \frac{\cosh\left(\sqrt{j\omega\tau} \cdot x\right)}{\cosh\left(\sqrt{j\omega\tau} \cdot L\right)}\right].$$

To understand if capacitive coupling can interfere with deep brain recordings, the extreme case was considered in which the electric field is uniform along the insulation but zero at the tip of the electrode.

$$g(L, j\omega) = 0.$$

In this configuration, the voltage at the amplifier is purely due to capacitive coupling. The effect of capacitive coupling was quantified by calculating the attenuation of the external electric field at the amplifier.

$$\frac{\mathrm{v}(0, j\omega)}{\mathrm{g}(\mathrm{j}\omega)} = 1 - sech\left(\sqrt{j\omega\tau} \cdot L\right).$$

This quantity was calculated for the frequencies between 0 and 40 kHz, which is the frequency range recorded by standard neural amplifiers [49]. Since the time constant defining this effect depends on the radius of the electrode, this analysis was repeated for electrodes of various thicknesses.

2.4.2 – Deep Brain Stimulation

2.4.2.1 – Electrical Circuit

The simplified circuit model of deep brain stimulation acts as a high-pass filter. While the resistivity and permittivity of neural tissue is nonlinear with respect to frequency, this effect can be approximated as a first-order high-pass filter with a cut-off frequency of 10 MHz (**Figure 2.5**). The amplitude of the pass-band is unity just outside the insulation, and decays logarithmically with distance from the electrode.

$$H_{stim}(r, j\omega) = \ln\left(\frac{r_b}{r}\right) \cdot \frac{j\omega}{j\omega + B}\ ; \qquad B = 10^7 MHz$$

$$h_{stim}(r, t) = F_t^{-1}\{H_{stim}(r, j\omega)\} = \ln\left(\frac{r_b}{r}\right) \cdot \left[\delta(\mathrm{t}) - \mathrm{B}e^{-\mathrm{B}t} \cdot u(t)\right].$$

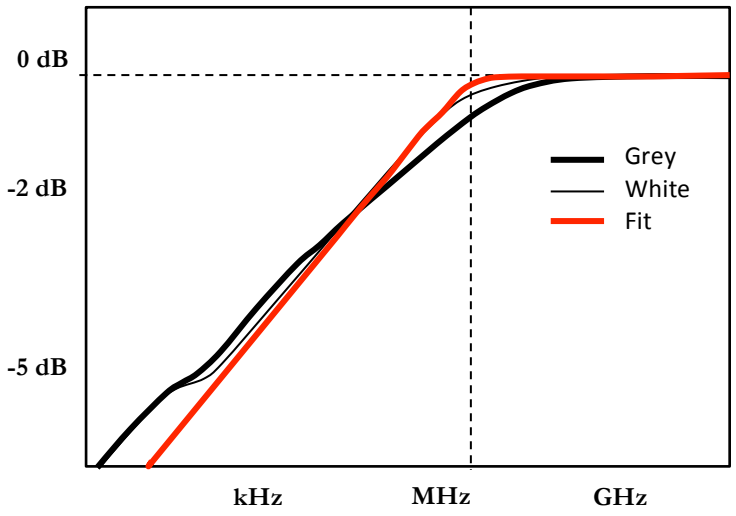

Figure 2.5: Frequency response for the simplified circuit model of deep brain stimulation calculated 10 microns away from the electrode. The response was calculated for the extreme cases of the brain being composed entire of either grey matter (bold black line) or white matter (thin black line). The effect was fit using a first order high-pass filter with a 10 MHz cut-off frequency (red line).

The voltage in the surrounding tissue will be the result of convolving this high-pass filter with the stimulation waveform.

$$v_{tissue}(r,t) = \int h_{stim}(r,T) \cdot v_{stim}(t-T)dT.$$

To visualize the effect of capacitive coupling, this filter was applied to a biphasic combination of a rectangular waveform and a decaying exponential (Appendix A.2) (**Table 2**).

$$\mathrm{v_{stim}(t)} = \mathrm{v_{rect}}(t-t_0) + v_{exp}(t-t_1)$$

$$\mathrm{v_{rect}}(t) = A_1 \cdot [u(t) - u(t-t_d)]$$

$$v_{exp}(t) = A_2 e^{-\frac{t}{\tau}} \cdot u(t).$$

A_1	$10V$
A_2	$10V$
t_d	$60\mu S$
τ	$60\mu S$

Table 2: Stimulation Parameters

To understand how the resulting voltage field effects nearby neurons, the activation function [50] was calculated for an axon passing perpendicular within 10 microns

of the electrode insulation. The voltage along the axon was extracted from the tissue.

$$v_{neuron}(x,t) = v_{tissue}\left(\sqrt{x^2+d^2}, t\right)$$
$$= \ln\left(\frac{r_b}{\sqrt{x^2+d^2}}\right) \cdot \left(v_{stim}(t) - B\int_0^{\infty} \mathrm{e}^{-\mathrm{BT}} \cdot v_{stim}(t-T)dT\right).$$

The activation function was computed by taking the second spatial derivative of the axon voltage.

$$v_{act}(x,t) = \frac{\delta^2}{\delta x^2} v_{neuron}(x,t)$$
$$= \frac{d^2-x^2}{(x^2+d^2)^2} \cdot \left(v_{stim}(t) - B\int_0^{\infty} \mathrm{e}^{-\mathrm{BT}} \cdot v_{stim}(t-T)dT\right).$$

2.4.2.2. – Computational Model

The spatial distribution of the stimulating voltage across the insulation was calculated using the COMSOL models of the standard and coaxial electrodes. The capacitive coupling effect was tested for stimulation frequencies of a kilohertz, megahertz, and gigahertz. Each stimulation frequency was applied independently to the top edge of the metal electrode in the form of a 10-volt sinusoid.

2.5 – Results

2.5.1 – Deep Brain Recording

Capacitive coupling does not affect deep-brain recordings. The insulation around the electrode blocks out the frequencies recorded by neural amplifiers (**Figure 2.6**). An electrode with a 50-micron radius attenuates the surrounding neural activity by more than 7 decibels. If surrounding activity has an amplitude of 100 millivolts, it will affect the neural recording by less than ten nanovolts. For thinner electrodes, the insulation filters out less of the surrounding activity, but this will only be a concern for electrodes with a radius smaller than 50 nanometers.

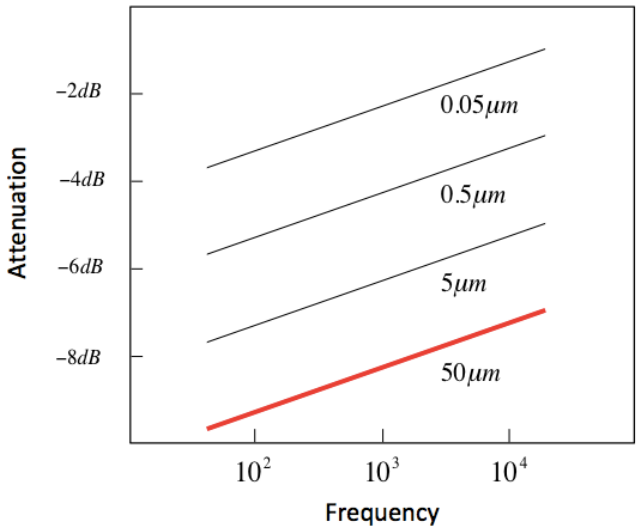

Figure 2.6. The attenuation of the surrounding neural activity during deep brain recording for electrodes of various thickness. The bottom red line represent an electrode with a radius of 50 microns.

2.5.2 – Deep Brain Stimulation

2.5.2.1 – Electrical Circuit

Capacitive coupling causes deep brain stimulation to leak across the insulation. The sharp discontinuities in the stimulation waveform cause large spikes of voltage in the surrounding tissue (**Figure 2.7a**). These spikes are brief, lasting less than a microsecond, but have amplitudes of 10 volts (**Figure 2.7b**). Pairing a positive rectangular waveform with a negative decaying exponential produces an unequal number of positive and negative spikes. The rectangular waveform produces a positive and a negative spike, while the decaying exponential produces only a negative spike.

The activation function of a neuron passing nearby the electrode during a positive spike is negative within 10 microns of the electrode, and positive outside it (**Figure 7C**). This suggests that neural activity is suppressed for neurons within 10 microns on either side of the electrode, while neural activity is facilitated for neurons further away. The opposite effect occurs during a negative spike.

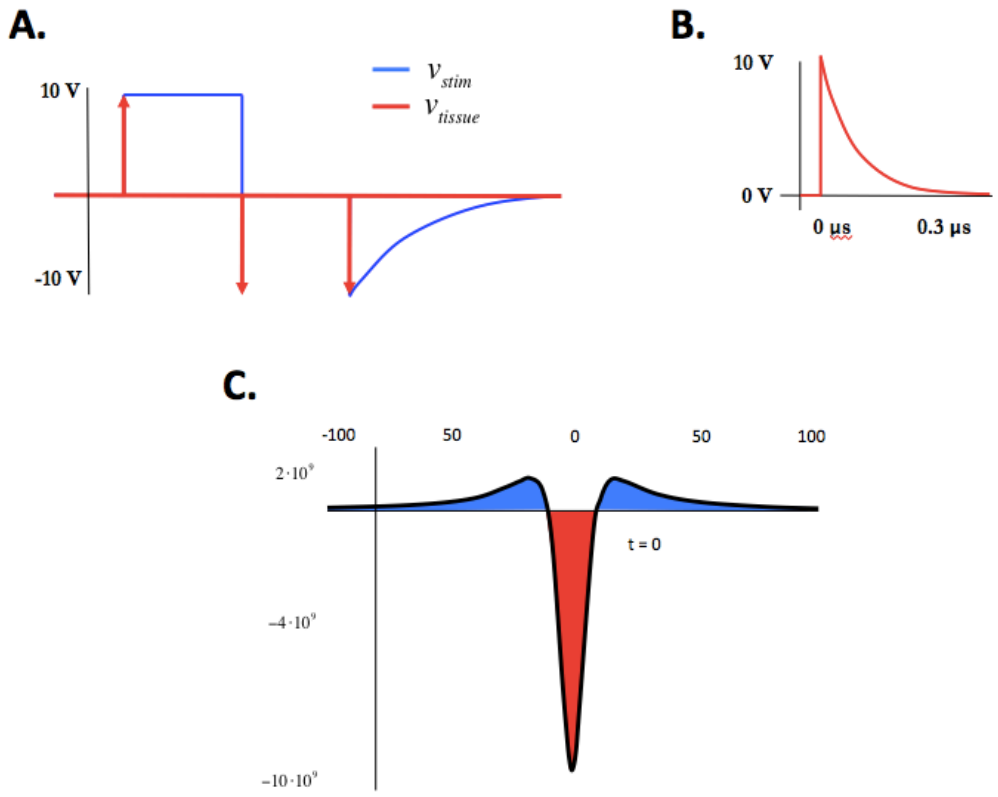

Figure 2.7: A) Tissue voltage caused by capacitive coupling during deep brain stimulation. B) Close up of the positive voltage spike in A. C) The activation function for a neuron passing perpendicularly within 10 microns of the electrode during the peak of the voltage spike (t = 0). Where the activation function is positive (blue regions) neural activity will be facilitated. Where the activation function is negative (red section) neural activity will be suppressed.

2.5.2.2 – Computational Model

The multiphysics model agrees with the results from the simplified circuit. The standard electrode acts as a high-pass filter with a cutoff frequency in the megahertz range. Stimulation frequencies of a kilohertz are blocked by the insulation, while stimulation frequencies of a megahertz and gigahertz leak into the surrounding tissue (**Figure 2.8a**). This effect is not seen in the coaxial electrode. The grounded layer of metal around the electrode shields the surrounding tissue from all three stimulation frequencies (**Figure 2.8b**).

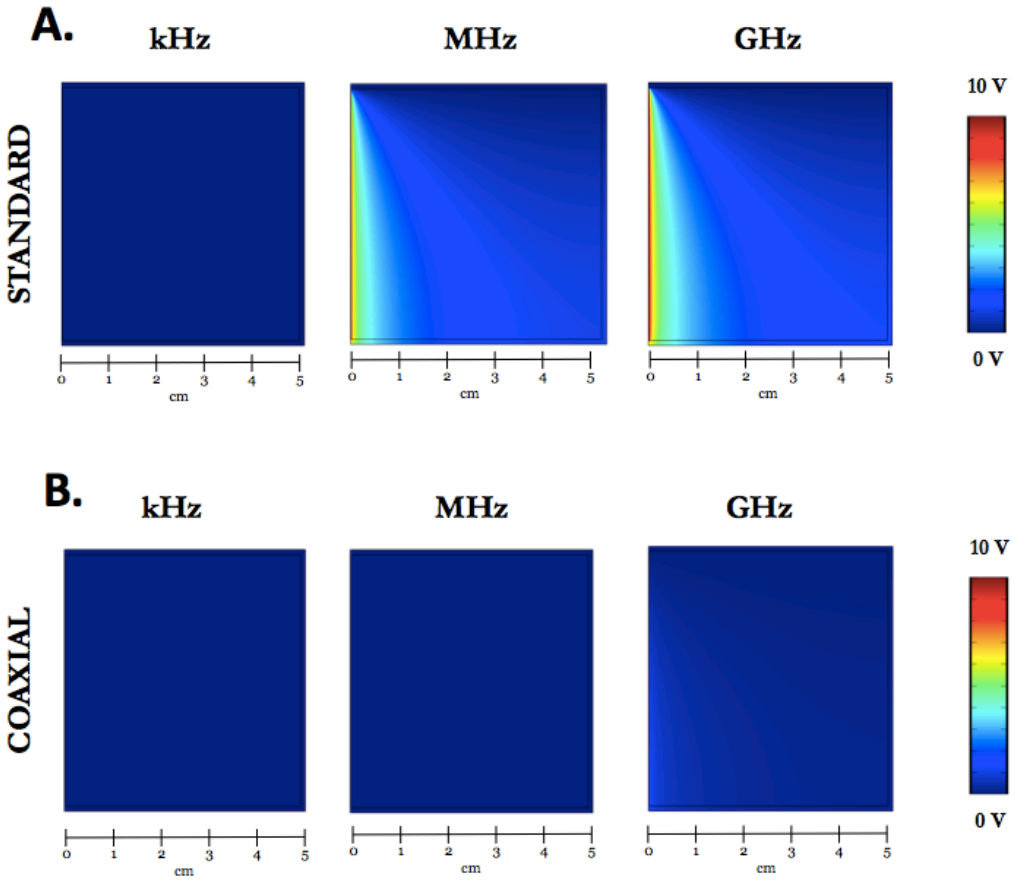

Figure 2.8: A) The spatial distribution of the stimulating voltage caused by capacitive coupling using a standard electrode, based on the COMSOL model Figure 2.4d. Each frequency was applied independently to the top of the electrode in the form of a 10 volt sinusoid. B) The spatial distribution of the stimulating voltage using a coaxial electrode, based on the COMSOL model Figure 2.4e.

2.6 - Discussion

Capacitive coupling raises serious concerns for deep brain stimulation. The insulation around the electrode allows high frequency stimulation to leak into the surrounding tissue. Standard waveforms used for stimulation have abrupt transitions between low and high voltage that occur in less than a microsecond [51]. These transitions are composed of extremely high frequencies (over 10 MHz) that will pass through the insulation, producing spikes of voltage in the brain. These spikes occur every time the stimulation waveform is applied, which can be as

frequent as 250 times a second [52]. These spikes will contribute to the electrical artifacts that distort neural recordings [24,25].

The fact that deep brain stimulation leaks into the surrounding tissue presents a problem for biphasic stimulation. Consider the effect of pairing a rectangular waveform and the decaying exponential on the surrounding tissue. The rectangular waveform produces a positive voltage spike followed shortly by a negative spike, while the decaying exponential produces only a negative voltage spike. These spikes of voltage will draw current from the electrode. This means that a portion of the current supplied by the stimulation circuitry will cross through the insulation, instead of reaching the tip of the electrode. The amount of current depends on the waveform, since the rectangle and the decaying exponential produce different numbers of voltage spikes.

The rectangle will push current through the insulation and then pull it back out. The negative decaying exponential will only pull current from the insulation. Since a portion of its total current comes from the insulation, the negative decaying exponential will fail to extract all of charge accumulated at the tip of the electrode. Pairing a positive rectangular wave with a negative decaying exponential will cause a loss of charge in the surrounding tissue, and a build up of charge at the tip of the electrode. This charge imbalance will accumulate throughout the duration of stimulation, which can last years [56].

A coaxial electrode will prevent deep-brain stimulation from leaking into the surrounding tissue. This will prevent damage to the nervous system, and will reduce stimulation artifacts generated in neural recordings. This coaxial electrode differs from commercially available concentric bipolar electrodes [53] in that the outer ring of metal is completely insulated and never contacts the surrounding tissue. This outer ring is also held to the stimulator ground.

While the coaxial electrode will protect the surrounding tissue, this device will not solve the problem of biphasic stimulation. Current will still cross the inner layer of insulation; it is simply diverted to the ground of the neural stimulator. While charge will not accumulate in the surrounding tissue, there will still be an incomplete extraction of charge from the tip of the electrode. To prevent a charge imbalance during biphasic stimulation, the positive and negative waveforms should be identical. This will force the negative waveform to extract the correct amount of charge from the tip of the electrode and from the insulation.

Capacitive coupling is not a concern for deep brain recording. The electrode insulation significantly attenuates the surrounding neural activity. Neural structures are too small and oscillate at frequencies too slow to cross through the insulation. As we create thinner electrodes, the influence of the surrounding neural activity will increase, but this will only become a concern once the diameter of the electrode shrinks below 100 nanometers.

2.7 – CITATIONS

[1] Galvani, Luigi. "D viribus electricitatis in motu musculari: Commentarius." Bologna: Tip. Istituto delle Scienze, 1791; 58 p.: 4 tavv. ft; in 4.; DCC. f. 70 (1791).

[2] Piccolino, Marco. "Luigi Galvani and animal electricity: two centuries after the foundation of electrophysiology." *Trends in neurosciences* 20.10 (1997): 443-448.

[3] Duchenne de Bologne, G. B. "The mechanism of human facial expression (RA Cuthbertson, Trans.)." *Paris: Jules Renard*(1862).

[4] Fritsch, Gustav, and Eduard Hitzig. "On the electrical excitability of the cerebrum." *Some papers on the cerebral cortex* (1960): 73-96.

[5] Caton, Richard. "Electrical Currents of the Brain." *The Journal of Nervous and Mental Disease* 2.4 (1875): 610.

[6] Berger, Hans. "On the electroencephalogram of man. Third report." *Electroencephalography and clinical neurophysiology*(1969): Suppl-28.

[7] Bullock, Theodore Holmes. "Neuron doctrine and electrophysiology." *Science* 129.3355 (1959): 997-1002.

[8] y Cajal, Santiago Ramón. *Neuron theory or reticular theory?: Objective evidence of the anatomical unity of nerve cells*. Editorial CSIC-CSIC Press, 1954.

[9] Bretag, Allan H. "The glass micropipette electrode: A history of its inventors and users to 1950." *The Journal of general physiology* (2017): jgp-201611634.

[10] Brown, KENNETH T., and T. N. Wiesel. "Intraretinal recording with micropipette electrodes in the intact cat eye." *The Journal of physiology* 149.3 (1959): 537-562.

[11] Green, J. D. "A simple microelectrode for recording from the central nervous system." *Nature* 182.4640 (1958): 962.

[12] Dowben, Robert M., and Jerzy E. Rose. "A metal-filled microelectrode." *Science* 118.3053 (1953): 22-24.

[13] Grundfest, Harry, et al. "Stainless Steel Micro-Needle Electrodes Made by Electrolytic Pointing." *Review of Scientific Instruments* 21.4 (1950): 360-361.

[14] Hubel, David H. "Tungsten microelectrode for recording from single units." *Science* 125.3247 (1957): 549-550.

[15] Maynard, Edwin M., Craig T. Nordhausen, and Richard A. Normann. "The Utah intracortical electrode array: a recording structure for potential brain-computer interfaces." *Electroencephalography and clinical neurophysiology* 102.3 (1997): 228-239.

[16] Becker, Hal C., et al. "A roentgenographic stereotaxic technique for implanting and maintaining electrodes in the brain of man." *Electroencephalography and clinical neurophysiology* 9.3 (1957): 533-543.

[17] Harris, Kenneth D., et al. "Accuracy of tetrode spike separation as determined by simultaneous intracellular and extracellular measurements." *Journal of neurophysiology* 84.1 (2000): 401-414.

[18] Wilson, Blake S., et al. "Better speech recognition with cochlear implants." *Nature* 352.6332 (1991): 236-238.

[19] Collinger, Jennifer L., et al. "High-performance neuroprosthetic control by an individual with tetraplegia." *The Lancet* 381.9866 (2013): 557-564.

[20] Aflalo, Tyson, et al. "Decoding motor imagery from the posterior parietal cortex of a tetraplegic human." *Science*348.6237 (2015): 906-910.

[21] Hochberg, Leigh R., et al. "Neuronal ensemble control of prosthetic devices by a human with tetraplegia." *Nature*442.7099 (2006): 164.

[22] Kaufman, Matthew T., Mark M. Churchland, and Krishna V. Shenoy. "The roles of monkey M1 neuron classes in movement preparation and execution." *Journal of neurophysiology* 110.4 (2013): 817-825.

[23] Barthó, Peter, et al. "Characterization of neocortical principal cells and interneurons by network interactions and extracellular features." *Journal of neurophysiology* 92.1 (2004): 600-608.

[24] Wagenaar, Daniel A., and Steve M. Potter. "Real-time multi-channel stimulus artifact suppression by local curve fitting." *Journal of neuroscience methods* 120.2 (2002): 113-120

[25] Hashimoto, Takao, Christopher M. Elder, and Jerrold L. Vitek. "A template subtraction method for stimulus artifact removal in high-frequency deep brain stimulation." *Journal of neuroscience methods* 113.2 (2002): 181-186.

[26] Smetters, Diana, Ania Majewska, and Rafael Yuste. "Detecting action potentials in neuronal populations with calcium imaging." *Methods* 18.2 (1999): 215-221.

[27] Tsien, Roger Y. "Fluorescence measurement and photochemical manipulation of cytosolic free calcium." *Trends in neurosciences* 11.10 (1988): 419-424.

[28] Stosiek, Christoph, et al. "In vivo two-photon calcium imaging of neuronal networks." *Proceedings of the National Academy of Sciences* 100.12 (2003): 7319-7324.

[29] Tian, Lin, et al. "Imaging neural activity in worms, flies and mice with improved GCaMP calcium indicators." *Nature methods* 6.12 (2009): 875.

[30] Wang, Jing W., et al. "Two-photon calcium imaging reveals an odor-evoked map of activity in the fly brain." *Cell* 112.2 (2003): 271-282.

[31] Yizhar, Ofer, et al. "Optogenetics in neural systems." *Neuron*71.1 (2011): 9-34.

[32] Nagel, Georg, et al. "Channelrhodopsin-1: a light-gated proton channel in green algae." *Science* 296.5577 (2002): 2395-2398.

[33] Matsuno-Yagi, Akemi, and Yasuo Mukohata. "Two possible roles of bacteriorhodopsin; a comparative study of strains of Halobacterium halobium differing in pigmentation." Biochemical and biophysical research communications 78.1 (1977): 237-243.

[34] Aravanis, Alexander M., et al. "An optical neural interface: in vivo control of rodent motor cortex with integrated fiberoptic and optogenetic technology." *Journal of neural engineering* 4.3 (2007): S143.

[35] Deisseroth, Karl. "Optogenetics." *Nature methods* 8.1 (2011): 26.

[36] Ibsen, Stuart, et al. "Sonogenetics is a non-invasive approach to activating neurons in Caenorhabditis elegans." *Nature communications* 6 (2015): 8264.

[37] Bernstein, Jacob G., Paul A. Garrity, and Edward S. Boyden. "Optogenetics and thermogenetics: technologies for controlling the activity of targeted cells within intact neural circuits." *Current opinion in neurobiology* 22.1 (2012): 61-71.

[38] Aston-Jones, Gary, and Karl Deisseroth. "Recent advances in optogenetics and pharmacogenetics." *Brain research* 1511 (2013): 1-5.

[39] Benabid, Alim Louis. "Deep brain stimulation for Parkinson's disease." *Current opinion in neurobiology* 13.6 (2003): 696-706.

[40] Limousin, Patricia, et al. "Electrical stimulation of the subthalamic nucleus in advanced Parkinson's disease." *New England Journal of Medicine* 339.16 (1998): 1105-1111.

[41] Okun, Michael S., et al. "Subthalamic deep brain stimulation with a constant-current device in Parkinson's disease: an open-label randomised controlled trial." *The Lancet Neurology*11.2 (2012): 140-149.

[42] Weaver, Frances M., et al. "Bilateral deep brain stimulation vs best medical therapy for patients with advanced Parkinson disease: a randomized controlled trial." *Jama* 301.1 (2009): 63-73.

[43] Engel, Andreas K., et al. "Invasive recordings from the human brain: clinical insights and beyond." *Nature Reviews Neuroscience* 6.1 (2005): 35.

[44] Robinson, David A. "The electrical properties of metal microelectrodes." *Proceedings of the IEEE* 56.6 (1968): 1065-1071.

[45] Cogan, Stuart F. "Neural stimulation and recording electrodes." *Annu. Rev. Biomed. Eng.* 10 (2008): 275-309.

[46] Jack, James Julian Bennett, Denis Noble, and Richard W. Tsien. "Electric current flow in excitable cells." (1975): 429-449.

[47] Blackrock Microsystem. Cerebus Amplifier Data Sheet. 2014

[48] Gabriel, Camelia. *Compilation of the Dielectric Properties of Body Tissues at RF and Microwave Frequencies*. KING'S COLL LONDON (UNITED KINGDOM) DEPT OF PHYSICS, 1996.

[49] Plexon. OmniPlex D Neural Data Acquisition System [data sheet] 2015

[50] Rattay, Frank. "Analysis of models for external stimulation of axons." *IEEE transactions on biomedical engineering* 10 (1986): 974-977.

[51] Laotaveerungrueng. A High-Voltage, High-Current Multi-Channel Arbitrary Waveform Generator ASIC for Neural Interface and MEMS Applications. [dissertation] [Cleveland]; Case Western Reserve University; 2011. 149 p.

[52] Medtronic. Activa PC Multi-program neurostimulator. Medtronic (2008)

[53] Microprobes Inc. Metal Electrodes Datasheet (2018)

[54] Rousche, Patrick J., and Richard A. Normann. "Chronic recording capability of the Utah Intracortical Electrode Array in cat sensory cortex." Journal of neuroscience methods 82.1 (1998): 1-15.

[55] Ferguson, John E., Chris Boldt, and A. David Redish. "Creating low-impedance tetrodes by electroplating with additives." Sensors and Actuators A: Physical 156.2 (2009): 388-393.

[56] Andrade, D. M., et al. "Long-term follow-up of patients with thalamic deep brain stimulation for epilepsy." *Neurology* 66.10 (2006): 1571-1573.

[57] Scheiner, Avram, J. Thomas Mortimer, and Uros Roessmann. "Imbalanced biphasic electrical stimulation: muscle tissue damage." *Annals of biomedical engineering* 18.4 (1990): 407-425.

STATE-ESTIMATION IN THE POSTERIOR PARITEAL CORTEX

The Brain

Figure 3.1: Examples of tetraplegic patients controlling the movement of a robotic limb from neural recordings in either A) motor cortex [7] or B) parietal cortex [8]

3.1 – Introduction

3.1.1 – Overview of Neural Prosthetics.

Patients suffering from high-cervical spinal injuries lose control of both their arms and their legs. These tetraplegic patients are locked into a wheelchair and require intensive assistance throughout daily life. A new technology (neural prosthetics) aims to assist these patients by giving them control over a robotic limb [1,2,3]. This is accomplished by implanting intracortical electrodes into brain regions closely associated with movement [4]. As a patient thinks about moving their hand, the neurons recorded by the electrodes modulate their firing patterns. Computer algorithms can then interpret changes in these patterns and predict the patient's intended action [5,6] [**Figure 3.1A,B**]. While there have been successful human trials [7,8,9], this technology is still in early stages of development. For these prostheses to be successful, researchers must accurately understand how neural activity relates to movement.

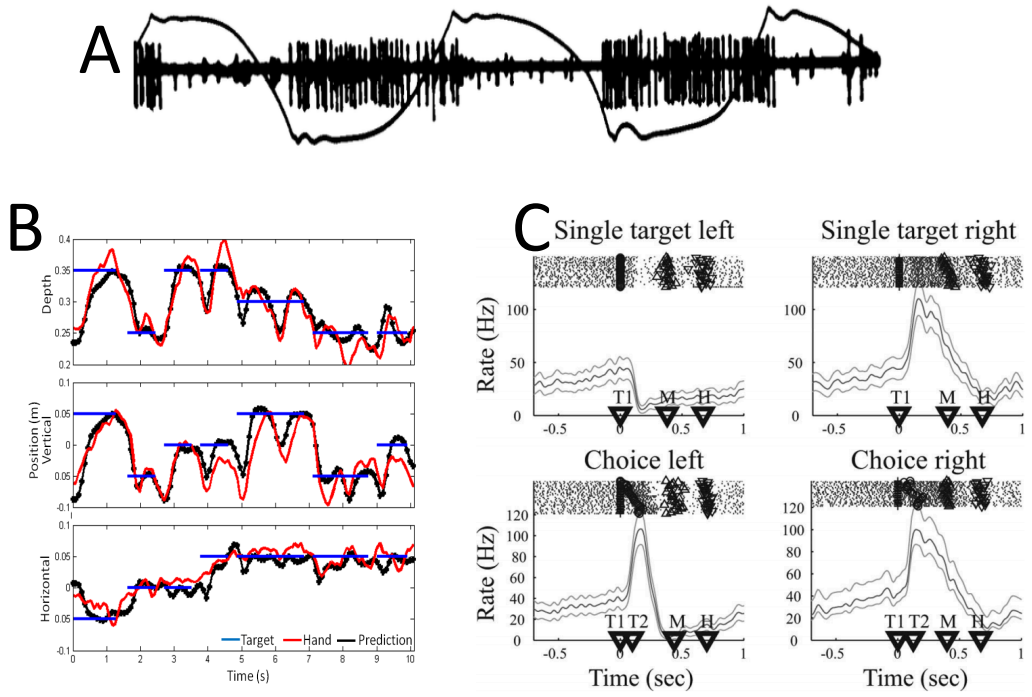

Figure 3.2: A) Raw spiking activity of a neuron from primary motor cortex recorded from a rhesus macaque monkey, superimposed on the animal's wrist position. This plot demonstrates the clear correlation between spiking activity in motor cortex and hand movement. [60] B) Offline reconstruction of the 3D hand position (black) from parietal activity (red) as a rhesus macaque monkey moves to various targets (blue) [13] C) Peristimulus time histogram demonstrating the preference of a parietal neuron to a specific goal location. Example parietal neuron increases activity when cued to move to the right goal. [14]

3.1.2 – Types of Movement Signals

There are many types of signals in the brain that relate to movement. Current neural prostheses focus on decoding kinematics signals, which is neural activity that directly correlates to the moment-by-moment movements of the hand. The brain region most extensively studied for this application is primary motor cortex (M1) [10,11] [**Figure 3.2a**]. Neurons in this brain area directly synapse onto the spinal neurons that activate our muscles. This places M1 at the final stage of the human motor system, and makes it the logical first place to look for a kinematic signal. Yet, kinematic signals do not need to reside in the motor cortex. Movement requires a complex interaction between sensory feedback and motor planning. Other brain areas outside of motor cortex are involved in this process and can also encode the

real-time kinematics of the hand. Recently, just such a signal has been discovered in the posterior parietal cortex [12,13] [**Figure 3.2b**]. The kinematic signal in the parietal cortex has proven strong enough to be successfully used for clinical applications in tetraplegic humans [8] [**Figure 3.1b**].

3.1.3 – Control Signals In Parietal Cortex.

The discovery of real-time hand kinematics in the parietal cortex was surprising. Traditionally, the parietal cortex was thought to encode cognitive signals, such as goal location [14,15,16] [**Figure 3.2c**], context [17,18], decision-making [19,14], sequential movements [20], and behavioral state [21]. The fact that the parietal cortex also encodes a kinematic signal has important applications for neural prosthetics. Prostheses built using purely kinematic signals produce slower and less accurate movements than our natural limbs. Evidence suggests that incorporating cognitive signals can improve the performance of neural prosthetics [22]. The discovery of a kinematic signal in the parietal cortex means that both cognitive and kinematic signals can be decoded from a single brain area. This would result in a less invasive implantation surgery, making these devices a safer option for patients. This makes the parietal cortex the ideal implantation site for neural prosthetics. For this to be successful, we need to better understand the nature of the kinematic signal in the parietal cortex.

3.1.4 – Sensorimotor Control.

Our bodies navigate through a complex and dynamic world. We must account both for our own movement and for changes in our environment. This is a complex physical problem. One approach successfully used in engineering is continuous sensorimotor control [23], which applies sensory feedback to adjust movement in real time [**Figure 3.3**]. In this feedback system, a *command signal* causally drives the movement of the limb. This command signal is also looped back into the brain as an efference copy to keep track of the motor output. The movement of the limb then generates a *sensory signal*, which reports to the brain the result of the motor

action. A *state-estimator* combines this sensory feedback with the efference copy to estimate the state of the limb. This state-estimator is used as an error signal to adjust the motor output, so that the limb produces the desired movement. State-estimation is a necessary signal for robust motor control during dynamic movement tasks [24,25,26].

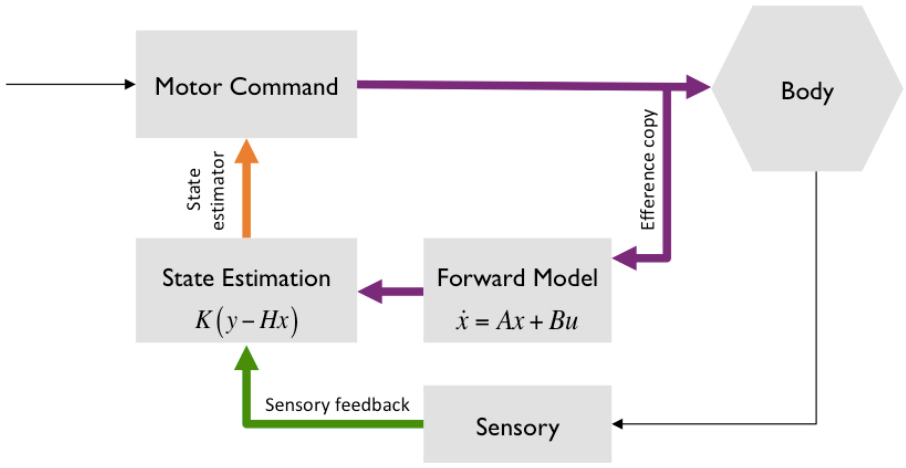

Figure 3.3: Example diagram of the sensorimotor feedback system. The motor command outputs a command signal (purple) that engages the body and is fed back into the brain as an efference copy. The body produces sensory information, which is also fed back into the brain (green) . The state estimator (orange) combines the efference copy with the sensory feedback to predict the state of the hand. The motor command incorporates this state-estimator into its control law to update the command signal.

3.1.5 – Anatomical Evidence of State-Estimation.

The parietal cortex is perfectly positioned in the sensorimotor pathway to act as a state-estimator. Classically, the parietal cortex is known as the 'association' area, as it receives a vast number of inputs from various sensory modalities, such as vision, somatosensation, audition, and the vestibular system [27,28]. For example, the parietal cortex is the final stage of the dorsal visual pathway (also known as the occipitoparietal pathway), which is involved in visually locating the position of objects and guiding visual motor tasks [29,30,31]. The efference copy is also fed into the parietal cortex, allowing it to monitor the command signal sent to the muscles [32]. This positions the parietal cortex between sensory and motor areas [33,34], which is a requirement for any cortical region that integrates these two signals.

3.1.6 – Clinical Evidence of State-Estimation.

Patients suffering from lesions in their parietal cortex present motor deficits that are in line with a damaged state-estimator [35]. In one study, patients were asked to make a series of finger movements, and were presented with visual feedback of either their own finger or the finger of an experimenter performing the same task [36]. These patients were unable to determine the ownership of the viewed finger. This suggests an inability to recognize differences between their internal efference copy and their visual feedback. Damage to the parietal cortex also interferes with making online corrections during reaching movements. Patients were asked to reach towards a target that would unexpectedly move once the patient initiated their reach. Patients with lesions in the parietal cortex failed to adjust to the new target location [37,38,39]. This failure suggests an inability to integrate sensory feedback into their motor plan.

Lesions in the parietal cortex can also result in a neurological disorder called Balint's syndrome [40], which includes a sensory-motor deficit known as optic ataxia [41]. These patients have otherwise healthy visual and motor systems, but demonstrate impaired movement during visually guided reaches. These patients will overshoot or undershoot their desired target, again suggesting a failure to incorporate sensory information into their motor plan (**Figure 3.4**) [41,42,43].

While clinical evidence has provided important insight into the function of the parietal cortex, lesion studies are an imperfect way of studying the brain. These lesions arise from natural causes, and thus may affect multiple functional areas in the brain and may be inconsistent across patients [40]. Also, these studies are conducted a significant time after the patient suffered their lesion, and their brain may have compensated for the loss of function. Their brain may use alternative cortical areas to accomplish a desired task. Changes in behavior could therefore be attributed to the alternative pathway and not necessarily to the loss of the lesioned

area [35]. As a result, it is difficult to tease out the precise role of a specific cortical area from human lesion studies alone.

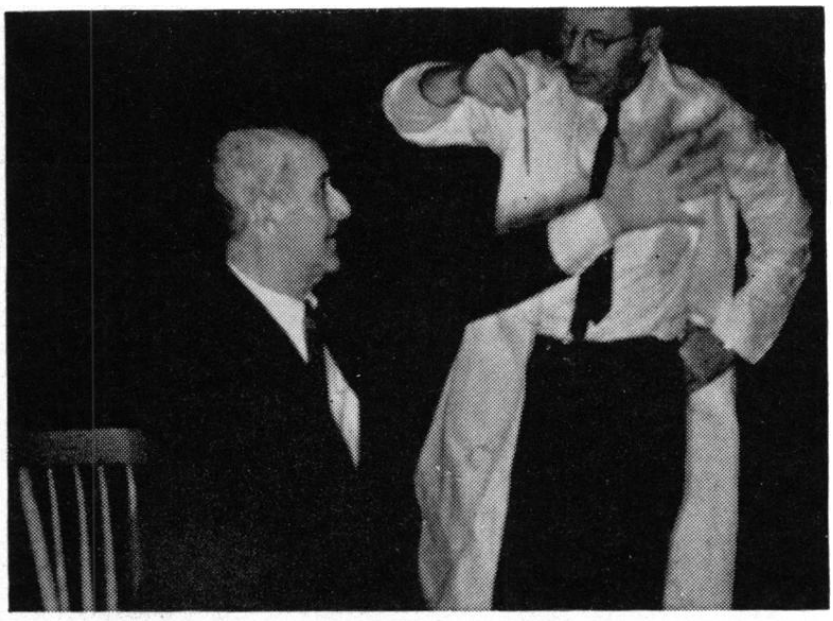

Figure 3.4: Example of patient suffering from optic ataxia. A patient with bilateral lesions in his parietal cortex fails to grasp a pen held by the experimenter, even though his visual and motor systems are intact. [43]

3.1.7 – Human Experiential Evidence of State-Estimation.

To expand upon the clinical results, human experiments have been performed using transcranial magnetic stimulation (TMS) [44]. Healthy subjects had a TMS coil positioned over their parietal cortex, which researchers used to temporarily disrupt neural activity in the region. In one experiment, subjects were asked to make finger movements in a virtual reality environment [45]. During a random subset of these movements, a visual delay was introduced between their actual finger movement and their displayed visual feedback. At the end of each movement the subjects were asked if they perceived visual feedback to occur in real-time or with a delay. The application of TMS to the subject's parietal cortex impaired their ability to notice the visual delay. This again suggests a failure to compare internal efference information with sensory feedback, similar to the finger ownership experiments in

lesion patients. Online movement correction was also studied using TMS in healthy subjects [46]. The subjects were cued to reach towards a desired goal, and once the subject initiated their reach, the goal moved. During TMS stimulation, subjects failed to adjust to the new location. Disrupting parietal activity using TMS produces similar behavioral effects as seen in the lesion patients, again supporting the idea that the parietal cortex plays an important role in integrating sensory and motor information.

There are strict limitations on the experiments that can be performed in humans [47]. Noninvasive methods (such as EEG [48], fMRI [49], and TMS [50]) have well documented tradeoffs between temporal and spatial resolution [51,52]. These investigational limitations prevent the direct assignment of a neural signal to a specific brain area. Only in extreme cases, such as tetraplegia [7,8,9] or severe forms of epilepsy [53,54], can researchers apply invasive techniques (Ecog and extracellular electrodes) to study neural activity in humans. These invasive experiments suffer from similar complications seen in lesion studies. These patients have diagnosed neurological issues, and so their brain activity may not be representative of healthy subjects. Therefore, the information that can be drawn from human experiments is limited.

3.1.8 – Nonhuman Primate Experiential Evidence of State-Estimation.

To further tease apart the neural mechanism in the parietal cortex, experiments were performed in nonhuman primates. In one such experiment, the parietal cortex of two nonhuman primates were temporarily inactivated using muscimole, a GABAa agonist that suppresses neural activity [55]. The animals had been trained to reach for targets on a computer screen. After the injection of muscimole, these animals consistently undershot their desired target [**Figure 3.5**]. This replicates the behavioral effect of optic ataxia, and again supports the idea that the parietal cortex is necessary to combine sensory and motor information.

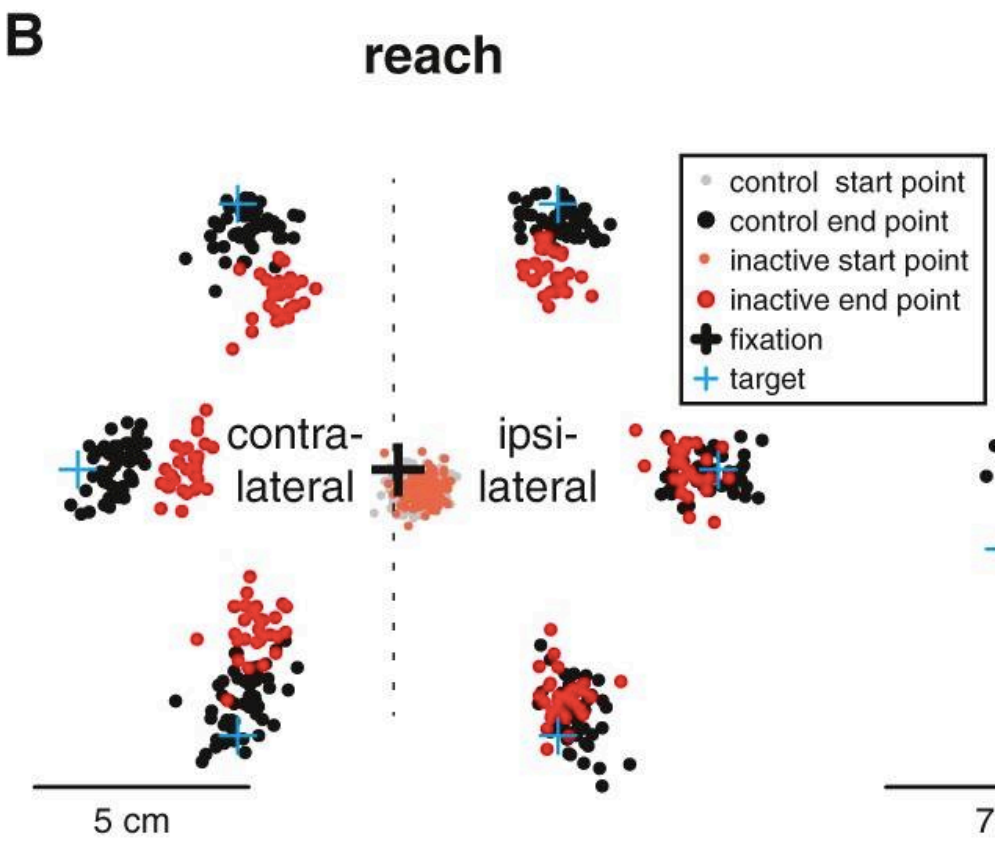

Figure 3.5: Reaching behavior of a nonhuman primate during parietal inactivation. The animal was placed in front of a touch-sensitive computer screen. The animal was trained to first touch the center position (black +) and was then cued to one of six possible goal locations (blue +). The animal removed their hand from the screen and reached for the target. The next location on the screen the animal touch was marked as the end point of their reach. The animal undershot the target during inactivation sessions (red), where the parietal cortex was injected with muscimole, compared to control sessions (black), where the parietal cortex was injected with saline, replicating the effect of optic ataxia. [55]

While these prior animal and human studies have focused on loss of function experiments in the parietal cortex, there is also correlative evidence that parietal cortex acts as a state-estimator. Neural signals need time to propagate through the nervous system. This means that a command signal that drives muscle activity must occur *before* movement, and a sensory signal that monitors feedback must occur *after* movement. This timing relationship was studied in the parietal cortex by computing the mutual information between hand movement and a window of neural activity. The window was shifted forwards and backwards in time to offset

the timing of the neural activity from the hand movement; shifting the window forward captured neural activity occurring after the movement, and shifting it backwards captured neural activity occurring before the movement. This produced an 'offset' tuning curve that displays the relative timing between the activity of an individual parietal neuron and the resulting hand movement [56]. Parietal activity recorded from nonhuman primates show this offset tuning curve peaks in mutual information at a 0 ms offset, suggesting an instantaneous relationship between parietal activity and hand movement (**Figure 3.6a**). The bulk of neurons in the posterior parietal cortex show this instantaneous relationship (**Figure 3.6b**), which means that the kinematic signal in the parietal cortex is too slow to drive movement, but too fast to be sensory feedback. This suggests the parietal cortex contains a forward model that predicts the current state of the hand [57]. Forward models would be expected in a state-estimator. As described above, command signals and sensory signals are out of sync with each other, and thus a forward model is needed to bring them into alignment.

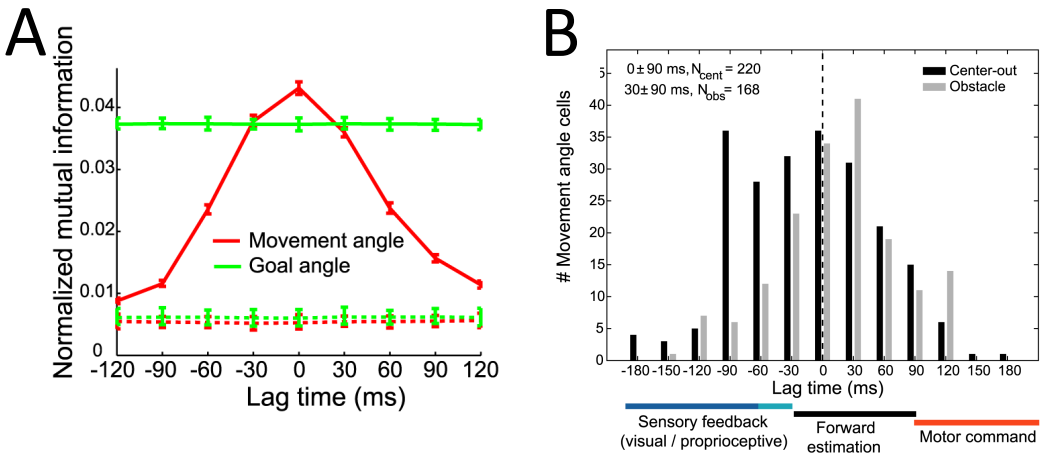

Figure 3.6: A) An offset tuning curve generated from a single parietal neuron. The mutual information was computed between a window of neural activity and the hand velocity. The window of neural activity was shifted forwards and backwards in time to study the timing relationship between parietal activity and hand movement. The peak of this curve is at 0ms, suggesting an instantaneous relationship between neural activity and movement. [56] B) A histogram of the optimal lag times for a collection of parietal neurons recorded during either a center-out task (black) or an obstacle avoidance task (grey). During the center-out task, the bulk of cells in the posterior parietal cortex show near instantaneous timing relationship with movement. During the obstacle avoidance task, the peak optimal lag time shifted forward by ~30 m. This shift forward during the obstacle task suggests that state-estimation is context dependent. [56]

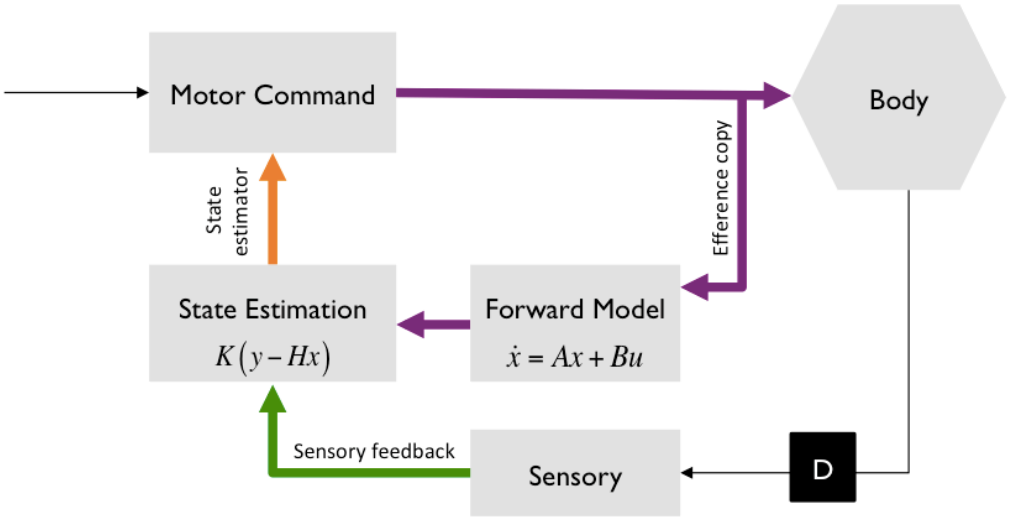

Figure 3.7: Example diagram of the sensorimotor feedback system with a delay element (D). This will cause the sensory feedback to lag the efference copy, which will disrupt the state-estimator.

3.2 – State-Estimation In Parietal Cortex

3.2.1 – Hypothesis

To provide causal evidence that the kinematic signal in the parietal cortex is a state-estimator, an artificial sensory delay was used to force a misalignment between the sensory feedback and the efference copy [**Figure 3.7**]. This misalignment has a unique effect on the offset tuning curves that can disassociate a state-estimator from sensory and command signals. If the parietal cortex encodes a sensory signal, the relative timing between neural activity and limb position should increase in proportion to the sensory delay [**Figure 3.8a**]. These sensory neurons will be unaware of the delay, and will process the old sensory information as if it were current. If the parietal cortex encodes a command signal, the relationship between neural activity and limb movement should be unaffected [**Figure 3.8b**]. The neurons will continue to correlate to muscle activity, and should show no significant change in encoding properties. A state-estimator will have a more complicated response. During a sensory delay, a state-estimator will unknowingly

combine the current efference copy with the delayed sensory feedback, resulting in incorrect predictions of the hand. If, as expected, the parietal cortex acts as a state-estimator, we would expect these incorrect predictions to cause a drop in correlation between neural activity and limb movement during a sensory delay [**Figure 3.8c**].

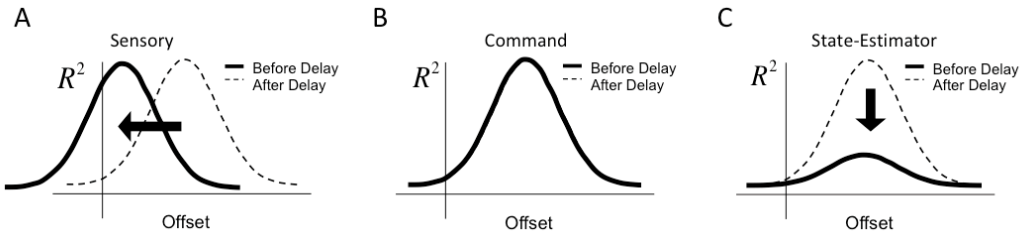

Figure 3.8: Expected effect of a sensory delay on the offset tuning curves for sensory, motor, and state-estimator signals. A) The peak decoding time for a sensory signal should shift backwards in time in proportion to the sensory delay. B) The command signal should be unaffected by the sensory delay. C) The state-estimator should show a drop in predictive strength after a sensory delay.

3.2.2 – Experimental Setup

To test this idea, we trained two nonhuman primates to make reaches in a virtual reality environment where their hand was displayed as a cursor on a screen (see methods). The animals had learned to guide the movement of the cursor by moving their own hand. The animals performed reaches with their hand position displayed either in real-time or with an artificial visual lag (**Figure 3.9a,b**). During these reaches, neural activity was recorded from intracortical arrays implanted in the parietal cortex (area5d) of both animals (**Figure 3.9c,b**). Monkey M had an additional intracortical array implanted in primary motor cortex (M1) (**Figure 3.9c**).

3.2.3 – Offset Tuning Analysis

We studied the effect of a sensory delay on the timing relationship between neural activity and hand movement. Linear regression was used to predict the hand velocity (x) from a sliding window of neural activity (f).

$$x(t) = \beta \cdot f(t - \tau).$$

Offsets (τ) of the window captured neural activity occurring either before or after the movement; positive offsets correspond to neural activity occurring *before* movement, and negative offsets correspond to neural activity occurring *after* movement. For each of these offsets, the strength of the linear regression was quantified using the adjusted coefficient of determination ($\bar{R}^2$), and the results formed an offset tuning curve (see methods).

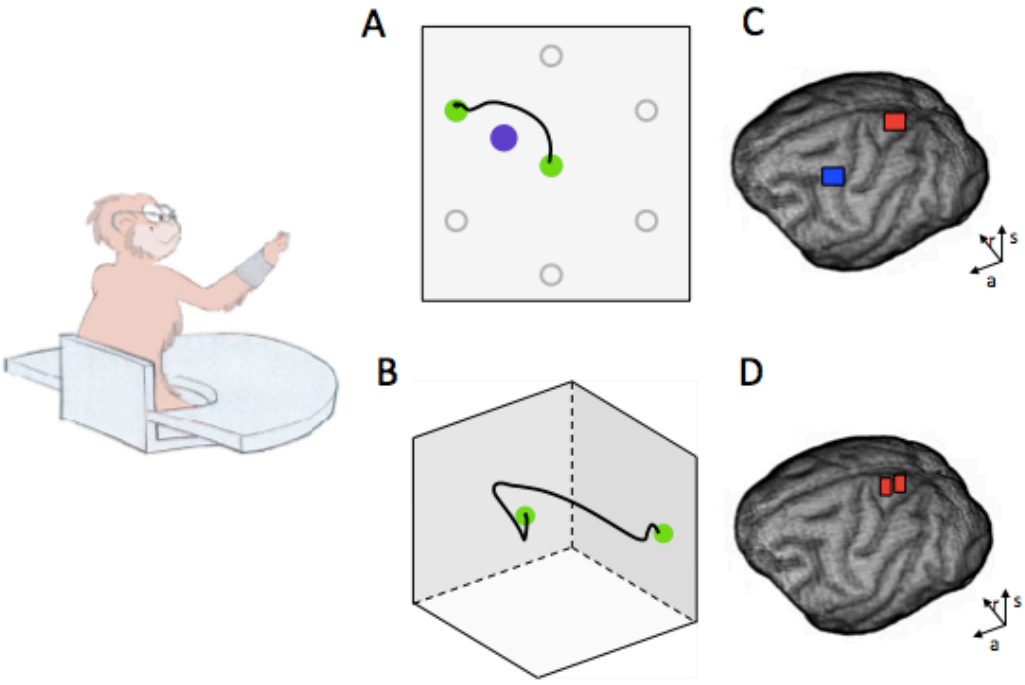

Figure 3.9: Reaching tasks and array locations. A) Example hand movement made by monkey M during the 2D center-out reaching task with obstacle avoidance. B) Example hand movement made by monkey R during the 3D sequential reaching task. C) Locations of Utah arrays implanted in parietal cortex (red) and motor cortex (blue) of monkey M superimposed on anatomical MRI scan of monkey M's brain. D) Locations of two floating microwire arrays (FMA) in the parietal cortex (red) of monkey R, superimposed on the anatomical scan of monkey M's brain.

Changes in the timing relationship between neural activity and hand movement were studied using a sliding window of experimental data. During the recording session, the animals performed hundreds of reaches. Offset tuning curves were generated using neural activity and behavioral data collected from a moving subset of 35 sequential reaches. This window of 35 reaches was scanned across the recording sessions in single trial increments, and an offset tuning curve was

calculated at each step. This resulted in a 2D heat-map that displayed changes in the offset tuning profile throughout the recording session. These heat-maps were computed independently for the real-time and delayed reaches, such that trials with and without the sensory delay were not mixed. Heat-maps were generated from multiple recording sessions and the results were averaged (monkey M, 18 sessions; monkey R, 6 lag sessions and 5 real-time sessions). In the case of monkey M, the parietal and motor arrays were processed independently.

3.2.4 – Idealized Signals

To confirm our hypothesis that a sensory delay will cause a decorrelation between parietal activity and movement, we studied the effect of a sensory delay on idealized versions of command, sensory, and state-estimator signals. Idealized signals were created from behavioral data of monkey M taken from the same sessions used in the neural analysis (see methods). A command signal ($f_{command}$) was created to directly correlate with the velocity of the hand (x) with added noise (σ):

$$f_{command}(t) = x(t) + \sigma(t).$$

A sensory signal ($f_{sensory}$) was created to correlate with the visual feedback of the hand (x), which includes a sensory delay (t_{delay}) that is zero during real-time reaches and 200ms during lag reaches:

$$f_{sensory}(t) = x\big(t - t_{delay}\big) + \sigma(t).$$

A state-estimator signal ($f_{estimator}$) was defined as the average between the command and sensory signals:

$$f_{estimator}(t) = \frac{1}{2} \cdot \big[f_{motor}(t) + f_{sensory}(t)\big].$$

The timing relationship between these idealized signals and hand movement was explored using the same offset tuning analysis applied to the real neural activity (see methods).

3.2.5 – Time-To-Contact Histograms

To study the behavioral effect of a sensory delay, we calculated the time required to complete the last centimeter of each reach (time-to-contact). This last section of the reach requires the animal to accurately acquire and hold a target. Histograms of the time-to-contact value were computed from the same sliding window of 35 trials used in the offset tuning analysis (see methods). This produced a time-to-contact histogram corresponding to each offset tuning curve. These histograms were computed and averaged across the same recording sessions used in the offset tuning analysis.

3.3 – Results

3.3.1 – Idealized Signals

The offset tuning analysis of the idealized signals agrees with our expectation of how a sensory delay will affect sensory, command, and state-estimator signals. In the real-time condition the three signals show identical offset tuning curves [**Figure 3.10a,b,c**]. The optimal window to predict the hand velocity coincides with the onset of the movement. The predictive strength of these signals decays as the window of neural activity was shifted away from this optimal offset time (moving along the y-axis). These tuning curves were robust, and did not change throughout the real-time reaches (along the x-axis). Each signal responded differently to the sensory delay. The optimal decoding time for the sensory signal was delayed by 200ms (a shift upwards on the y-axis), which is in proportion to the sensory delay [**Figure 3.10d**], the command signal was unaffected [**Figure 3.10e**], and the state-estimator showed a drop in predictive strength (approximately 66%) [**Figure 3.10f**]. These offset tuning profiles did not change throughout the delayed sessions.

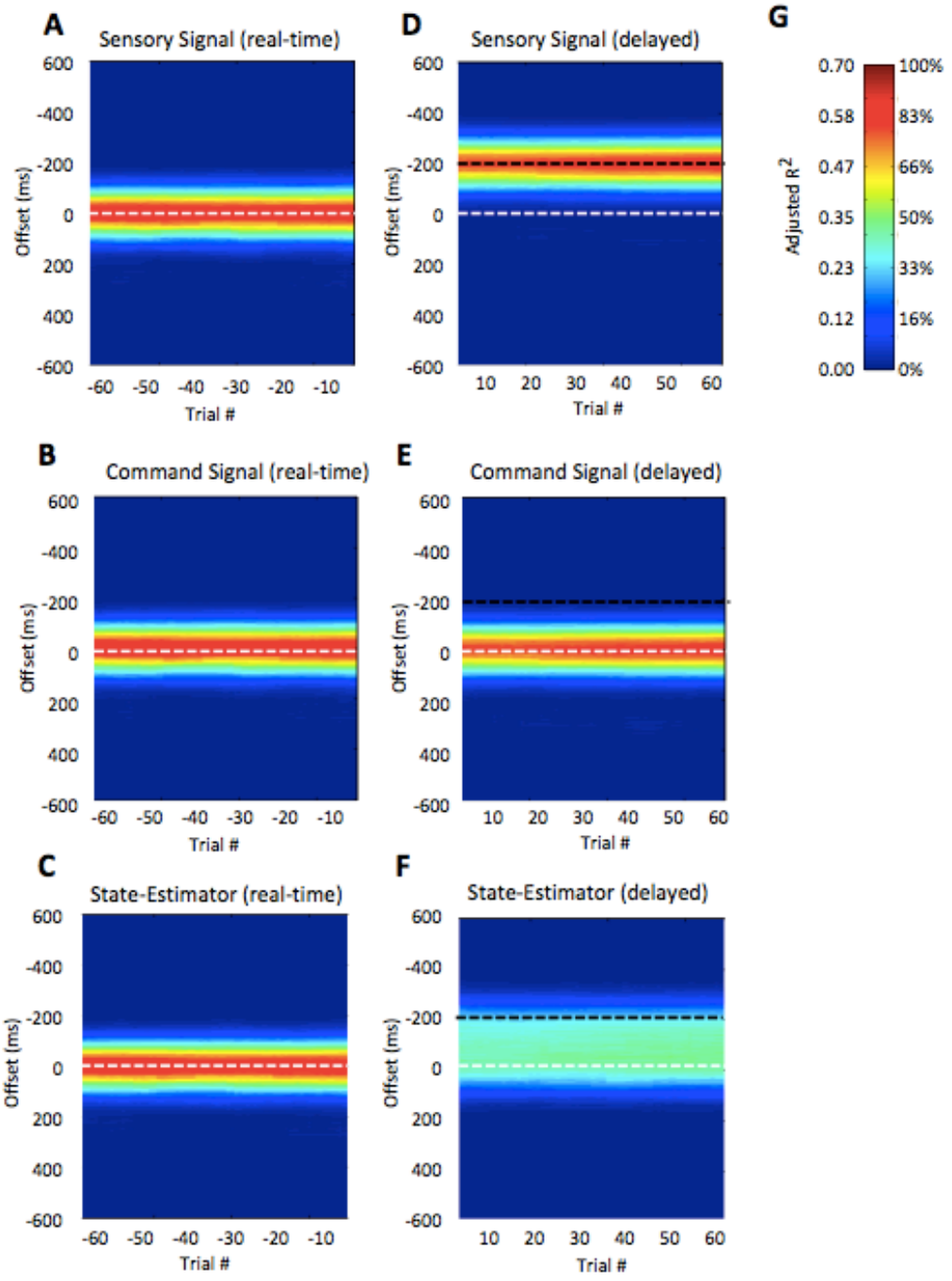

Figure 3.10: Offset tuning analysis of the idealized signals during the real time conditions for A) sensory signal, B) command signal, and C) state-estimator, and during the delayed condition for D) sensory signal, E) command signal, and F) state-estimator. G) The color scale used across all plots.

3.3.2 – Offset Tuning Analysis

Spiking activity of parietal neurons in both monkey M and monkey R shows clear tuning to hand velocity during real-time reaches. The optimal time to decode hand movements occurs approximately with the onset of the movement. As the window of neural activity is shifted from this optimal lag time (along the y-axis), the predictive strength of the parietal cortex decays. This offset tuning profile was consistent through out the recording sessions during real-time hand reaches (**Figure 3.11a, Figure 3.12a**). Spiking activity in the motor cortex of monkey M showed a similar offset tuning profile during real-time reaches (**Figure 3.11g**). At the onset of the visual delay there was a significant drop in the predictive strength of the parietal cortex (approximately 50%) (**Figure 3.11b, Figure 3.12b**). As the animals perform additional reaches with the visual delay (20 trials for monkey M, and 60 trials for monkey R), the offset tuning profile of the parietal cortex gradually returned. The recovered tuning profile showed no significant change in the optimal decoding time. This drop and recovery was seen in the parietal cortex of both animals. In motor cortex, there was a slight drop in the predictive strength (15%) during the visual lag, but the general tuning profile remained constant and did not improve over time (**Figure 3.11h**).

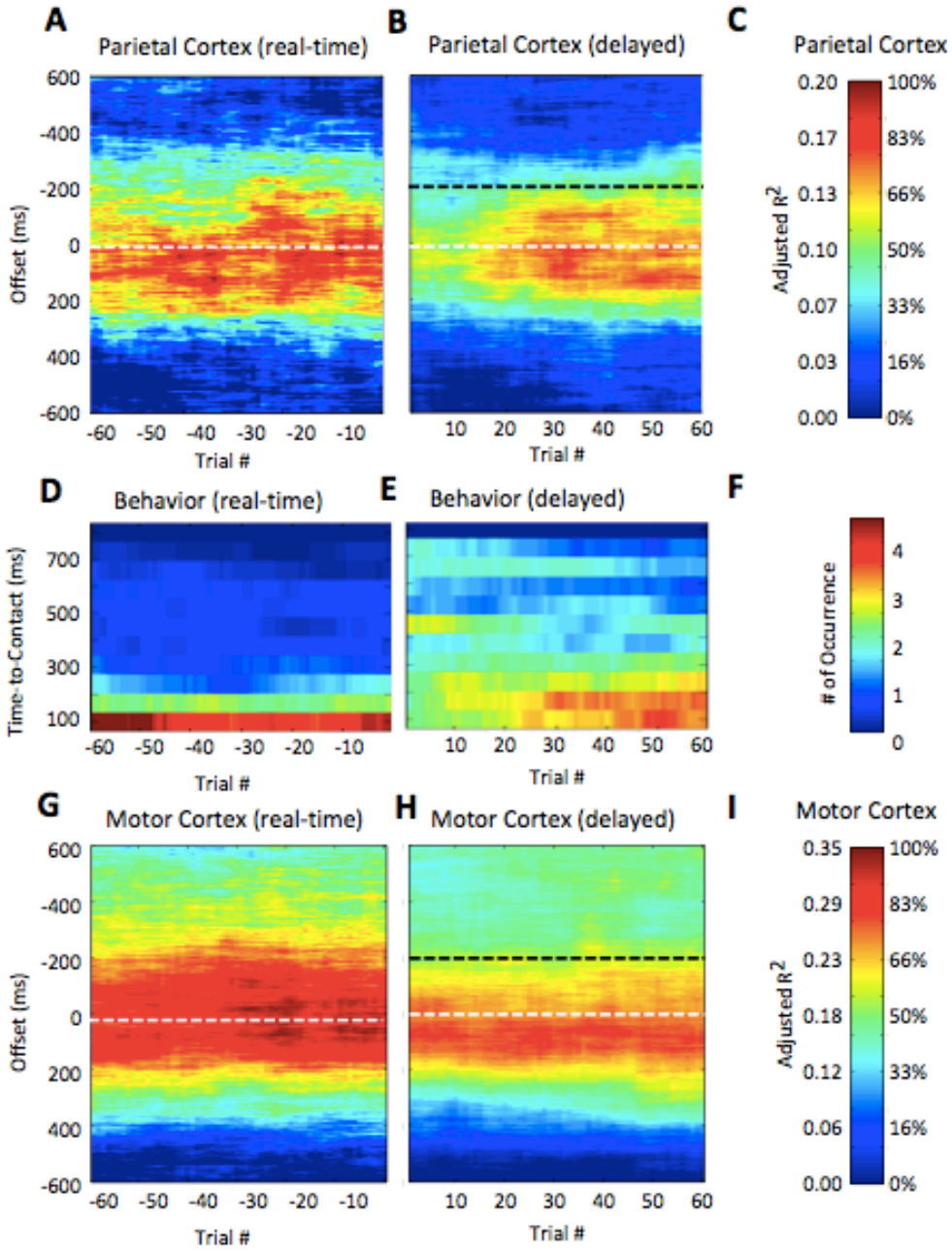

Figure 3.11: Monkey M. Offset tuning analysis of parietal neurons during A) real-time, B) delayed reaches, and the corresponding color scales. Dashed black line represents the sensory delay. C). Histogram analysis of time-to-contact values during D) real-time, E) delayed reaches, and the corresponding color scale F). Offset tuning analysis of motor neurons during G) real-time, H) delayed reaches, and the corresponding color scales I).

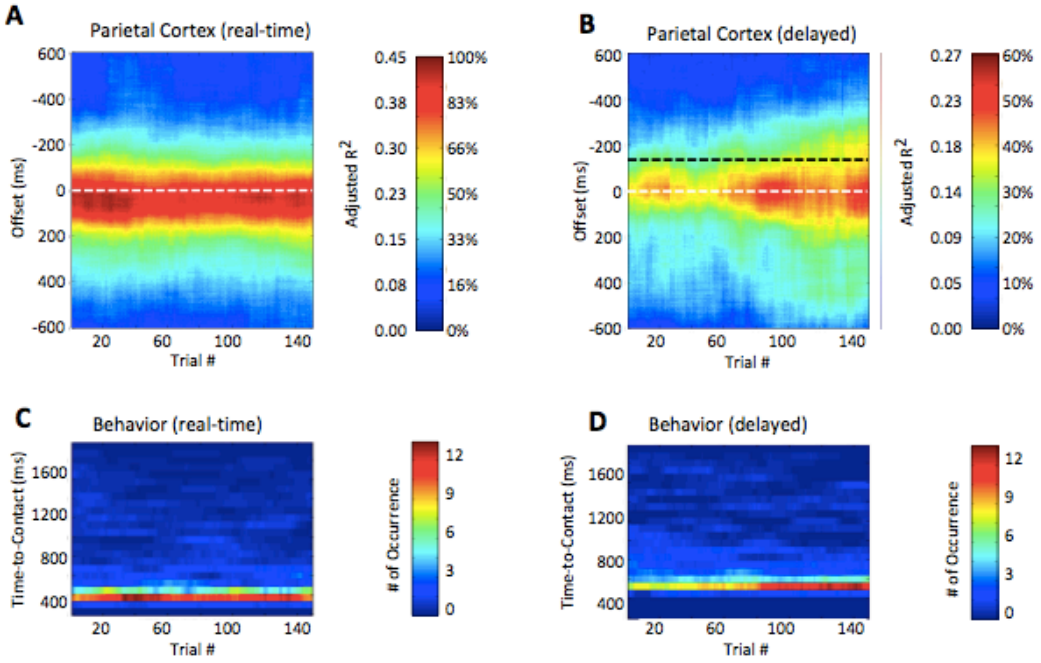

Figure 3.12: Monkey R. Offset tuning analysis of parietal neurons during A) real-time and B) delayed reaches. The dashed lack line corresponds to the sensory delay. Histogram analysis of time-to-contact values during C) real-time and D) delayed reaches

3.3.3 – Time-to-Contact

During real-time trials the animals acquired the target with quick and consistent hand movements (**Figure 3.11d, Figure 3.12c**). At the onset of the delay, reaching the target became difficult. Both animals were slower and more variable in their movements (**Figure 3.11e, Figure 3.12d)**. As the animals performed additional reaches in the delayed condition, their performance improved (25 trials monkey M, and ~80 trials monkey R). The animals were still slower than their real-time behavior, but their reaches were more consistent. This improvement in behavior occurred on the same timescale as the recovery of the predictive strength in the parietal cortex.

This gradual behavioral improvement can be seen in the trajectory of the animal's hand [**Figure 3.13a**]. At the onset of the delay, the animals attempted to produce the same movement used during the real-time reaches. As this proved difficult in completing the task [**Figure 3.13b**], the animals adjusted their path to the target. In the case of monkey M, his hand moved closer to the obstacle during the delayed reaches. It was as if during real-time reaches monkey M was focused more on avoiding the obstacle and less on acquiring the target, but that this priority switched during the delayed reaches (teaching a monkey to avoid an obstacle was the most difficult aspect of the behavioral training).

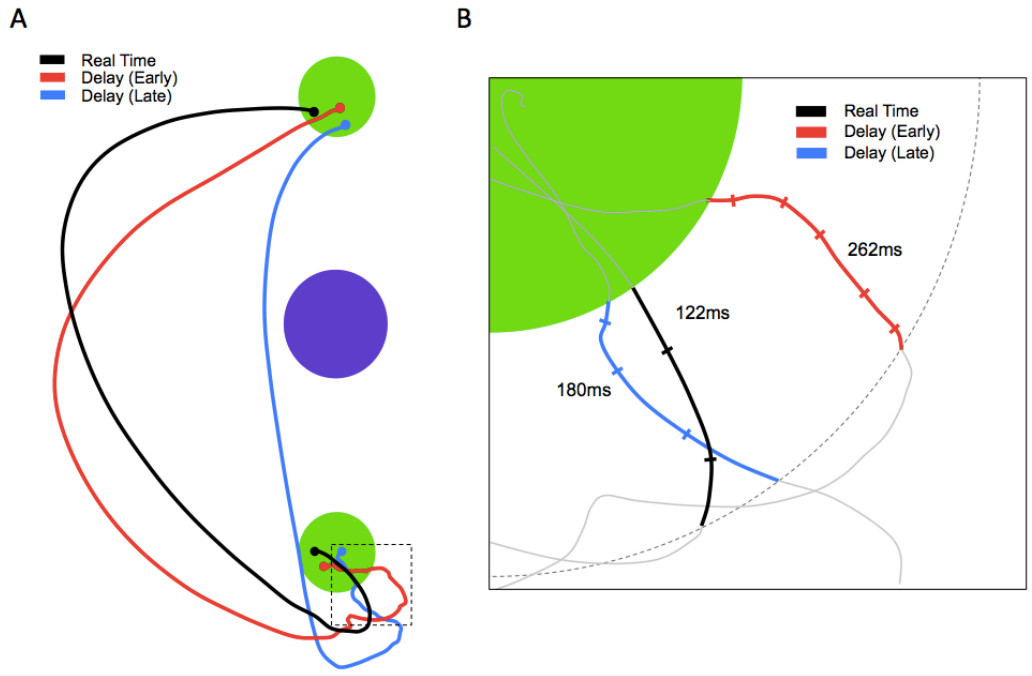

Figure 3.13: Example reaches performed by monkey M during the center-out task. Reaches began at the top (green circle), avoided the obstacle (purple), and ended at the bottom (green circle). Three typical reaches are displayed: real-time (black), early lag (red) and late lag (blue). B) Close up of bottom right corner of the target. The example reaches are displayed in grey, except when within one centimeter of the target. The dashes on each trace mark the hand position every 50 ms. Each trace is labeled with total time to complete the last centime of the reach.

3.4 – Discussion

3.4.1 – State-estimation in Parietal Cortex

The response of parietal cortex to a sensory delay presents causal evidence that the parietal cortex encodes a state-estimator. At the onset of the delay, there is a large drop in the correlation between parietal activity and hand movement. This decorrelation fits with our reasoning that the combination of old sensory information with a current efference copy will incorrectly predict the hand velocity. This effect is mirrored in the idealized version of a state-estimator. Primary motor cortex does not show this effect, and its response matches the behavior of the idealized command signal. Since primary motor cortex is well understood to drive muscle activity, the agreement between M1 and the idealized command signal was expected and supports our modeling of sensorimotor signals.

3.4.2 – Adaptation Effect

As the animals performed additional reaches with the sensory delay, the correlation between parietal activity and hand movement returned. This suggests that parietal cortex adapts to the sensory delay. This proves that parietal cortex is sensitive to, but not dominated by sensory feedback. For this adaptation to occur the parietal cortex must recognize the delay in visual feedback. Since a sensory delay does not distort the visual information, this delay can only be recognized in comparison with an unaffected signal, i.e. the efference copy. Parietal cortex could recover predictive strength by either shifting weight to the efference copy and ignoring the sensory feedback, or compensating for the delay by predicting further into the future from the delayed sensory information. Since visual feedback is necessary for the reaching tasks, the latter effect is most likely.

3.4.3 – Drop in R2 in both Parietal and Motor

During the sensory delay, both the motor cortex and the recovered parietal cortex show a slight decrease in predictive strength. While it is possible that these brain areas contain a sensory signal that is lost during the visual delay, this drop in

predictive strength could be an artifact of the coefficient of determination. The coefficient of determination depends on two quantities: the predictive strength of the neural activity (βf) and the distribution of the hand velocities (x). The animals change their behavior in response to the sensory delay; both animals slow down and make fine adjustments to acquire the target. This alters the distribution of hand velocities to include more fine hand movements.

We intentionally chose, for clarity, the simplest regression model between neural activity and movement. While linear regression successfully shows the connection between spiking activity and hand velocity, this method only captures the first-order characteristic of the relationship. Coarse arm movements may be well modeled by linear regression, while fine hand movements may require a more nuanced relationship.

In this visual delay experiment, the animals made more fine hand movement during the delayed reaches compared to real-time reaches. Therefore, the linear regression between neural activity and hand velocity is tested more often on fine hand movements during delayed reaches than in real-time reaches. This would cause the delayed condition to have a lower coefficient of determination than the real-time condition, even though the underlying relationship between neural activity and movement has not changed. This means that a behavioral change could directly account for the slight decrease in predictive strength seen in both motor and parietal cortex during the delayed reaches.

This effect cannot explain the drop and recovery of the predictive strength in the parietal cortex. Neural activity was recorded simultaneously from both motor cortex and parietal cortex in monkey M. These neural signals predicted the exact same hand movements. If the adaptation effect were simply a product of the animal's behavior, motor cortex would be equally affected.

3.4.4 – Misalignment of visual and somatosensation

The decorrelation of the parietal cortex could result from a misalignment between visual feedback and somatosensation, and not depend on the efference copy. This is unlikely because the animals performed reaches in free-space and in a virtual reality environment. The animals could not rely on tactile feedback to complete the task, making vision the dominant sensory input.

3.4.5 – Application for BMI

The adaptation of parietal cortex to a sensory delay has important implications for neural prosthetics. A spinal injury damages the axons of the corticospinal neurons that reside in primary motor cortex. Amputation studies show that the cortex undergoes massive reorganization after such an injury [58]. This means that models of cortical activity developed in the intact animal may imperfectly translate to the spinalized human. Not only is the parietal cortex further removed from the injury (and thus may undergo less reorganization), the parietal cortex can also adapt to misalignments. The parietal cortex region compensates for discrepancies between the intended movement and the resulting sensory feedback. This means the parietal cortex will work with the decoding algorithm to ensure the correct action is taken, making the parietal cortex the ideal location for implanting neural prosthetics.

3.5 – Methods

3.5.1 – General Methods

Two adult male rhesus macaques (Macaca mulatta) were used in this study. All surgical and animal care procedures were done in accordance with the National Institutes of Health Guide for the Care and Use of Laboratory Animals and were approved by the California Institute of Technology Institutional Animal Care and Use Committee. Monkey M was implanted with two electrode arrays (Utah arrays; Blackrock): one in area 5D of the posterior parietal cortex, and one in motor cortex (Appendix B). Monkey R was implanted with two electrode arrays (Floating Microelectrode Arrays; MicroProbes): both in area 5D of the posterior parietal

cortex. The implantation sites were located using anatomical MRI scans. The parietal arrays were placed medial to the postcentral dimple, abutting the intraparietal sulcus. The motor array was placed medial to the spur of the arcuate sulcus, abutting the central sulcus. Spiking activity was recorded using Plexon and Blackrock neural signal processors, and the Plexon Offline Sorter was used for spike sorting.

3.5.2 – Behavioral Task

Monkey M and monkey R performed reaches using their dominant hand in free-space with head-fixation and free-gaze. The animal's hand position was tracked using an Optotrak imaging system and was displayed as a cursor on a computer monitor (Appendix B). The animal's view of their own hand was blocked, forcing the animals to rely on the cursor for visual feedback.

3.5.2.1 - Monkey M: 2D Center-Out with Obstacle Avoidance

The horizontal components of monkey M's hand position were displayed as a cursor on a monitor mounted horizontally over the animal's workspace. The animal looked down at the monitor, and performed hand reaches in the space underneath it. Monkey M initiated a reach by guiding a cursor to a target illuminated in the center of his workspace. While holding the cursor in the center position, the animal was cued to a goal selected at random from six possible locations. These goals were placed 9 cm from the center position and arranged symmetrically in a ring. After 500 ms, the illuminated target jumped from the center position to the cued location, and the animal was allowed to make his reach [**figure 3.9a**]. A large obstacle was illuminated directly between the center and goal positions to prevent straight hand movements. If the cursor collided with this obstacle, the trial was reset, and the animal was required to recenter his hand. If the animal successfully avoided the obstacle, acquired the goal, and held the goal position for 750 ms, a liquid reward was issued.

Recording sessions were broken into three sequential phases; real-time, lag, and wash-out. The first ~300 reaches (real-time) were performed with the hand position displayed in real-time. The next ~600 reaches (lag) were performed with an artificial 200 ms lag between the animal's hand position and the cursor position. For the last ~300 reaches (wash-out) the lag was removed, and the reaches were performed in real-time [wash-out data was not analyzed]. The exact number of reaches in each phase was randomized to prevent the animal from predicting the transitions. There was no rest period between transitions.

3.5.2.2 - Monkey R: 3D Sequential Reaches

Monkey R's hand position was displayed using a 3D computer monitor and polarized shutter glasses. During the task, the animal was cued to one of 27 goal locations. These goals were arranged on a 3x3x3 grid spaced 10 cm apart. Once the animal moved the cursor to the cued location, and held the position for 300 ms, the next reach was initiated [**figure 3.9b**]. A new goal location was randomly selected from the 26 remaining positions, and the process was repeated. After eight successful reaches, a liquid reward was issued.

There were two types of recording sessions for monkey R; real-time or lag. In real-time recording sessions, all reaches were performed with the hand position displayed in real-time. In lag recording sessions, all reaches were performed with an artificial 150 ms lag between the animal's hand position and the position of the cursor. Recording sessions were randomized, to prevent the animal from predicting the type of recording session.

3.5.3 – Neural Analysis

Hand velocity was predicted from neural activity using data from a sliding window of 35 sequential trials. Both neural activity and velocity data were discretized into consecutive non-overlapping 100ms time-bins. These time-bins were extracted from each trial starting when the cursor exited the initial position and ended when

the goal was acquired. Velocity data was discretized by selecting the instantaneous velocity of the hand at the end of each time-bin. Neural activity was discretized independently for each neural unit by counting the number of spikes occurring within the time-bins. The discretized neural units (*f*) were combined to form a multivariate linear regression model of the hand velocity (*x)*.

$$x = \beta f, \qquad \beta = \frac{f^T x}{f^T f}.$$

Regression models were built independently for each axis of movement (for monkey M: x and y; for monkey R: x, y, and z). The predictive strength of the neural activity was quantified by averaging the adjusted coefficient of determination ($\bar{R}^2$) [59] across each axis of movement. The adjusted coefficient of determination describes the proportion of variance in the hand velocity that can be predicted by neural activity while accounting for both the number of neural units (*p*) and the number of time bins (*n*) used in the model:

$$\bar{R}^2 = 1 - \frac{n-1}{n-p-1} \cdot \left[1 - \frac{\sum(x_i - \beta f_i)^2}{\sum(x_i - \bar{x})^2}\right].$$

3.5.4 – Offset Tuning Curve

The timing relationship between hand velocity and neural activity was explored by shifting the window of neural activity used for the regression model. A series of timing offsets (ranging from -600 ms to 600 ms, in 1ms increments) were subtracted from the spike times of the neural data. For each offset, the shifted neural activity was rediscretized and the predictive strength was recalculated. These timing offsets force the regression model to use neural data occurring either before or after the movement (positive offsets capture neural data occurring before the movement, and negative offsets capture neural data occurring after the movement).

3.5.5 – Behavioral Analysis

The distance between the cursor and the target was calculated at 10 ms intervals during each trial. The time-to-contact value was defined as the amount of time between when the cursor first approached within one centimeter of the target and

when the cursor contacted the target. Time-to-contact values were grouped according to the sliding window of 35 trials used in the offset tuning analysis. Histograms were computed for each group by counting the number of time-to-contact values occurring within a range of intervals.

3.5.6 – Idealized Signals

Idealized motor, sensory, and state-estimator signals were generated by adding noise to the hand velocity of monkey M. The noise (σ) was drawn from a Gaussian distribution with a standard deviation set to 20% of the standard deviation of the hand velocity. These idealized signals were used to predict the velocity of the hand. Offset tuning curves were created using the same method applied to the neural activity, except the idealized signals were discretized by selecting the value at the end of each time bin. The timing offsets shifted the idealized signals backwards and forwards in time in relation to the hand velocity. Offset tuning curves were generated from the same sliding window of data used in the neural analysis.

3.6 – CITATIONS

[1] Hatsopoulos, Nicholas G., and John P. Donoghue. "The science of neural interface systems." *Annual review of neuroscience* 32 (2009): 249-266.

[2] Schwartz, Andrew B., et al. "Brain-controlled interfaces: movement restoration with neural prosthetics." *Neuron* 52.1 (2006): 205-220.

[3] Andersen, R. A., et al. "Cognitive neural prosthetics." *Trends in cognitive sciences* 8.11 (2004): 486-493.

[4] Schwartz, Andrew B. "Cortical neural prosthetics." *Annu. Rev. Neurosci.* 27 (2004): 487-507.

[5] Wu, Wei, et al. "Bayesian population decoding of motor cortical activity using a Kalman filter." *Neural computation* 18.1 (2006): 80-118.

[6] Vargas-Irwin, Carlos E., et al. "Decoding complete reach and grasp actions from local primary motor cortex populations." *Journal of neuroscience* 30.29 (2010): 9659-9669.

[7] Hochberg, Leigh R., et al. "Neuronal ensemble control of prosthetic devices by a human with tetraplegia." *Nature*442.7099 (2006): 164.

[8] Aflalo, Tyson, et al. "Decoding motor imagery from the posterior parietal cortex of a tetraplegic human." *Science*348.6237 (2015): 906-910.

[9] Collinger, Jennifer L., et al. "High-performance neuroprosthetic control by an individual with tetraplegia." *The Lancet* 381.9866 (2013): 557-564.

[10] Serruya, Mijail D., et al. "Brain-machine interface: Instant neural control of a movement signal." *Nature* 416.6877 (2002): 141.

[11] Wessberg, Johan, et al. "Real-time prediction of hand trajectory by ensembles of cortical neurons in primates." *Nature* 408.6810 (2000): 361.

[12] Mulliken, Grant H., Sam Musallam, and Richard A. Andersen. "Decoding trajectories from posterior parietal cortex ensembles." *Journal of Neuroscience* 28.48 (2008): 12913-12926.

[13] Hauschild, Markus, et al. "Cognitive signals for brain–machine interfaces in posterior parietal cortex include continuous 3D trajectory commands." *Proceedings of the National Academy of Sciences* 109.42 (2012): 17075-17080.

[14] Scherberger, Hansjörg, and Richard A. Andersen. "Target selection signals for arm reaching in the posterior parietal cortex." *Journal of Neuroscience* 27.8 (2007): 2001-2012.

[15] Scherberger, Hansjörg, Murray R. Jarvis, and Richard A. Andersen. "Cortical local field potential encodes movement intentions in the posterior parietal cortex." *Neuron* 46.2 (2005): 347-354.

[16] Musallam, Sam, et al. "Cognitive control signals for neural prosthetics." *Science* 305.5681 (2004): 258-262.

[17] Brozović, Marina, Alexander Gail, and Richard A. Andersen. "Gain mechanisms for contextually guided visuomotor transformations." *Journal of Neuroscience* 27.39 (2007): 10588-10596.

[18] Gail, Alexander, and Richard A. Andersen. "Neural dynamics in monkey parietal reach region reflect context-specific sensorimotor transformations." *Journal of Neuroscience* 26.37 (2006): 9376-9384.

[19] Cui, He, and Richard A. Andersen. "Posterior parietal cortex encodes autonomously selected motor plans." *Neuron* 56.3 (2007): 552-559.

[20] Baldauf, Daniel, He Cui, and Richard A. Andersen. "The posterior parietal cortex encodes in parallel both goals for double-reach sequences." *Journal of Neuroscience* 28.40 (2008): 10081-10089.

[21] Hwang, Eun Jung, and Richard A. Andersen. "Brain control of movement execution onset using local field potentials in posterior parietal cortex." *Journal of Neuroscience* 29.45 (2009): 14363-14370.

[22] Yu, Byron M., et al. "Mixture of trajectory models for neural decoding of goal-directed movements." *Journal of neurophysiology* 97.5 (2007): 3763-3780.

[23] Desmurget, Michel, and Scott Grafton. "Forward modeling allows feedback control for fast reaching movements." *Trends in cognitive sciences* 4.11 (2000): 423-431.

[24] Jordan, Michael I., and David E. Rumelhart. "Forward models: Supervised learning with a distal teacher." *Cognitive science*16.3 (1992): 307-354.

[25] Wolpert, Daniel M., Zoubin Ghahramani, and Michael I. Jordan. "An internal model for sensorimotor integration." *Science* 269.5232 (1995): 1880-1882.

[26] Goodwin, Graham C., and Kwai Sang Sin. *Adaptive filtering prediction and control*. Courier Corporation, 2014.

[27] Mountcastle, Vernon B., et al. "Posterior parietal association cortex of the monkey: command functions for operations within extrapersonal space." *Journal of neurophysiology* 38.4 (1975): 871-908.

[28] Press, Critchley M. Hafner. "New York, NY: 1953." *The parietal lobes*.

[29] Haaxma, R., and H. G. Kuypers. "Intrahemispheric cortical connexions and visual guidance of hand and finger movements in the rhusus monkey." *Brain* 98.2 (1975): 239-260.

[30] Mishkin, Mortimer, Leslie G. Ungerleider, and Kathleen A. Macko. "Object vision and spatial vision: two cortical pathways." *Trends in neurosciences* 6 (1983): 414-417.

[31] Goodale, Melvyn A., and G. Keith Humphrey. "The objects of action and perception." *Cognition* 67.1-2 (1998): 181-207.

[32] Andersen, Richard A., et al. "Multimodal representation of space in the posterior parietal cortex and its use in planning movements." *Annual review of neuroscience* 20.1 (1997): 303-330.

[33] Andersen, Richard A., and Christopher A. Buneo. "Intentional maps in posterior parietal cortex." *Annual review of neuroscience* 25.1 (2002): 189-220.

[34] Culham, Jody C., Cristiana Cavina-Pratesi, and Anthony Singhal. "The role of parietal cortex in visuomotor control: what have we learned from neuroimaging?." *Neuropsychologia* 44.13 (2006): 2668-2684.

[35] Shadmehr, Reza, and John W. Krakauer. "A computational neuroanatomy for motor control." *Experimental brain research*185.3 (2008): 359-381.

[36] Sirigu, Angela, et al. "Perception of self-generated movement following left parietal lesion." *Brain* 122.10 (1999): 1867-1874.

[37] Pisella, L., et al. "An ‘automatic pilot’for the hand in human posterior parietal cortex: toward reinterpreting optic ataxia." *Nature neuroscience* 3.7 (2000): 729.

[38] Desmurget, M., et al. "Role of the posterior parietal cortex in updating reaching movements to a visual target." *Nature neuroscience* 2.6 (1999): 563.

[39] Gréa, Hélène, et al. "A lesion of the posterior parietal cortex disrupts on-line adjustments during aiming movements." *Neuropsychologia* 40.13 (2002): 2471-2480.

[40] Andersen, Richard A., et al. "Optic ataxia: from Balint's syndrome to the parietal reach region." *Neuron* 81.5 (2014): 967-983.

[41] Perenin, M-T., and A. Vighetto. "Optic ataxia: A specific disruption in visuomotor mechanisms: I. Different aspects of the deficit in reaching for objects." *Brain* 111.3 (1988): 643-674.

[42] Allison, R. S., et al. "A follow-up study of a patient with Balint's syndrome." *Neuropsychologia* 7.4 (1969): 319-333.

[43] Cogan, David G. "Ophthalmic manifestations of bilateral non-occipital cerebral lesions." *The British journal of ophthalmology* 49.6 (1965): 281.

[44] Rossi, Simone, et al. "Safety, ethical considerations, and application guidelines for the use of transcranial magnetic stimulation in clinical practice and research." *Clinical neurophysiology* 120.12 (2009): 2008-2039.

[45] MacDonald, Penny A., and Tomáš Paus. "The role of parietal cortex in awareness of self-generated movements: a transcranial magnetic stimulation study." *Cerebral Cortex* 13.9 (2003): 962-967.

[46] Della-Maggiore, Valeria, et al. "Stimulation of the posterior parietal cortex interferes with arm trajectory adjustments during the learning of new dynamics." *Journal of Neuroscience* 24.44 (2004): 9971-9976.

[47] Council for International Organizations of Medical Sciences. "International ethical guidelines for biomedical research involving human subjects." *Bulletin of medical ethics* 182 (2002): 17.

[48] Niedermeyer, Ernst, and FH Lopes da Silva, eds. *Electroencephalography: basic principles, clinical applications, and related fields*. Lippincott Williams & Wilkins, 2005.

[49] Huettel, Scott A., Allen W. Song, and Gregory McCarthy. *Functional magnetic resonance imaging*. Vol. 1. Sunderland: Sinauer Associates, 2004.

[50] Wassermann, Eric M. "Risk and safety of repetitive transcranial magnetic stimulation: report and suggested guidelines from the International Workshop on the Safety of Repetitive Transcranial Magnetic Stimulation, June 5–7, 1996." *Electroencephalography and Clinical Neurophysiology/Evoked Potentials Section* 108.1 (1998): 1-16.

[51] Grinvald, Amiram, and Rina Hildesheim. "VSDI: a new era in functional imaging of cortical dynamics." *Nature Reviews Neuroscience* 5.11 (2004): 874.

[52] Van Gerven, Marcel, et al. "The brain–computer interface cycle." *Journal of neural engineering* 6.4 (2009): 041001.

[53] Rutishauser, Ueli, et al. "Human memory strength is predicted by theta-frequency phase-locking of single neurons." *Nature* 464.7290 (2010): 903.

[54] Lachaux, Jean-Philippe, et al. "Measuring phase synchrony in brain signals." *Human brain mapping* 8.4 (1999): 194-208.

[55] Hwang, Eun Jung, et al. "Inactivation of the parietal reach region causes optic ataxia, impairing reaches but not saccades." *Neuron* 76.5 (2012): 1021-1029.

[56] Mulliken, Grant H., Sam Musallam, and Richard A. Andersen. "Forward estimation of movement state in posterior parietal cortex." *Proceedings of the National Academy of Sciences*105.24 (2008): 8170-8177.

[57] Mulliken, G. H., and R. A. Andersen. "Forward models and state estimation in posterior parietal cortex." *The cognitive neurosciences IV* (2009): 599-611.

[58] Sanes, Jerome N., et al. "Rapid reorganization of adult rat motor cortex somatic representation patterns after motor nerve injury." *Proceedings of the National Academy of Sciences* 85.6 (1988): 2003-2007.

[59] Montgomery, Douglas C., Elizabeth A. Peck, and G. Geoffrey Vining. *Introduction to linear regression analysis*. Vol. 821. John Wiley & Sons, 2012.

[60] Evarts, EDWAHD V. "Pyramidal tract activity associated with a conditioned hand movement in the monkey." *Journal of Neurophysiology* 29.6 (1966): 1011-1027.

RECOVERY OF VOLUNTARY MOVEMENT AFTER SPINAL INJURY

The Spinal Cord

4.1 – Background

4.1.1 – History of the Spinal Injury

The clinical treatment of spinal cord injury has dramatically improved over the pass 70 years [1]. Until relatively recently, spinal cord injuries were life threatening. In the 1930's there was an 80% mortality rate within the first 2 years of injury [2]. The outlook was so bleak that in 1945 General George S Patton refused medical treatment after suffering a spinal injury from a car accident, and he died 13 days later [3]. The main cause of death was sepsis, typically resulting from complications in the urinary system (75% of deaths prior to 1969 were caused by renal failure or urinary tract infection) [4]. Thankfully, this is no longer the case. Methods have since been developed for treating the bladder and other issues associated with the injury [5], and patients can now expect to live well into their sixties [6].

In addition to managing the secondary complications that arise from spinal injury, effort has focused on engaging neurons in the spinal cord as a treatment for paralysis. Intensive rehabilitation using body weight harnesses and treadmills has demonstrated marked improvement in the balance, weight bearing, and gait of paralyzed patients [7,8,9,10]. These treatments force sensory feedback into the spinal cord, which reinvigorates neural circuits damaged by the injury. Until recently, recovery from this rehabilitation had been limited to patients with incomplete spinal injuries [11,12]. A new approach (spinal stimulation) improves upon this treatment by directly activating the neurons in the spinal cord with

electrical stimulation [13]. This treatment has enabled paraplegic patients with clinically complete spinal injuries to regain weight bearing while standing, and even limited voluntary movement [14,15,16]. While this new treatment holds incredible promise for patients suffering from spinal injury, aspects of the treatment are yet to be fully understood. In particular, how are these motor complete patients regaining voluntary movement, and how can this recovery be improved?

4.1.2 – Reflex Circuits

Spinal stimulation can trace its origins back to the study of reflex circuits conducted over a hundred years ago [17,18]. Reflex circuits are local connections of neurons in the spinal cord that process sensory information and produce movement without input from the brain. An example of a reflex circuit is seen in the patellar tendon test used commonly by doctors. A tap of a hammer on the knee stretches a muscle spindle in the quadriceps, which sends a sensory signal into the spinal cord. This sensory signal directly activates the motor neuron innervating the quadriceps, causing the patient to kick. This occurs locally in the spinal cord without input from the brain, and is used by doctors to judge the neurological health of a patient. These reflex circuits were initially thought to form the basis of walking. A chain of these circuits could monitor sensory feedback from the body and activate the muscles accordingly to stabilize movement [19].

4.1.3 – Central Pattern Generation

Experiments soon proved that not even sensory input (a key component of the reflex circuit) was needed to generate complex muscle activity. In 1911, Brown demonstrated this fact in the spinalized cat by severing the afferent neurons that provide sensory feedback [20]. Despite a complete lack of input from the brain or sensory information from the limbs, the cat produced rhythmic leg movements, similar to walking [**Fig 4.1**]. This proved the existence of a neural circuit in the spinal cord that can self generate stepping-like behavior. Movement therefore is not simply a response to external stimuli, but is internally generated. The neurons

responsible for this oscillatory leg movement became known as the ‘central pattern generator’ [21,22]. Since its discovery in the cat, these oscillatory neural circuits have been found across the animal kingdom in examples such as locusts [23], lamprey [24], tadpoles [25], salamanders [26], and rats [27]. Evidence also suggests that central pattern generators exist in nonhuman primates [28] and humans [29,30,31]. These oscillating neural circuits are thought to form the basis of rhythmic movements like walking, swimming, and flying [32].

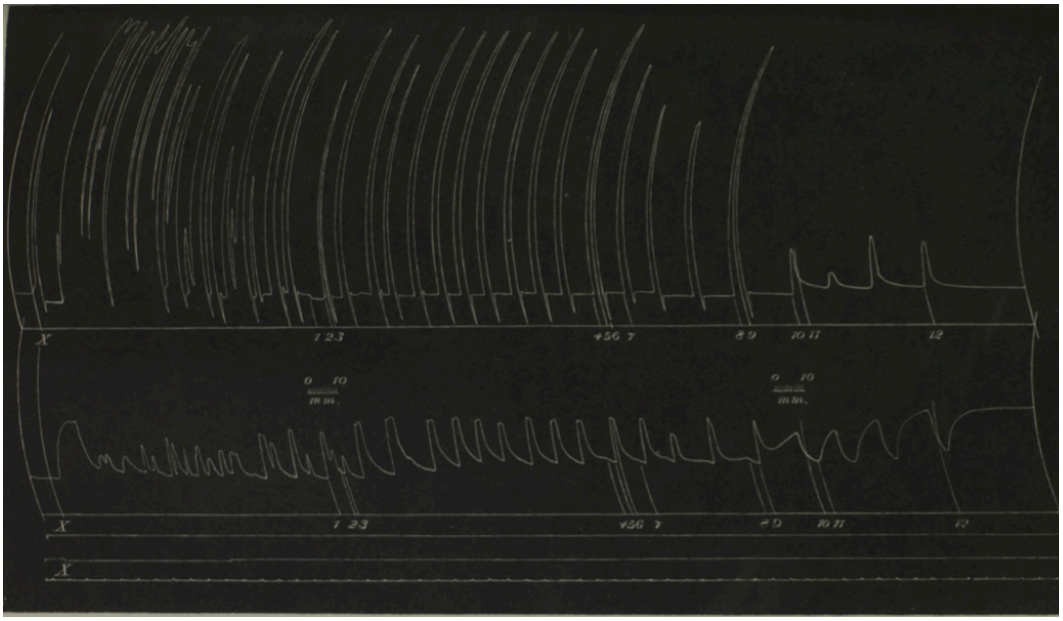

Figure 4.1: Oscillating muscle activity generated by a spinalized and deafferented cat. This leg movement occurred without input from the brain or sensory feedback. [20]

4.1.4 – Distributed Control / Automaticity

The existence of the central pattern generator is proof that motor control is distributed across the nervous system. While the cortex is critical in generating voluntary movement, neural circuits in the spinal cord are responsible for much of our muscle coordination. This ‘automaticity’ in the spinal circuitry means that basic movements like standing and walking on flat ground are controlled locally in the spinal cord and do not require much input from the brain [33]. These spinal circuits play an important role in controlling natural movement [34,35], but quickly enter

into a nonfunctional state after a spinal injury (Figure 4.1 shows that the oscillating leg movement in the spinalized cat stops within seconds after injury). It therefore became an obvious goal to reengage these spinal circuits as a treatment for paralysis, which would assist in movements that do not require brain input, such as stabilizing posture and bearing weight during standing.

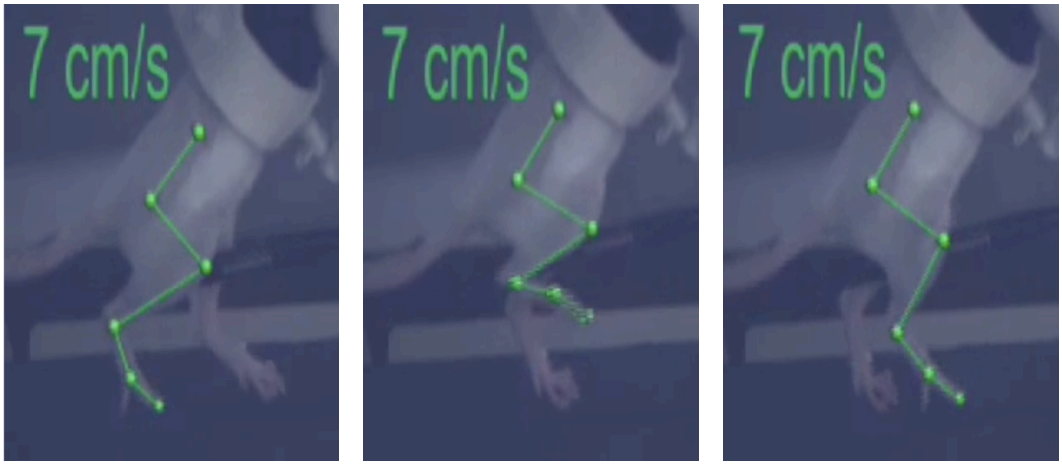

Figure 4.2: Example stepping behavior performed by a spinalized rat receiving 40-Hz stimulation across its lumbosacral enlargement (L1/S2 spinal levels). [46]

4.1.5 – Reactivation Of The Spinal Circuitry

Early attempts to reengage the central pattern generator in spinalized animals used pharmacological agents, such as L-dopa [36,37], strychnine [38], clonidine [39], Ap5 [40], and quipazine [41,42]. These drugs were used to selectively activate or inhibit specific types of neurons in the spinal cord. The careful combination of these drugs could reactivate the central pattern generator and produced fictive stepping movement from the hindlimbs of spinalized cats and rodents. In addition to pharmacology, electrical stimulation has also been used to trigger this stepping behavior. Early approaches involved decerebrated cats [43]. This injury destroys the input from the cerebral cortex, but preserves the connection between the spinal cord and the brainstem. Low electrical stimulation in the brainstem of decerebrated cats, at a rhythmic 20 Hz, could elicit walking, and increasing the stimulation

would evoke galloping or trotting behavior [44]. It was eventually found that targeting the electrical stimulation to the lower spinal cord (across the lumbosacral enlargement) could also produced stepping behavior in rodents that had suffered a mid-thoracic spinal injury [45,46]. These rodents could perform robust stepping behavior on a treadmill while bearing their own body weight [**Fig 4.2**].

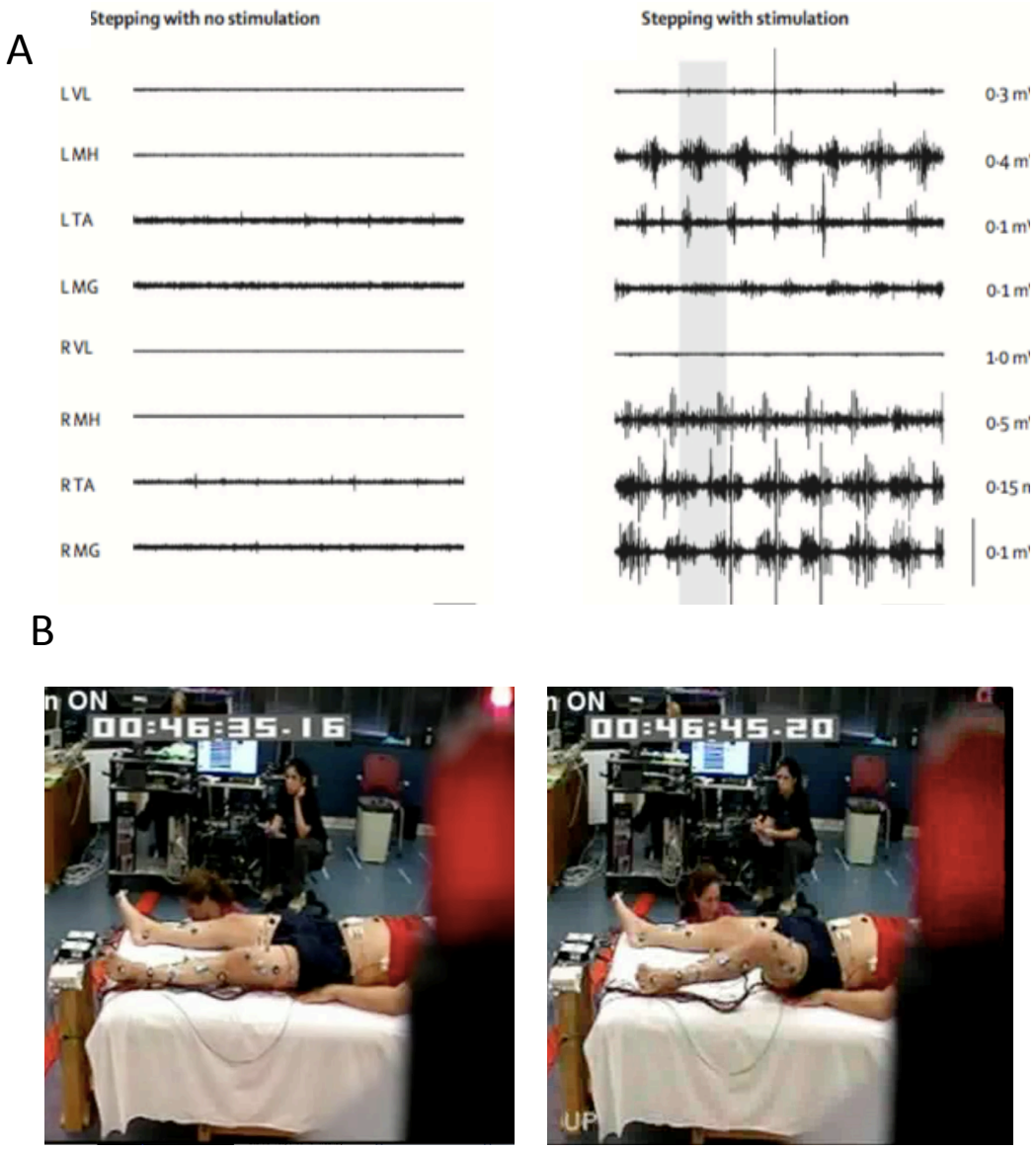

Figure 4.3: A) Example EMG activity of a paraplegic patient during step training with epidural stimulation turned off (left) or on (right). Epidural stimulation evokes clear alternating muscle activity in paraplegic humans. B) Example of paraplegic patient lifting his leg while receiving epidural stimulation. [14]

4.1.6 – Human Clinical Trials

The success of these animal experiments led to human clinical trials. Paraplegic patients were implanted with an array of stimulating electrodes over their lumbosacral enlargement, in the epidural space between their vertebra and spinal cord [14,15]. By carefully selecting the stimulation patterns, the patients were able to achieve full weight bearing during standing and locomotor-like stepping behavior [**Fig 4.3a,b**]. Remarkably, these patients also regained voluntary movement [16]. The patients could lift their leg [**Fig 4.3c**], flex their ankle, or wiggle their toe, but only when receiving spinal stimulation. This recovery demonstrates that stimulation of the lumbosacral enlargement enables communication to cross a patient's injury site. This effect has since been repeated in patients using noninvasive transcutaneous electrodes [15].

4.1.7 – 'Discomplete' Spinal Injury

The recovery of voluntary movement was surprising. The foundational research had been conducted in animals with completely transected spinal cords, where recovery was not possible. In fact, during surgery, a piece of gel foam was commonly inserted into the injury site to block any potential regrowth [47]. The first patient in the clinical trials was intentionally selected because he had been diagnosed with a complete spinal injury (ASIA A, no motor control and no sensory feedback). Researchers could therefore trust that any movement resulting from the treatment was generated locally by his spinal circuitry. There was no expectation that the patient would regain voluntary leg movement.

It turns out that spinal injuries in humans are rarely complete transections. Postmortem analysis shows that neural pathways commonly survive even in the most severe cases [48]. This results in a 'discomplete' injury [49], which presents clinically as a motor complete spinal injury, but maintains a dormant subset of supraspinal connections. The recovery of voluntary movement is proof that spinal stimulation can transform these dormant connections into functional pathways.

4.1.8 – Alternative Injury Models

To understand the mechanism enabling the recovery of voluntary movement, spinal stimulation must be studied in injury models that replicate the discomplete nature of human spinal injuries. An example of such an injury is the contusion [50,51,52]. In this injury, the spinal cord of an animal is exposed and a blunt force is applied using a small piston. Adjusting the force applied by the piston controls the severity of the injury. While this technique replicates the blunt force trauma typically experienced in humans, there can be variability in the resulting injury and there is lack of control over which neural pathways are damaged.

A more precise injury model is the staggered double hemisection [53]. In this injury, a lateral incision is made halfway across the spinal cord at one spinal level and a second lateral incision is made halfway across the spinal cord on the opposite side at a different spinal level. This injury severs all direct projections from the brain, and results in paralysis [**Fig. 4.4a**]. Yet, this injury leaves a tract of healthy tissue in between the two incisions that has the potential to reorganize into a functioning pathway [54]. This potential for reorganization was observed by inducing the hemisections in two separate surgeries [55]. After the first hemisection, the animal is initially paralyzed on the ipsilateral side of the incision, but over time spontaneously regains control of their paralyzed limb. This recovery is mediated by propriospinal neurons that reorganize locally around the injury site [55]. When this recovered animal receives the second hemisection, they again become paralyzed (this time in both legs), and again spontaneously recover [**Fig 4.4b**].

This proves that the tissue between the staggered hemisections can form a functional pathway to and from the brain. The same tract of tissue survives after the simultaneous injury, but the animal is permanently paralyzed, which fits the definition of discomplete. We therefore chose to use the simultaneous double

hemisection to study the effect of spinal stimulation on the recovery of voluntary movement.

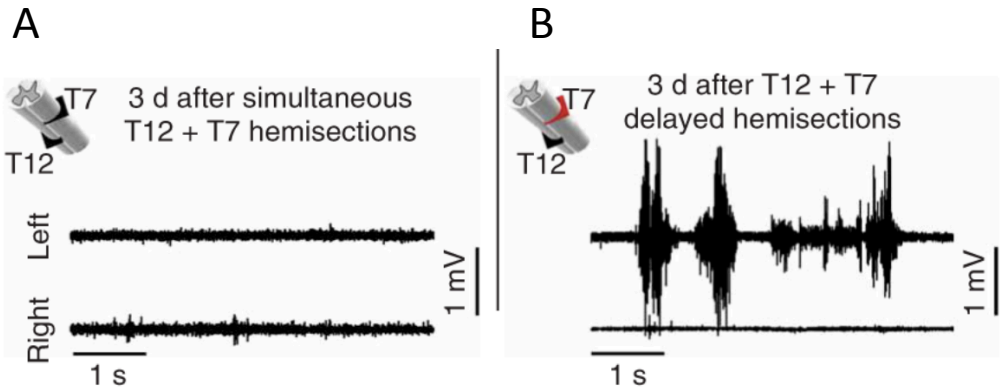

Figure 4.4: EMG recordings from the tibialis anterior muscles after b) simultaneous double hemisection or b) delayed double hemisections. Animals that received delayed hemisections recovered activity in their hindlimb muscle, while animals that received a simultaneous double hemisection did not. [55]

4.1.9 – Behavioral Task

In addition to a discomplete injury model, a new behavioral task is needed to study the recovery of voluntary movement. Traditional behaviors studied with spinal stimulation involve complex movements such as treadmill stepping. A previous attempt to model the recovery of voluntary movement involved a complex locomotor task requiring a rodent to modulate walking gaits while climbing stairs [56]. In this task, it is unclear what aspect of muscle activity is due to supraspinal control and what is generated locally at the spinal cord. It is also unclear when and how the brain is interacting with the spinal circuitry.

The ideal task is simple, discrete, stereotyped, repeatable, and locked to an external stimulus. By coupling the animal's behavior to an external stimulus, event-related techniques [57] can be leveraged to study how neural signals throughout the nervous system are involved in recovery. With this in mind, we developed a simplified behavioral task in the rodent. Rodents were trained to kick their right hindlimb in response to an auditory cue. This behavior was trained in their uninjured state, and their response was studied after a simultaneous double

hemisection. The purpose of this initial work is to (a) characterize this simple behavioral task and (b) use the task to explore the voluntary control recovery mechanism.

4.2 – Recovery of Voluntary Movement in the Rodent

4.2.1 – Beep-kick Task

Rodents (adult; female; Sprague-Dawley rats; 250-300g) were trained to kick their right hindlimb in response to an auditory cue (3 kHz tone; 250 ms duration) (**Fig 4.5**). Correct responses were reinforced with a food reward. Typical sessions lasted between 15-30 minutes, and contained ~100 trials. The timing of the beep was randomized to prevent the rodent from predicting the trial onset. During the task, the rodent was secured via a harness onto a mount suspended over the lap of the experimenter. The rodent's hindlimbs hung unrestricted in free space. A computer speaker was placed near the mount, and the auditory cue was played at a comfortable volume.

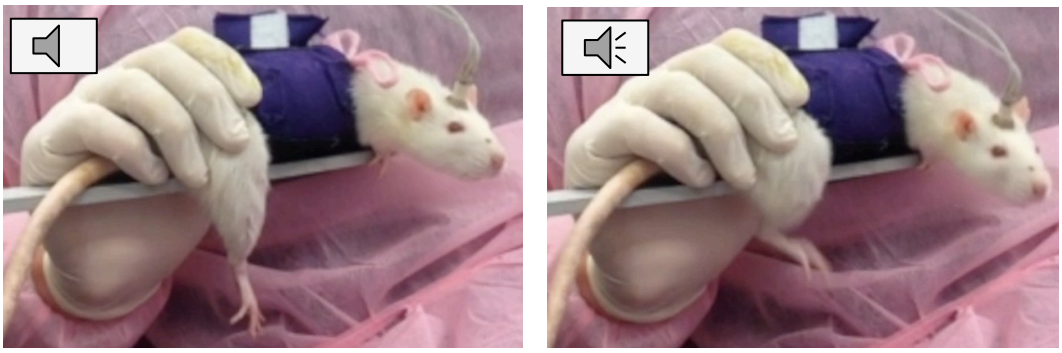

Figure 4.5: Example behavior during the beep-kick task from an uninjured rodent. The animal lifts their leg in response to an auditory cue.

4.2.1.1 – Treated Rodents

Six rodents were implanted with EMG recording electrodes in the hindlimbs and epidural stimulating electrodes over the L1/S2 spinal levels. After implantation, the rodents were trained on the beep-kick task for one month to engrain the behavior

and to collect pre-injury data. These pre-injury sessions served as a baseline of the natural connection between the brain and the spinal cord, and were performed without spinal stimulation. The rodents then received a simultaneous spinal double hemisection (left T7, right T10) (**Fig 4.6**). After injury, the rodents received therapy consisting of multi-hour stimulation sessions, followed by treadmill step training. One month after injury, the treadmill step training was replaced with the beep-kick task. Two months after injury, the multi-hour stimulations were stopped, and the rodents were only stimulated during the beep-kick task. Beep-kick sessions were recorded both with and without spinal stimulation after injury. Four months after injury, the rodents were euthanized and their spinal tissue was collected for histology.

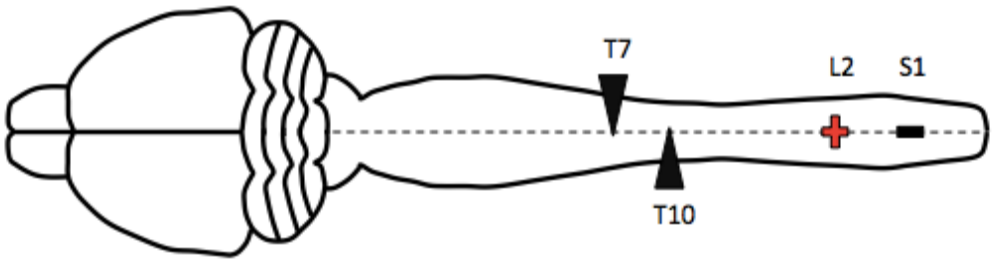

Figure 4.6: Schematic displaying the placement of the mid-thoracic spinal injury and the epidural electrode.

4.2.1.2 – Untreated Rodents

Two additional rodents received the same surgery and training as the treated animals, but were never spinally stimulated. Three months after injury, the control rodents were retrained on the beep-kick task. This training was attempted for five days, and was done to ensure the control rodents had not forgot the task.

4.2.1.3 – Untrained Rodents

Two additional rodents received the same surgery as the treated animals, but were not trained on the beep-kick task. Instead, they were exposed to 'sham' sessions, where the beep triggered a reward regardless of behavior. These sessions were

recorded before and after the spinal injury. The post-injury 'sham' sessions were conducted with spinal stimulation.

4.2.1.4 – Incomplete Injury Rodents

Two rodents recovered walking and weight bearing within days of the spinalization injury. These animals could perform the beep-kick task without spinal stimulation. These animals were not included in the treated group, but their post-injury behavior was recorded and their spinal tissue was preserved for histological analysis.

4.2.2 – Novel Sessions and Startle Sessions

Control experiments were conducted to ensure that the behavior was not a reflex to the auditory stimulus. These tests were conducted with the treated group of rodents in the same experimental setup. In *novel sessions*, the auditory cue was replaced with a sound the animals had not heard before (chirp; 500Hz ->1kHz frequency sweep; 250 ms duration) played at the same volume. In *startle sessions*, the cue was replaced with a burst of noise (white noise; 250 ms duration) played at a much louder volume (85 dB). These experiments were conducted after the injury, and the rodents were not rewarded.

4.2.3 – On/Off Stimulation

Spinal stimulation was toggled on an off in a subset of beep-kick sessions performed by the treated group. The toggling of the stimulation occurred randomly to prevent the animals from predicting the transitions.

4.2.4 – Pharmacology (Quipazine & Strychnine)

The neural pathways involved in the post-injury behavior were explored using quipazine (nonspecific $5HT_2$ agonist) and strychnine (glycine antagonist). These drugs are known to improve stepping and standing in spinalized animals, and the dosages were based off prior studies [38,58]. The treated rodents were injected intraperitoneally with either quipazine (0.2-0.35 mg/kg) or strychnine (0.2 mg/kg).

The drugs were given ten minutes to take effect, after which the rodents performed the beep-kick task with spinal stimulation. Injections were spaced 48 hours apart, with each rodent performing multiple quipazine sessions and multiple strychnine sessions. The drugs were never mixed. The stepping benefits of quipazine were quantified using treadmill step testing. Additional beep-kick sessions with quipazine were conducted in rodents before injury.

4.2.5 – Histology

The severity of the simultaneous double hemisections was confirmed in postmortem analysis. The injury sites were sliced along the horizontal plane to capture both hemisections, and an astrocyte stain was used to delineate the borders of each injury and the midline of the spinal cord. These regions were manually identified across multiple sections in the spinal cord (space 200 microns apart) and were compiled to form a 3D model of the injury.

The lumbar region of each animal was cut in coronal sections and stained for the neural activity marker c-fos. This marker is expressed in neurons after a period of increased activity. Prior to euthanasia, the rodents performed the beep-kick task for 45 minutes, after which they were returned to their home cage (see methods). The rodents were perfused one hour later, which allowed the neurons to express the c-fos protein. During post-mortem analysis, c-fos was colocalized with a stain for neuron cell bodies (NeuN) to identify active neurons in the lumbar region. This was performed using a custom semi-automated image processing method.

In a subset of animals, the motor pools innervating the trained hindlimb were identified by a percutaneous injection of a cholera toxin B tracer (CT-B) into the tibialis anterior muscle. This tracer is absorbed by the axons of the motor neurons in the muscle and transported to their cell bodies, which are located in the spinal cord. This tracer served as a guide to locate the motor pools involved in the recovered behavior.

4.3 – Results

4.3.1 – Beep-kick Task

Before injury, the rodents demonstrated a clear behavioral response to the auditory cue. Burst of EMG activity from the tibialis anterior (TA) of the trained hindlimb closely aligned with the onset of the beep (**Fig 4.7a**). The behavioral response of the uninjured animal can also be seen in video recordings of the task (**sup video1**). Two months after the spinal injury, the treated animals could again perform the beep-kick task, but only when receiving spinal stimulation. Bursting activity from the trained TA muscle aligned with the auditory cue during spinal stimulation, but the response of the injured animal was slower and more variable (**Fig 4.7b**). This effect is also seen in the video recordings of the task (**sup video2**). Without stimulation, the spinalized rodent failed to generate any significant EMG activity (**Fig 4.7c**).

The behavioral response was compared before and after injury by computing histograms of the timing of bursting activity in the TA muscle (**Fig 4.8**). These histograms show that bursting activity from the TA muscle did not occur randomly, but aligned to the auditory cue both before injury and after (Pearson Chi-Squared, $p < 10^{-10}$ across all animals and condition). Before injury, the animals had a fast and consistent response to the cue, with an average median response occurring 652 milliseconds after the cue. After injury, the animals had a slower and more variable response, with an average median response occurring 1768 milliseconds after the cue.

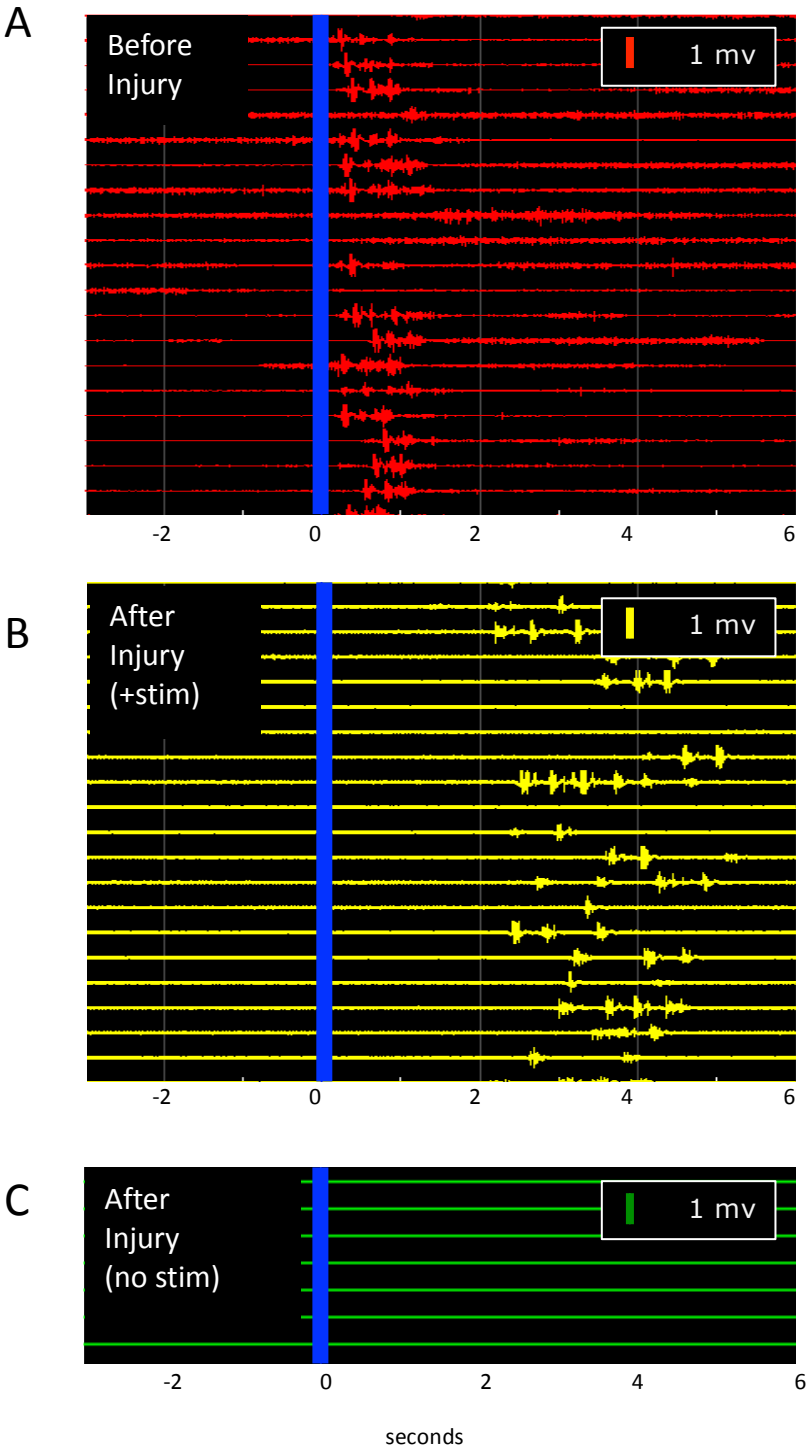

Figure 4.7: Raster plots of EMG activity from the tibialis anterior muscle (TA) of the trained hindlimb from a single rodent A) before injury, B) after injury with spinal stimulation, and C) after injury without spinal stimulation. EMG activity was segmented 3 seconds before the auditory cue, and 6 seconds after. Raster plots show EMG activity taken from consecutive beep-kick trials.

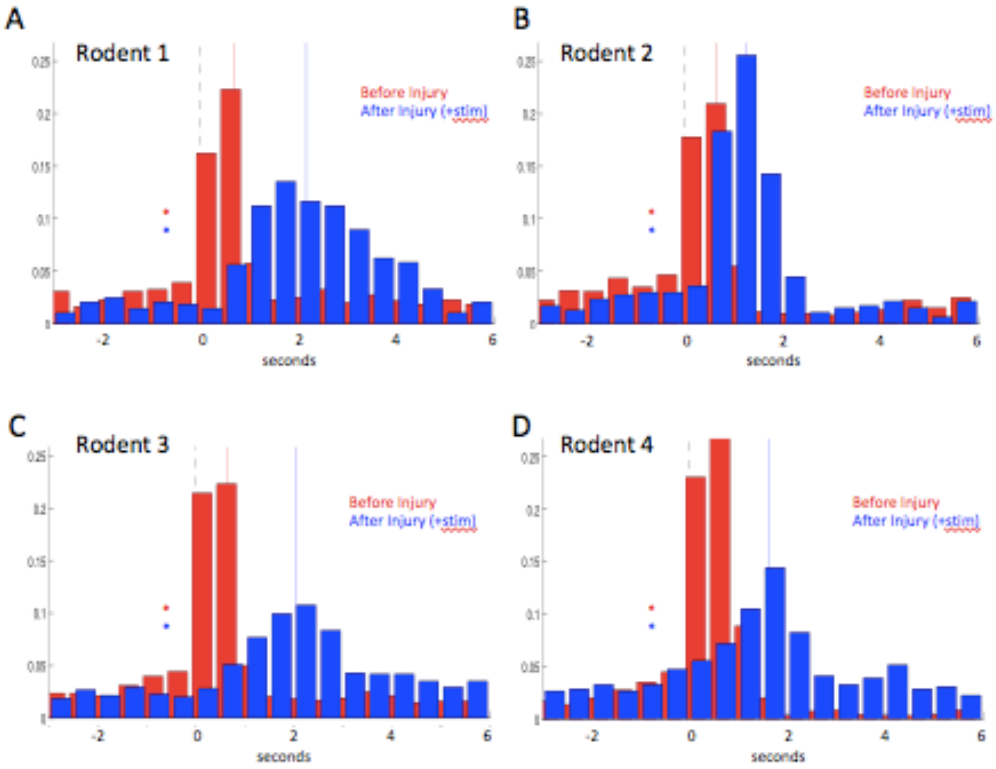

Figure 4.8: Histograms of the onset of TA bursting activity compared before injury and after injury (with stimulation). In both conditions across all four rodents, the distribution of onset times was significantly different than random (Pearson Chi-Squared, $p < 10^{-10}$). A) Rodent 1: Before Injury - 1232 burst over 325 trials (median response 0.70 seconds) , After Injury - 480 burst over 307 trials (median response 2.16 seconds), B) Rodent 2: Before Injury - 1203 bursts over 273 trials (median response 0.62 seconds) After Injury - 469 burst over 208 trials (median response 1.24 seconds), C) Rodent 3: Before Injury - 1359 bursts over 325 trials (median response 0.64 seconds), After Injury - 744 bursts over 142 (median response 2.03 seconds), D) Rodent 4: Before Injury - 938 bursts over 269 trials (median response 0.65 seconds), After Injury - 485 burst over 199 trials (median response 1.64 seconds)

The untreated rodents showed a clear behavioral response before injury, but failed to recover after spinalization (**Fig 4.9a,b**). The untrained animals failed to produce muscle activity in response to the auditory cue both before and after injury (**Fig 4.9c,d**). The incomplete injury rodents showed a clear response to the auditory cue before and after injury, both without spinal stimulation. The incomplete injury

rodents showed a similar delayed and variable response as seen in the treated group (**Fig 4.9e,f**).

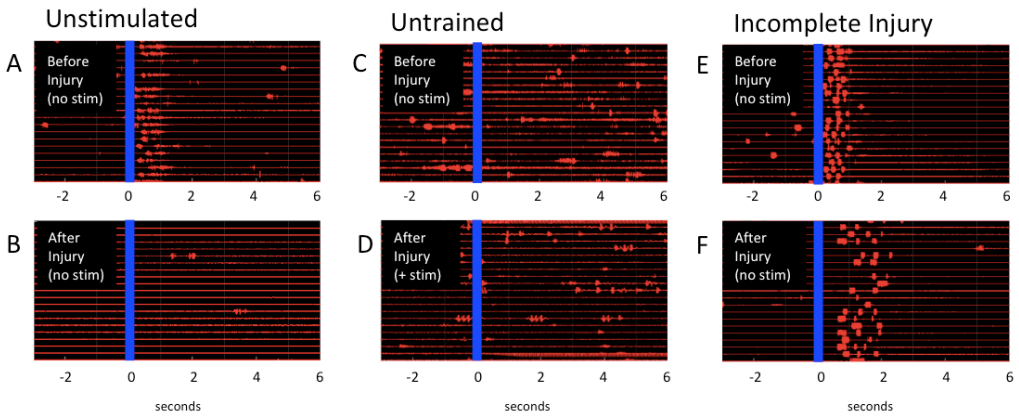

Figure 4.9: Raster plots of the trained TA muscle of the untreated rodent group [A: before injury, B: after injury], the untrained rodent group [C: before injury, D: after injury], and the incomplete injury group [E: before injury, FL after injury].

4.3.2 – Muscle Response Before and After Injury

Before injury, the treated rodents generated a clear and unilateral response in their trained limb (**sup video1**). After injury, these spinalized rodents produced a weaker and bilateral response in both hindlimbs, similar to fictive stepping (**sup video2**). Changes in muscle activity were studied by cross-correlating the EMG power between the muscle groups (see methods). Before injury, the rodents showed weak correlation between their trained and untrained TA muscles. After injury, there is a peak in correlation occurring at a 300ms offset between these muscle groups (**Fig 4.10a**). This means that a burst of activity in the trained TA was followed 300 ms later by a burst in the untrained TA. Cross correlation was also performed between the TA and vastus lateralis muscle (VL) in the trained hindlimb, which showed a similar increase in correlation after injury (**Fig 4.10b**).

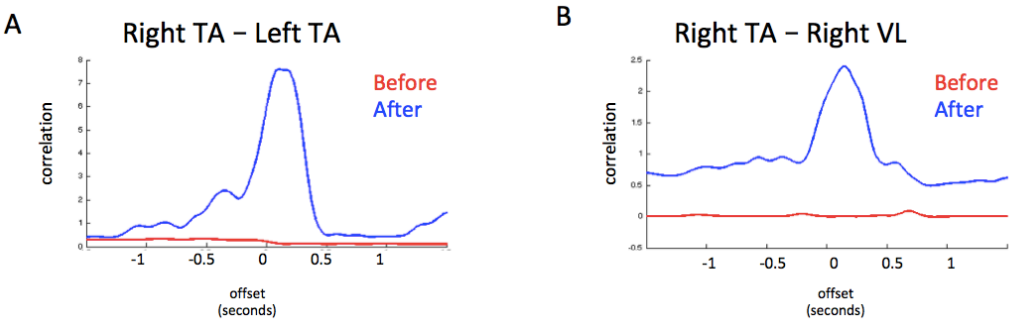

Figure 4.10: Cross-correlation of EMG power between A) the trained TA muscle and the untrained TA muscle, and B) the trained TA muscle and the vastus lateralis muscle (VL), before and after injury (with stimulation).

One animal in the treated group showed a unique behavioral response after injury. On some days she failed to generate visible movement in her hindlimbs, but produced a consistent and sustained muscle contraction in her untrained TA muscle (**Fig 4.11a**). No significant muscle activity was observed in her trained TA muscle (**Fig 4.11b**). The untrained TA muscle shows a clear increase in EMG power in response to the auditory cue (**Fig 4.11c**).

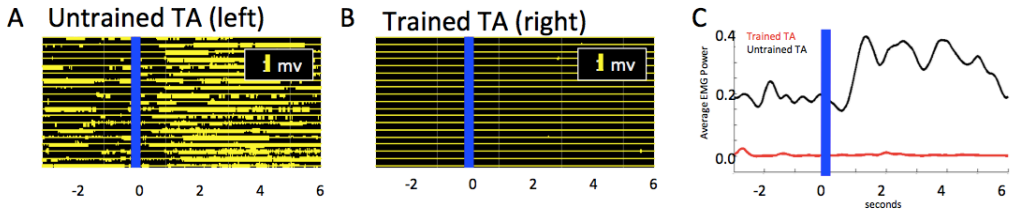

Figure 4.11: Raster plots from A) the untrained TA and B) the trained TA muscles of a treated rodent. Data taken from session where the animal failed to produce visible movement but contracted her untrained limb. C) The EMG power (low pass filter < 1Hz) generated from the untrained limb (black) vs. the trained limb (red) averaged over 91 trials.

4.3.3 – Adaptation Effect

The rodent's behavior at 4 months post-injury was compared to their average performance 2 months post-injury. There was no consistent improvement in the response time of the spinalized rodents. One animal performed faster than her initial

recovery, one animal performed the same, and two animals performed slower (**Fig 4.12**).

One animal showed spontaneous leg movement without spinal stimulation 4 months after injury (**Fig 4.13a**), but this behavior was not correlated to the auditory cue. This animal had been tested at 3 months post injury and failed to produce any noticeable muscle activity without spinal stimulation (**Fig 4.13b**).

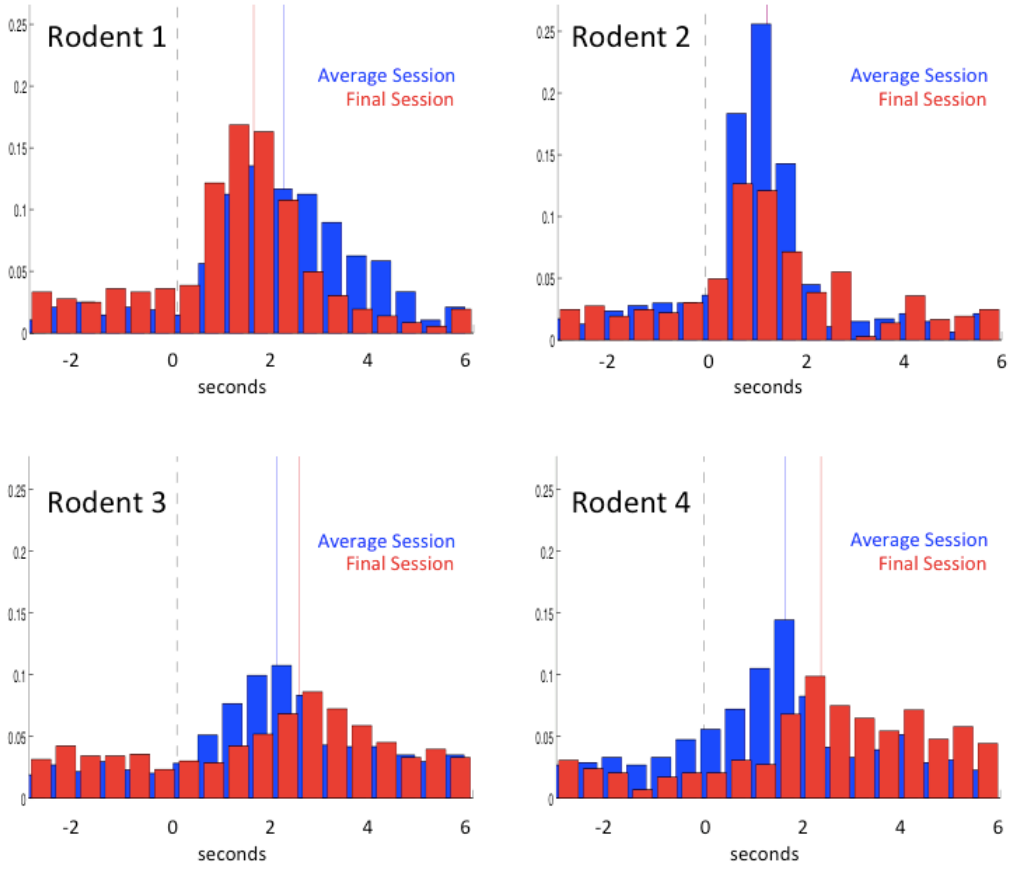

Figure 4.12: Histograms of TA busting onset compared between after session after injury (with stimulation) and the final session recorded at 4 months post-injury (with stimulation). In both conditions across all four rodents, the distribution of onset times was significantly different than random (Pearson Chi-Squared, $p < 10^{-10}$). A) Rodent 1: Average Session – 480 burst over 307 trials (median response 2.17 seconds) , Final Session – 362 burst over 99 trials (median response 1.54 seconds), B) Rodent 2: Average Session - 469 burst over 208 trials (median response 1.24 seconds), Final Session – 364 burst over 84 trials (median response 1.25 seconds), C) Rodent 3: Average Session – 744 bursts over 142 trials (median response 2.03 seconds), Final Session – 732 bursts over 82 (median response 2.47 seconds), D) Rodent 4: Average Session – 485 bursts over 199 trials (median response 1.64 seconds), Final Session – 294 burst over 81 trials (median response 2.37 seconds)

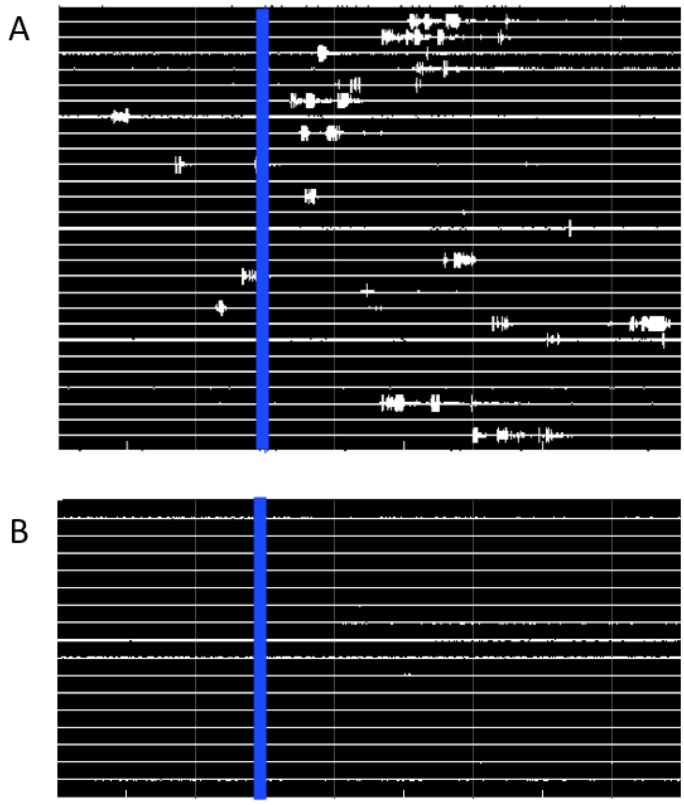

Figure 4.13: A) Raster plots of spontaneous EMG activity generated by a treated rodent without spinal stimulation. B) Raster plot of EMG activity recorded from the same rodent in a previous non-stimulated session.

4.3.4 – Novel Tone and Startle Recording

The treated rodents failed to produce muscle activity when the auditory cue was replaced with a novel tone. EMG activity during these novel sessions was significantly lower and failed to show any significant tuning (**Fig 4.14a**).

The startle response was both qualitative and quantitatively different than the beep-kick behavior. The startle response was a slight muscle twitch, in contrast to the large leg movements during the beep-kick task. The onset of the startle response

was also significantly shorter than the beep-kick response, and the muscle activity was more stereotyped than the beep-kick behavior (**Fig 4.14b**).

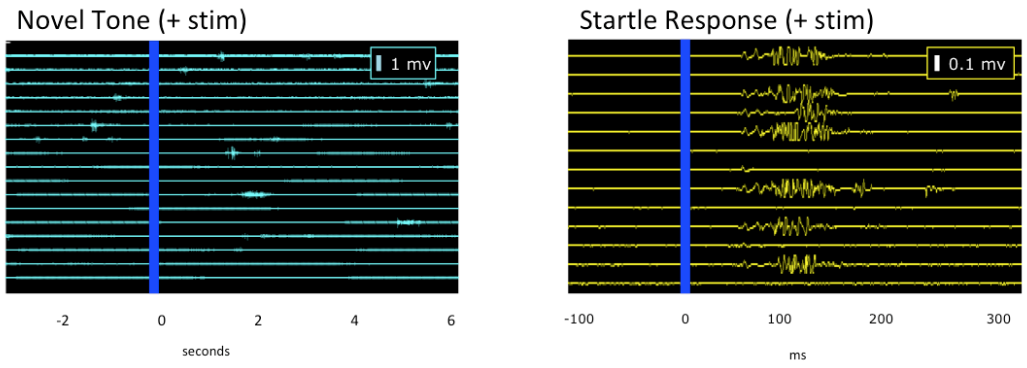

Figure 4.14: A) Raster plots of the treated animals response to the novel tone (chirp) while receiving spinal stimulation. B) Raster plots showing the startle response generated by a loud unexpected noise. Note that the timescale and the voltage scale are different.

4.3.5 – On/Off Experiment

Toggling the spinal stimulation on and off caused an immediate change in behavior (**sup video3**). The spinalized rodents could clearly and consistently respond to the auditory cue during spinal stimulation, but the behavior disappeared when the stimulator was turned off (**Fig 4.15**). When the stimulator was turned back on, the behavior returned. This effect was immediate. When the stimulator was turned off, the rodent failed to perform in the next trial. When the stimulator was turned back on, the behavior returned within the next trial. This behavior was seen across the treated group of rodents.

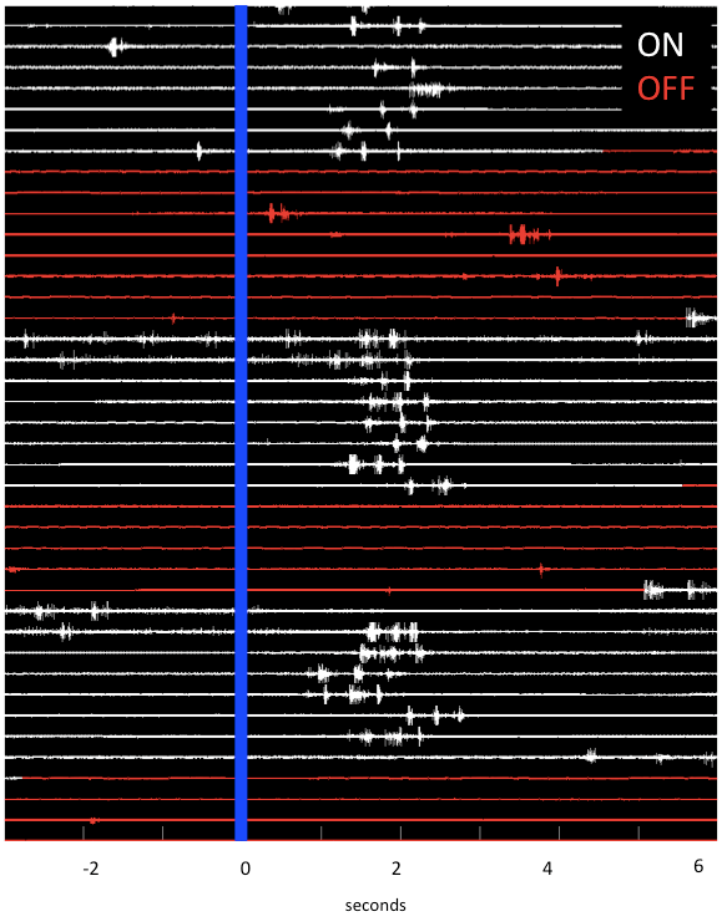

Figure 4.15: Raster plot showing the loss and recovery of muscle activity when spinal stimulation is either turned off (red) or on (white). The traces correspond to consecutive trials, and the transition between red and white shows when the stimulator was turned on or off.

4.3.6 – Pharmacology (Quipazine & Strychnine)

The administration of either quipazine or strychnine produced spontaneous leg movements in all animals. Despite the increased muscle activity, animals dosed with strychnine were capable of performing the beep-kick task (**Fig 4.16b**). The combination of strychnine and spinal stimulation resulted in a faster response time when compared to spinal stimulation alone (**Fig 4.16a**).

While quipazine produced similar amounts of spontaneous muscle activity as strychnine, the administration of the drug interfered with the animal's performance

(**Fig 4.16c**). Treadmill testing demonstrated that the dosage of quipazine, while interfering with the beep-kick task, improves muscle coordination during stepping (**Fig 4.17a,b**). Beep-kick sessions conducted before the injury showed that quipazine does not interfere with the uninjured animal (**Fig 4.17c**).

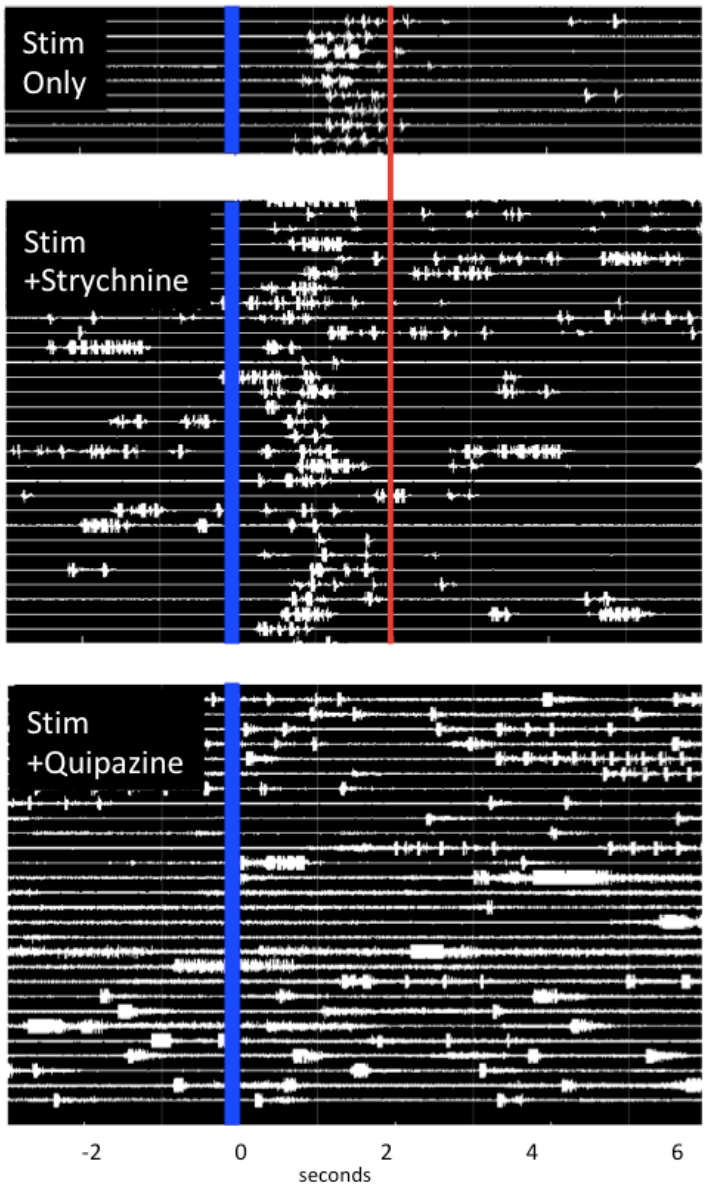

Figure 4.16: Raster plots comparing behavior when provided either A) spinal stimulation only, B) spinal stimulation plus strychnine, or C) spinal stimulation plus quipazine.

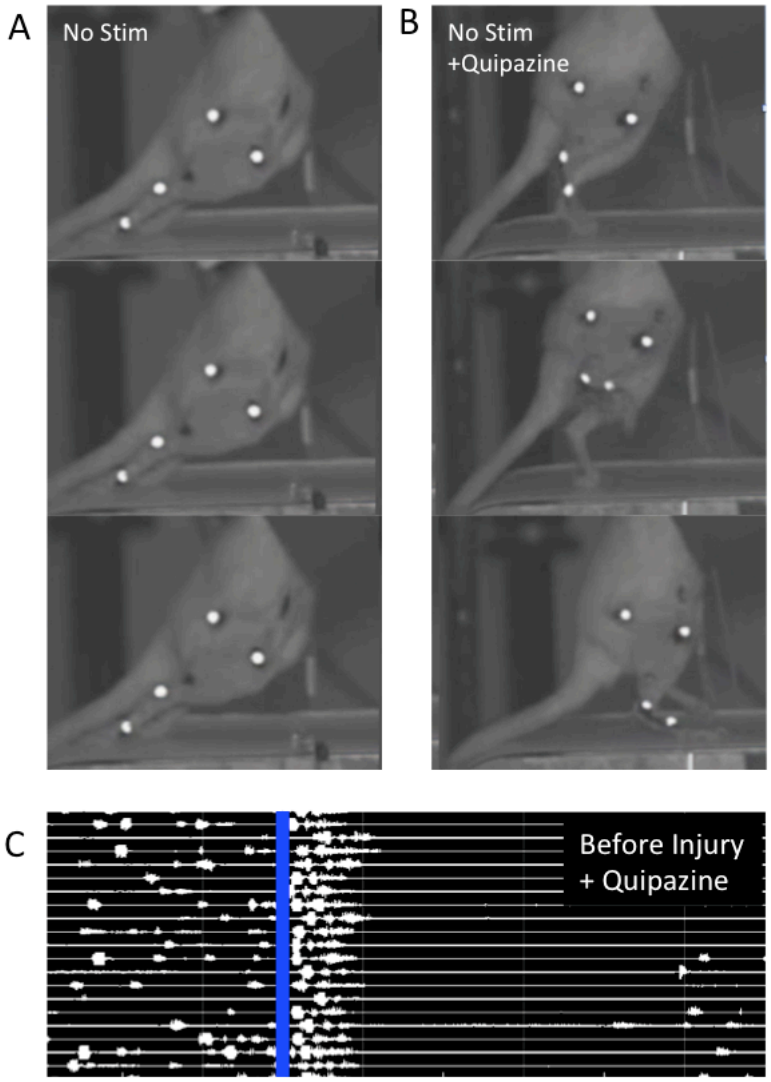

Figure 4.17: A) Stepping performance of the spinalized rodents without stimulation. B) Stepping performance of spinalized rodents with quipazine. C) Raster plot of the effect of quipazine on uninjured animals.

4.3.7 – Histology

Astrocytes stains of the injury site confirm the location and severity of the hemisections (**Fig 4.18a**). The 3D model confirmed that the injury occurred through out the spinal cord (**Fig 4.18b**). A common morphology in the injury sites seen across rodents was a large cyst at the lower T10 hemisection and an atrophy of neural tissue at the upper T7 hemisection.

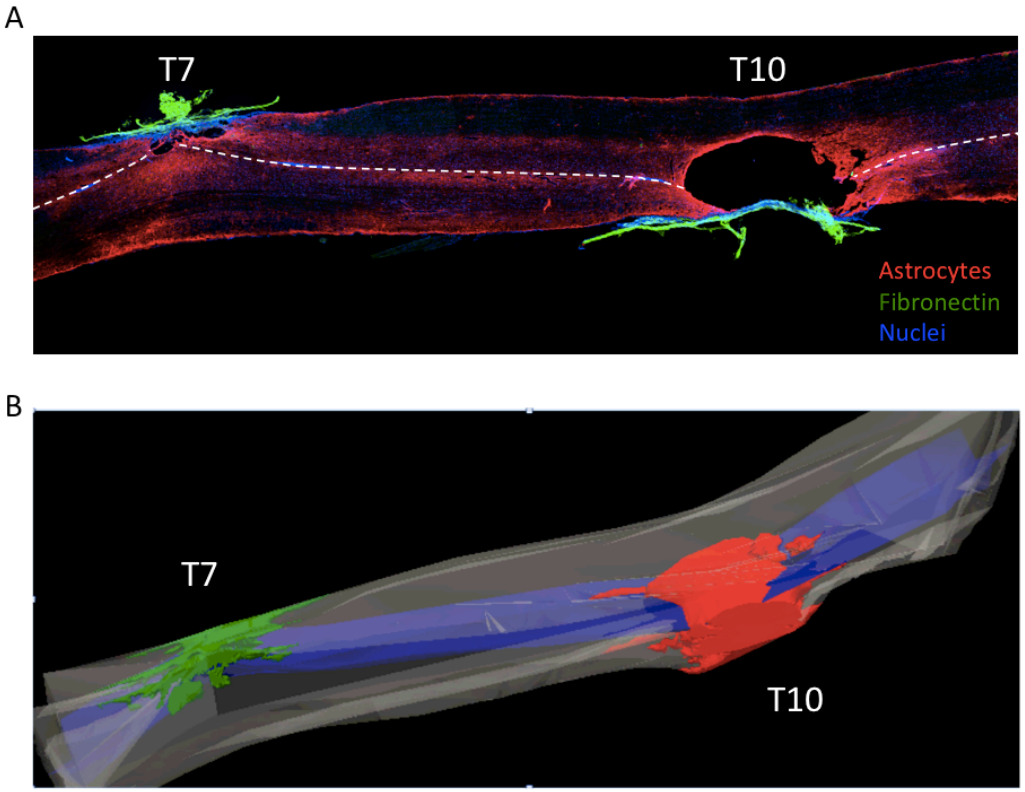

Figure 4.18: A) Horizontal section of an injury site from the spinalized rodent. The tissue is stained for astrocytes (red), fibronectin (green), and cell nuclei (blue). The midline of the spinal cord was marked following the central canal (dotted white). The hemisection at spinal level T7 can be seen as an atrophy of the spinal tissue. The hemisection at spinal level T10 shows the formation of a large cyst. B) A 3D reconstruction of the injury site compiled from multiple horizontal sections of the spinal cord (spaced 200 microns apart). The T7 hemisection is labeled in green, and the T10 hemisection is labeled in red. The midline of the spinal cord labeled in blue across the spinal cord. This 3D model shows that the injury sites pass through the entire depth of the spinal cord.

Neural activity in the lumbosacral enlargement was studied using immunofluorescence staining for the c-fos protein, which is expressed in neurons that undergo a sustained increase in the firing of action potentials. Before perfusion, all rodents were placed in the experimental set up. The treated rodents (with spinal stimulation) and the incomplete injury rodents (without spinal stimulation) successfully performed the kicking task. The untreated rodents were not stimulated, and failed to generate leg movement, while the untrained rodents were stimulated, and also failed to generate leg movement.

Active neurons were manually identified by colocalizing c-fos (1:1500) with NeuN (1:1500), a marker for neuron cell bodies, in eight coronal sections of spinal tissue taken from each animal spaced evenly between the L1 and L4 spinal levels. All rodents showed a significant number of active neurons primarily located in the dorsal horns (**Fig 4.19d**). To study the spatial distribution of the active neurons, the coronal sections were discretized into a grid and the number of active cells in each grid element was counted. The result was spatially smoothed and the sections were aligned to the central canal. Data from the untreated and untrained rodents was combined into a control group, since neither cohort generated muscle activity prior to perfusion. The spatial distribution of active neurons in this control group was compared against the treated and incomplete rodents. Comparisons were made by computing a one-way ANOVA at each grid element, which determines the likelihood that the cell counts from the two groups are drawn from the same distribution. Grid elements with likelihood greater than 0.5% were ignored.

Comparing the control group against the combined data from the treated and incomplete injury rodents shows that animals performing the kicking task modulated neural activity only on the trained side of their spinal cord, with increased neural activity near the central canal and decreased neural activity in the lateral spinal nucleus (**Fig 4.19a**). Comparing only the treated rodents against the control group shows broader activation of neural activity along the medial side of the dorsal horn on the trained side, as well as an additional region of increased neural activity in lamina 3/4 of the dorsal horn on the untrained side (**Fig 4.19b**). Both regions of increased activity in the dorsal horns overlap with areas that normally receive dense projections from the corticospinal tract [12]. Contrasting the treated rodents against the incomplete injury rodents shows that the only significant difference between the groups is increased activity in the lamina 3/4 region on the untrained side of the treated rodents (**Fig 4.19c**). The active region near the central canal is populated with cholinergic neurons, which were identified using a CHaT stain (1:500). There were zero CHaT positive neurons that coexpressed the c-fos

protein, meaning that cholinergic neurons did not contribute to the increased activity seen in rodents performing the kicking task.

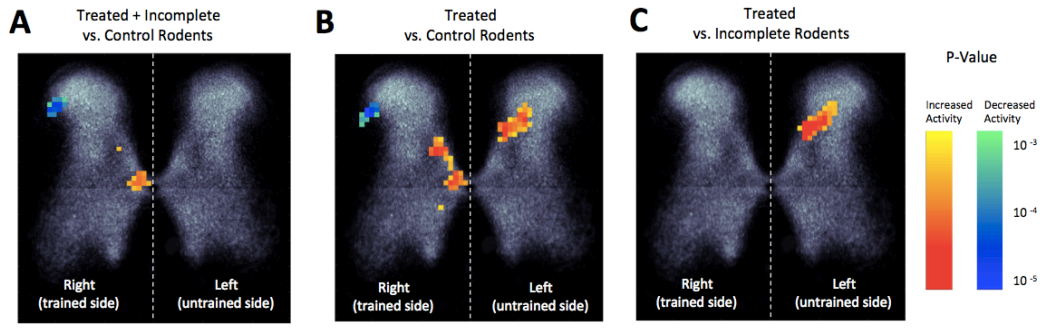

Figure 4.19 Comparisons of the spatial distribution of neural activity in the lumbosacral enlargement. Regions of red denote increased activity and regions in blue denote decreased activity. Active neurons were identified in eight sequential coronal sections from the lumbosacral enlargement of each animal by colocalizing c-fos (1:1500) and NeuN (1:1500). The coronal sections were discretized into a grid, and the number of active cells in each element were counted. A one-way ANOVA was calculated at each grid element comparing either A) the combined data from the treated and incomplete rodents against the control rodents (untreated and untrained) B) just the treated rodents against the control group, or C) the treated rodents against the incomplete injury rodents. D) Compares the average number of active cells in each coronal section in the treated rodents vs the control group.

5HT axons were not present in the lumbar region of the treated rodents **(Fig 4.20a)**, but 5HT axons were observed in the incomplete injury rodents (**Fig 4.20b**).

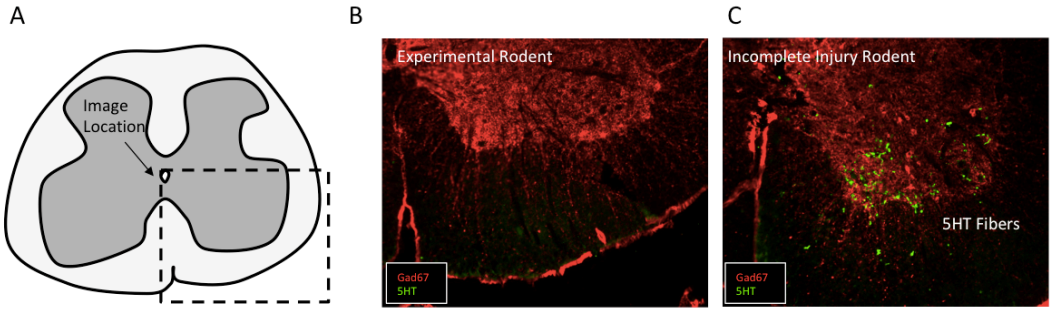

Figure 4.20: A) Schematic of image locations in B and C. These images were taken from the right ventral horn of coronal section in the lumbar region. B) No 5HT axons are present in the treated animals. C) 5HT axons are clearly seen in the incomplete injury rodents (green)

4.4 – Discussion

Spinal stimulation directly enables the recovery of voluntary movement after a motor complete spinal injury in the rodent. Recovery occurs within seconds of the

stimulation being applied and disappears within seconds of stimulation being removed. The animal's response to the cue is slower and less specific than their pre-injury behavior.

4.4.1 – Delayed Response

The simultaneous double hemisection destroys the direct monosynaptic connections between the brain and the spinal circuitry. The delayed response time could be caused by a) increased transmission delays due to a new multisynaptic pathway, or b) a weakened supraspinal input needing additional time to accumulate in the spinal circuitry to cross a movement threshold. Results from the strychnine and incomplete injury rodents suggest that this delay is due to a weakened supraspinal input.

Strychnine is a glycine antagonist, which reduces inhibition in the spinal circuitry. Animals administered strychnine produce spontaneous leg movements, suggesting this reduced inhibition lowers the threshold for muscle activity. Strychnine will not effect the transmission time of an action potential along a neuron. Therefore, the time required for the supraspinal input to propagate down to the spinal circuitry should be the same with and without strychnine. Spinalized rodents respond faster to the auditory cue when dosed with strychnine. This faster response is likely the result of the spinal circuitry requiring less supraspinal input to trigger movement.

The improved response time also suggests that the supraspinal input reaches the spinal circuitry well before movement in the non-strychnine condition. The delay between the arrival of the input and the resulting movement is then a function of the sensitivity of the spinal circuitry and the accumulation rate of the supraspinal input.

The delayed response in the incomplete injury rodents also supports the idea of a weakened supraspinal input. These animals maintained 5HT axons in their lumbar region after injury. The primary source of 5HT fibers is from the raphe nuclei in the

brainstem, which proves that these animals maintained monosynaptic connections to the brain. If the delayed response time was caused by transmission delays along a multisynaptic pathway, then these animals should not be affected. Yet the incomplete injury rodents showed a delayed response after spinalization.

4.4.2 – Muscle Coordination

Our results show that spinal stimulation directly enables the recovery of voluntary movement after a spinal injury, and that the mechanism of recovery occurs within seconds of treatment. The recovered supraspinal input is delayed and has decreased muscle specificity. This loss of specificity is seen both in the bilateral and stereotyped leg movements and in the broader and bilateral activation of neurons in the lumbosacral enlargement. This broad activity pattern suggests a more generalized spinal circuit is engaged after the injury. The areas of increased activity overlap with regions that traditionally receive dense cortical projections. This suggests that the recovered pathway likely engages the same input to the spinal circuitry that was used before injury. Therefore the reorganization after injury does not require the spinal circuitry to search for the new supraspinal input. The asymmetrical nature of the c-fos expression pattern may be due to either the recovered spinal circuit or the asymmetry of the hemisections (Left T7, Right T10). This could be teased apart by flipping the injury sites and looking for a corresponding change in the c-fos expression pattern. If the asymmetry flips sides, then the recovered circuit is linked to the injury site. If the asymmetry is unaffected, then the recovered circuit is linked to behavior.

4.4.3 – Long Term Effects of Spinal Stimulation

There was no significant improvement across the rodents at four months post injury compared to two months post injury, but additional experiments are needed to study the long-term effects of spinal stimulation on recovery. The nonstimulated muscle activity from one rodent at the four-month mark suggests that spinal stimulation can cause a lasting reorganization in the nervous system. Prior work shows that the

neural tissue between the double hemisections can form a functioning pathway, without the need for stimulation, if the hemisections are induced at different times [55]. Spinal stimulation may facilitate the formation of this same pathway after the simultaneous injury, which does not naturally show this recovery.

4.4.4 – Serotonin

The disruptive effect of quipazine on the beep-kick task suggests that serotonin plays an important role of the recovered pathway. Quipazine does not affect the uninjured rodent, which proves that the drug does not interfere with the auditory system or the brain's ability to issue a motor command. Step testing in spinalized rodents also shows that quipazine engages the spinal circuitry in a positive and biologically relevant manner. Strychnine produces similar stepping behavior in the spinalized rodent, but does not disrupt voluntary movement. This suggests that the loss of behavior during the beep-kick task is not simply the result of an over-engaged spinal circuit. Since neither the brain nor the spinal circuitry are negatively impacted by the drug, the likely culprit for the disruption of voluntary movement is the pathway connecting the two.

Quipazine is a nonspecific serotonin agonist. This drug binds with 5HT receptors, which could alter the firing properties of neurons along the recovered pathway. This would introduce noise in the recovered communication channel between the brain and spinal circuits, and thereby prevent supraspinal input from reaching the spinal circuitry.

The behavioral results from quipazine will guide future anatomical studies of the recovered pathway. Since serotonin is primarily generated in the raphe nuclei, the brainstem is likely an important node in the recovered connection between the motor cortex and spinal circuitry. Histology can now be targeted to look for changes in the synaptic wiring between the motor cortex and structures in the brainstem.

The expression pattern of 5HT receptors can also be studied in the injury site. Prior work shows that a functional pathway between the hemisections can be created locally by propriospinal interneurons. The absence of 5HT fibers in the lumbar regions of the treated animals proves that the recovery of voluntary movement is not the result of regrown serotonergic axons. While the serotonergic neurons from the brainstem do not directly reach the spinal circuitry, they may synapse onto the reorganized propriospinal neurons. This could be studied by looking for changes in expression patterns of 5HT receptors near the injury site.

4.4.5 – Decreased C-fos Activity in the Lateral Spinal Nucleus

Decreased activity in the lateral spinal nucleus suggests that the treated rodents attempted to engage a specific and trained spinal network. This region of the spinal cord is the entry point of afferent fibers that relay sensory information from the limb. Our results show that while the recovered movement involves both hindlimbs, only sensory feedback from the trained limb is suppressed. During training, the rodents likely formed a spinal circuit controlling the trained limb that listened for supraspinal input and ignored sensory feedback. The asymmetry of sensory suppression after injury suggests that the treated rodents attempted to reengage this trained spinal circuit.

4.4.6 – Mechanism of Spinal Stimulation

The stimulating electrodes are sutured to the Dura on the dorsal side of the rodent's lumbosacral enlargement. Large nerve bundles travel in and out spinal cord on this dorsal side. The decreased activity in the lateral spinal nucleus also suggests that the main effect of spinal stimulation is not due to the activation of these afferent fibers that enter into the spinal cord through the lateral spinal nucleus. If this were the case, we would expect to see increased activation in the lateral spinal nucleus on both sides of the spinal cord when comparing the treated rodents against the incomplete injury rodents. Also, the similar total number of active cells

in the treated and untreated rodents suggests that spinal stimulation does not simply increase neural activity, but somehow regulates activity in the spinal network.

4.4.7 – Characterization of the Beep-Kick Task

These results are proof that the beep-kick task is a reliable and effective tool for studying the recovery of movement. This task requires minimal equipment and training, and was recovered in all animals that were tested after spinal injury. The control studies show that performance during the beep-kick task is the result of a trained behavior enabled by spinal stimulation. The untreated animals, as well as the nonstimulation and on/off recordings from the treated rodents, are proof that spinal simulation is necessary for behavior to occur. Yet, the untrained animals prove that spinal stimulation is not sufficient to generate behavior. These untrained animals are also proof that behavior is not a confound of the animal adjusting their body position while receiving the food reward. Finally, the novel tone and startle sessions prove that behavior is not simply triggered by an auditory stimulus, but is a trained response to a specific sound, and can therefore be treated as voluntary movement

4.4.7 – Future work

The next step is to combine this task with cortical recordings. Spiking activity from neurons in the motor cortex can be correlated to the onset of the auditory cue. The response properties of these cortical neurons can be studied as the spinal stimulation is turned on and off, or for changes in stimulation intensity and frequency. By identifying the region of cortex involved in recovery, we can begin to tease apart the functional and anatomical properties of the recover pathway between the brain and spinal circuits. This behavioral task can also be used to optimize the spinal stimulation treatment. The stimulation pattern can be altered, the electrode positions can be adjusted, or different drugs can be tested, and the effect on voluntary movement can be studied. Results from this work can then guide the treatment of

patients suffering from spinal injury to assist in their recovery of voluntary movement.

4.5 – Methods

4.5.1 – Spinal Stimulation

The lumbosacral enlargement was electrically stimulated using a pair of electrodes implanted in the epidural space, between the Dura and the vertebra, at spinal levels L2 and S1 (Appendix C). Stimulation parameters were based on previous studies (40 Hz; L2 [+] / S1 [-]; voltage-controlled; monophasic; 0.2 ms rectangular pulse; Grass S88 Stimulator) [46]. A stimulation threshold was established for each animal by slowly increasing the voltage until muscle activity was evoked (typically 1-4 volts). The stimulating voltage was then set to 80%-90% of this threshold. Stimulation equipment was independent of the beep-kick task, and was not modulated to evoke the behavioral response.

4.5.2 – EMG Recording

Muscle activity was recorded from bipolar EMG electrodes embedded into the muscle tissue (Appendix C). EMG signals were differentially amplified (A-M system; Model 3500) and band-pass filtered between 1 Hz and 5kHz. The signals were digitized (National Instruments; BNC-2111) and recorded to hard drive (LabView; custom). EMG data was processed offline using custom analysis software (MATLAB; 2015) (Appendix C).

4.5.3 – EMG Analysis

EMG activity of the tibialis anterior in the trained hindlimb was segmented around each trial (3 seconds before beep, 6 seconds after). EMG bursts were extracted using a thresholding method. To test for significance, a timing histogram of the burst onsets was computed, and a Pearson's Chi-Squared coefficient was calculated to test the likelihood that the timing distribution of TA activity was drawn from a

uniform distribution. EMG power in the tibialis anterior (EMG_{ta}) was also cross-correlated with EMG power (EMG_{other}) from either the left tibialis anterior or the right vastus lateralis. The EMG power was defined as the instantaneous power in the raw EMG signal, band-passed filtered between 0.1 Hz and 20 Hz.

$$f(\tau) = \int EMG_{ta}(t+\tau) \cdot EMG_{other}(t)dt.$$

4.5.4 – Therapy

After injury, the rodents received therapy sessions every other night. These sessions consisted of multi-hour subthreshold stimulation, followed by treadmill step training.

Subthreshold stimulation sessions have been described previously [59]. Spinal stimulation (40 Hz; L2 [+] / S1 [-]; voltage-controlled; monophasic; 0.2 ms rectangular pulse; Grass S88 Stimulator) was set to 80% of motor threshold. The rodent's headplug were connected to a long stimulating cable on a swivel, which allowed the animal to move freely around their home cage. EMG activity was not recorded during these sessions. Typical sessions lasted three hours.

Treadmill step training has been described previously [59]. The rodents were suspended in a harness above a treadmill to perform bipedal stepping. Spinal stimulation (40 Hz; L2 [+] / S1 [-]; voltage-controlled; monophasic; 0.2 ms rectangular pulse; Grass S88 Stimulator) was set between 80-90% of motor threshold. The treadmill speed was varied to evoke different stepping patterns. Kinematics were not recorded during these sessions. Typical sessions lasted fifteen minutes.

4.5.5 – Beep-kick Training

Each rodent was trained by pairing the auditory cue with the vibration of a small motor temporarily taped to the rodent's right hindlimb (Appendix C). The initial vibration provoked a leg movement, which was positively reinforced with a food

reward. The intensity of vibration was slowly lowered over multiple trials, until the rodent performed the task with the motor turned off. Once the rodent reliably performed the task, the motor was removed completely. This behavior took approximately one week to train, but one animal acquired the task in a single session.

4.5.6 – Quipazine Step Testing

Step testing was similar to the treadmill step training described above. Rodents were suspended in a harness above a treadmill to perform bipedal stepping. Kinematics were recorded using video tracking software and visual markers placed on the rodent's hindlimbs. Baseline stepping kinematics were recorded immediately before the quipazine injection and without spinal stimulation. Rodents were then injected intraperitoneally with quipazine (0.3 mg/kg), and the drug was given ten minutes to take affect. The treadmill step testing was then repeated, again without spinal stimulation.

4.5.7 – Perfusion

Rodents were anesthetized with ketamine and xylazine, and killed by intracardial perfusion of formaldehyde [%4]. The spinal column was coarsely dissected and fixed over night. The spinal cord was then finely dissected and split into three blocks. The first block contained the lumbosacral enlargement, the second block contained the injury site, and the third block contained tissue above the injury site. The block containing the injury site was horizontally sliced and slide mounted, while the other blocks were coronally sliced and free floated.

4.5.8 – C-FOS Immunohistochemistry

The process for c-fos staining has been described previously [60]. Just before euthanasia, the rodents performed the beep-kick task. These sessions lasted 45 minutes, after which the rodents were returned to their home cage. The rodents were perfused one hour later. The treated rodents (n=4) were spinally stimulated,

and successfully performed the task. The untreated rodents (n=2) were not stimulated, and failed to perform the task. The untrained rodents (n=2) were stimulated, but also failed to perform the task. The incomplete injury rodents (n=2) were not stimulated, but successfully performed the task.

4.6 – CITATIONS

[1] Strauss, David J., et al. "Trends in life expectancy after spinal cord injury." *Archives of physical medicine and rehabilitation*87.8 (2006): 1079-1085.

[2] Rehabilitation of the individual with spinal cord injury

[3] Donovan WH. Spinal Cord Injury—Past, Present, and Future. *The Journal of Spinal Cord Medicine*. 2007;30(2):85-100

[4] Schurch, Brigitte, Cécile Tawadros, and Stefano Carda. "Dysfunction of lower urinary tract in patients with spinal cord injury." *Handbook of clinical neurology*. Vol. 130. Elsevier, 2015. 247-267

[5] Silver, John Russell. *History of the treatment of spinal injuries*. Springer Science & Business Media, 2012

[6] White, Non-Hispanic, and Non-Hispanic Black. "Spinal cord injury (SCI) facts and figures at a glance." *National spinal cord injury statistical center, facts and figures at a glance* (2016)

[7] Norman, Kathleen E., et al. "A treadmill apparatus and harness support for evaluation and rehabilitation of gait." *Archives of physical medicine and rehabilitation* 76.8 (1995): 772-778.,

[8] Hesse, S., et al. "Treadmill training with partial body weight support compared with physiotherapy in nonambulatory hemiparetic patients." *Stroke* 26.6 (1995): 976-981.

[9] Field-Fote, Edelle C. "Combined use of body weight support, functional electric stimulation, and treadmill training to improve walking ability in individuals with chronic incomplete spinal cord injury." *Archives of physical medicine and rehabilitation*82.6 (2001): 818-824.

[10] Hesse, Stefan, et al. "Restoration of gait in nonambulatory hemiparetic patients by treadmill training with partial body-weight support." *Archives of physical medicine and rehabilitation* 75.10 (1994): 1087-1093.

[11] Hornby, T. George, David H. Zemon, and Donielle Campbell. "Robotic-assisted, body-weight–supported treadmill training in individuals following motor incomplete spinal cord injury." *Physical therapy* 85.1 (2005): 52-66.

[12] Barbeau, H., et al. "Does neurorehabilitation play a role in the recovery of walking in neurological populations?." *Annals of the New York Academy of Sciences* 860.1 (1998): 377-392.

[13] Ichiyama, R. M., et al. "Hindlimb stepping movements in complete spinal rats induced by epidural spinal cord stimulation." *Neuroscience letters* 383.3 (2005): 339-344.

[14] Harkema, Susan, et al. "Effect of epidural stimulation of the lumbosacral spinal cord on voluntary movement, standing, and assisted stepping after motor complete paraplegia: a case study." *The Lancet* 377.9781 (2011): 1938-1947.

[15] Gerasimenko, Yury P., et al. "Noninvasive reactivation of motor descending control after paralysis." *Journal of neurotrauma* 32.24 (2015): 1968-1980.

[16] Angeli, Claudia A., et al. "Altering spinal cord excitability enables voluntary movements after chronic complete paralysis in humans." *Brain* 137.5 (2014): 1394-1409.

[17] Sherrington, Charles. *The integrative action of the nervous system*. CUP Archive, 1910.

[18] Sherrington, Charles Scott. "Observations on the scratch‐reflex in the spinal dog." *The Journal of physiology* 34.1-2 (1906): 1-50.

[19] Sherrington, C. S. "On reciprocal innervation of antagonistic muscles.—Eighth note." *Proc. R. Soc. Lond. B*. Vol. 76. No. 509. The Royal Society, 1905.

[20] Brown, T. Graham. "The intrinsic factors in the act of progression in the mammal." *Proc. R. Soc. Lond. B*. Vol. 84. No. 572. The Royal Society, 1911.

[21] Marder, Eve, and Dirk Bucher. "Central pattern generators and the control of rhythmic movements." *Current biology* 11.23 (2001): R986-R996.

[22] Ijspeert, Auke Jan. "Central pattern generators for locomotion control in animals and robots: a review." *Neural networks* 21.4 (2008): 642-653.

[23] Wilson, Donald M. "The central nervous control of flight in a locust." *Journal of Experimental Biology* 38.2 (1961): 471-490.

[24] Cohen, Avis H., and Peter Wallén. "The neuronal correlate of locomotion in fish." *Experimental brain research* 41.1 (1980): 11-18.

[25] Sillar, Keith T., Carolyn A. Reith, and J. O. E. McDEARMID. "Development and aminergic neuromodulation of a spinal locomotor network controlling swimming in Xenopus larvae." *Annals of the New York Academy of Sciences* 860.1 (1998): 318-332.

[26] Cabelguen, Jean-Marie, Céline Bourcier-Lucas, and Réjean Dubuc. "Bimodal locomotion elicited by electrical stimulation of the midbrain in the salamander Notophthalmus viridescens." *Journal of Neuroscience* 23.6 (2003): 2434-2439.

[27] Cazalets, J. R., Y. Sqalli‐Houssaini, and F. Clarac. "Activation of the central pattern generators for locomotion by serotonin and excitatory amino acids in neonatal rat." *The Journal of physiology* 455.1 (1992): 187-204.

[28] Fedirchuk, Brent, et al. "Pharmacologically evoked fictive motor patterns in the acutely spinalized marmoset monkey (Callithrix jacchus)." *Experimental brain research* 122.3 (1998): 351-361.

[29] Gerasimenko, Yu P., A. N. Makarovskii, and O. A. Nikitin. "Control of locomotor activity in humans and animals in the absence of supraspinal influences." *Neuroscience and behavioral physiology* 32.4 (2002): 417-423.

[30] Calancie, Blair, et al. "Involuntary stepping after chronic spinal cord injury: evidence for a central rhythm generator for locomotion in man." *Brain* 117.5 (1994): 1143-1159.

[31] Dimitrijevic, Milan R., Yuri Gerasimenko, and Michaela M. Pinter. "Evidence for a spinal central pattern generator in humans." *Annals of the New York Academy of Sciences* 860.1 (1998): 360-376.

[32] Grillner, S. "Control of locomotion in bipeds, tetrapods, and." (1981).

[33] Edgerton, V. Reggie, et al. "Plasticity of the spinal neural circuitry after injury." *Annu. Rev. Neurosci.* 27 (2004): 145-167.

[34] Orlovskii, G. N., and A. G. Fel'dman. "Classification of lumbosacral neurons by their discharge pattern during evoked locomotion." *Neurophysiology* 4.4 (1972): 311-317.

[35] Baev, Konstantin V. "Introduction." *Biological Neural Networks: Hierarchical Concept of Brain Function*. Birkhäuser Boston, 1998. 1-6.

[36] Barbeau, H., and S. Rossignol. "Initiation and modulation of the locomotor pattern in the adult chronic spinal cat by noradrenergic, serotonergic and dopaminergic drugs." *Brain research* 546.2 (1991): 250-260.

[37] Grillner, S., and P. Zangger. "On the central generation of locomotion in the low spinal cat." *Experimental Brain Research* 34.2 (1979): 241-261.

[38] De Leon, R. D., et al. "Hindlimb locomotor and postural training modulates glycinergic inhibition in the spinal cord of the adult spinal cat." *Journal of neurophysiology* 82.1 (1999): 359-369.

[39] Forssberg, H., and S. Grillner. "The locomotion of the acute spinal cat injected with clonidine iv." *Brain research* (1973).

[40] Giroux, Nathalie, et al. "Effects of intrathecal glutamatergic drugs on locomotion. II. NMDA and AP-5 in intact and late spinal cats." *Journal of neurophysiology* 90.2 (2003): 1027-1045.

[41] Feraboli‐Lohnherr, Delphine, Jean‐Yves Barthe, and Didier Orsal. "Serotonin‐induced activation of the network for locomotion in adult spinal rats." *Journal of neuroscience research* 55.1 (1999): 87-98.

[42] Barbeau, H., and S. Rossignol. "The effects of serotonergic drugs on the locomotor pattern and on cutaneous reflexes of the adult chronic spinal cat." *Brain research* 514.1 (1990): 55-67.

[43] Shik, Mark L., and Grigori N. Orlovsky. "Neurophysiology of locomotor automatism." *Physiological reviews* 56.3 (1976): 465-501.

[44] Shik, M. Lo. "Control of walking and running by means of electrical stimulation of the midbrain." *Biophysics* 11 (1966): 659-666.

[45] Iwahara, T., et al. "Spinal cord stimulation-induced locomotion in the adult cat." *Brain research bulletin* 28.1 (1992): 99-105.

[46] Courtine, Grégoire, et al. "Transformation of nonfunctional spinal circuits into functional states after the loss of brain input." *Nature neuroscience* 12.10 (2009): 1333.

[47] Barbeau, Hughes, and Serge Rossignol. "Recovery of locomotion after chronic spinalization in the adult cat." *Brain research* 412.1 (1987): 84-95.

[48] Kakulas, Byron A. "Pathology of spinal injuries." *Central Nervous System Trauma* 1.2 (1984): 117-126.

[49] Sherwood, Arthur M., Milan R. Dimitrijevic, and W. Barry McKay. "Evidence of subclinical brain influence in clinically complete spinal cord injury: discomplete SCI." *Journal of the neurological sciences* 110.1 (1992): 90-98.

[50] Gale, Karen, Harry Kerasidis, and Jean R. Wrathall. "Spinal cord contusion in the rat: behavioral analysis of functional neurologic impairment." *Experimental neurology* 88.1 (1985): 123-134.

[51] Gruner, John A. "A monitored contusion model of spinal cord injury in the rat." *Journal of neurotrauma* 9.2 (1992): 123-128.

[52] Basso, D. Michele, Michael S. Beattie, and Jacqueline C. Bresnahan. "Graded histological and locomotor outcomes after spinal cord contusion using the NYU weight-drop device versus transection." *Experimental neurology* 139.2 (1996): 244-256.

[53] Arvanian, Victor L., et al. "Combined delivery of neurotrophin-3 and NMDA receptors 2D subunit strengthens synaptic transmission in contused and staggered double hemisected spinal cord of neonatal rat." *Experimental neurology* 197.2 (2006): 347-352.

[54] Bernstein, Deborah R., and Dennis J. Stelzner. "Plasticity of the corticospinal tract following midthoracic spinal injury in the postnatal rat." *Journal of Comparative Neurology* 221.4 (1983): 382-400.

[55] Courtine, Gregoire, et al. "Recovery of supraspinal control of stepping via indirect propriospinal relay connections after spinal cord injury." *Nature medicine* 14.1 (2008): 69.

[56] van den Brand, Rubia, et al. "Restoring voluntary control of locomotion after paralyzing spinal cord injury." *science*336.6085 (2012): 1182-1185.

[57] Luck, Steven J. *An introduction to the event-related potential technique*. MIT press, 2014.

[58] Gerasimenko, Yury P., et al. "Epidural spinal cord stimulation plus quipazine administration enable stepping in complete spinal adult rats." *Journal of neurophysiology* 98.5 (2007): 2525-2536.

[59] Gad, Parag, et al. "Sub-threshold spinal cord stimulation facilitates spontaneous motor activity in spinal rats." *Journal of neuroengineering and rehabilitation* 10.1 (2013): 108.

[60] Ichiyama, Ronaldo M., et al. "Step training reinforces specific spinal locomotor circuitry in adult spinal rats." *Journal of Neuroscience* 28.29 (2008): 7370-7375.

CORTICAL RECORDING AND SPINAL STIMULATION

5.1 – Overview

This thesis has focused on the use of electrodes to interact with neural circuits involved in voluntary movement.

The first study was on the electrode itself. This work showed that the insulation coating the metal electrode acts as a capacitor, coupling the voltage on the electrode to the surrounding neural tissue. This causes large spikes of voltage in the surrounding tissue during deep brain stimulation. These spikes have the potential to damage neural tissue and will induce electrical artifacts in neural recordings. To block this effect, a coaxially shielded electrode should be used. This coaxial electrode will be useful for reducing the electrical artifacts generated by the spinal stimulation in future experiments that combine spinal stimulation with cortical recordings.

The second study was on neural circuits in the parietal cortex and their role in hand movements. This research provides causal evidence that the parietal cortex encodes a state-estimator, combining sensory information with the efference copy to predict the movement of the hand. State-estimation is an important signal in motor control for guiding complex movement through a dynamic environment [35]. To test this idea, a visual delay was used to force a misalignment between sensory feedback and the efference copy. The parietal cortex unknowingly combines this delayed sensory feedback with the current efference information, resulting in poor predictions of the movement of the hand. Parietal activity eventually recovers predictive strength, showing that the parietal cortex is adaptive to sensory delays. This helps elucidate the role of the parietal cortex during movement and can help guide the development of neural prosthetics.

The last study focused on the use of spinal stimulation to restore voluntary movement after a motor complete spinal injury. Rodents were trained to kick their hindlimb in response to an auditory cue. They then received a spinal injury in the form of a simultaneous double hemisection, which resulted in paraplegia. By electrically stimulating their lumbosacral enlargement, the rodents were able to kick in response to the auditory cue. This work characterizes the new behavioral task in the rodent and begins to study the mechanism enabling the recovery of voluntary movement after spinal injury.

Future work will combine the cortical recording techniques used in the parietal study with the behavioral task developed in the spinal stimulation research to explore plasticity in the nervous system after a spinal injury. For voluntary movement to recover after a motor complete spinal injury, the nervous system must undergo massive reorganization. Understanding the functional and anatomical changes that enable this recovery will expose new sites for therapeutic intervention, which will improve treatment options for paralyzed patients. This recovery also offers an opportunity to study how the brain and spinal circuitry interact to generate movement. Corticospinal communication can be studied in two different states in the same animal (before and after injury), which will allow us to tease apart the aspects of this corticospinal interaction that are necessary for movement.

The following sections cover new experiments that will use cortical recording, stimulation, inactivation, and histological techniques to tease apart the recovered pathway. These sections will also discuss how the recovery of voluntary movement can be used as a tool for understanding how movement is encoded in the nervous system.

5.2 – Functional and Anatomical Mapping

5.2.1 – Cortical Stimulation

The first step is to identify the cortical regions involved in the recovery of voluntary movement. The obvious place to examine is motor cortex. Neurons in the motor cortex are arranged in a topographical layout that corresponds to the muscles they activate [2] [**Fig 5.1a**]. Prior studies show that after an amputation of a limb, this cortical map adjusts such that the area that once controlled the lost limb is coopted by the surviving body parts [3] [**Fig 5.1b**]. A similar effect should be seen after a spinal injury; the hindlimb area of the motor cortex should be taken over by the forelimbs. The first experiment is to study how this cortical map responds to spinal stimulation.

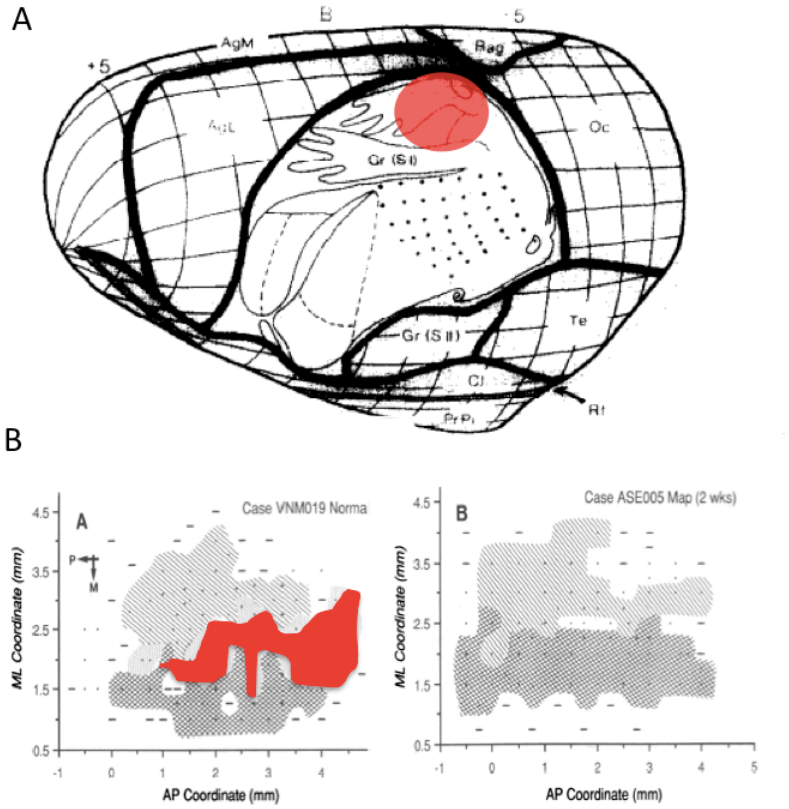

Figure 5.1: A) Example of the topographical layout of the rat's motor cortex. The hindlimb region is highlighted in red [2]. B) The response of a rat's motor cortex to an amputation. Initially, electrically stimulating the region in red evoked movement in the rodent's whiskers. Stimulation of the light grey region evoked movement from the rodent's eyelid. Stimulation of the dark grey evoked movement of the rodent's forearm. After severing the nerve innervating the whiskers, stimulation of the previously red region evoked movement either in the eyelid (light grey) or forearm (dark grey) [3].

Cortical maps can be generated by stimulating at various locations across the motor cortex, using either single electrodes or cortical arrays (such as the Utah array). The resulting muscle activity can be correlated to the location of cortical stimulation, showing which areas of motor cortex produce hindlimb movement. These cortical maps can be compared before and after injury, as well as with and without spinal stimulation. During spinal stimulation, do the hindlimbs reclaim their original cortical space, or do they colonize a new location? How quickly does this reorganization occur (the on/off experiments (Section 4.3.5) suggest this happens in seconds)? Is there an increased latency between stimulation and response? How does muscle activity respond to increased stimulation intensities/frequencies? Is there a change in muscle specificity resulting from the stimulation?

The cortical area can be further dissected using optogenetic tools, like channelrhodopsin [4]. This is a light sensitive protein that when exposed to blue light (480 nm) will trigger neural activity. Unlike electrical stimulation, which indiscriminately activates nearby neurons, channelrhodopsin can be targeted to activate a specific subset of neurons [5]. In particular, it would be interesting to see how the Betz cells (which form a major component of the corticospinal tract destroyed by the spinal injury) are involved in recovery.

5.2.2 – Cortical Recording

Once the important cortical area has been identified, the activity of cortical neurons can be recorded during the beep-kick task. These experiments can be performed using single unit electrodes or cortical arrays. The spiking activity of cortical neurons can be aligned to the onset of the beep, forming raster plots [**Figure 5.2a**]. Cortical activity can be averaged across trials forming peristimulus histograms (PSTH). These are standard tools that will allow the response properties of cortical neurons to be compared before and after injury, and with and without spinal stimulation. Does the activity of these cortical neurons correlate to stimulus onset? To muscle activity? Does the strength of these correlations diminish after injury? Is

there an increased latency between cortical activity and muscle activity? How does this change when the stimulator is turned off (i.e. on/off experiments)?

Calcium imaging is an alternative recording method that could be used during the beep-kick task. Standard electrode arrays have problems with stimulation artifacts, low spatial sampling, and the inability to distinguish cell type. Since calcium imaging uses a fluorescent calcium indicator to monitor neural activity, this method is immune to electrical artifacts that are produced during stimulation of the lumbosacral enlargement [6]. Calcium imaging also records neural activity with a microscope, which captures images with subcellular resolution. This affords a greater sampling of neurons in the cortical area, as well as maintaining their spatial locations. Calcium imaging can also be genetically targeted [7], allowing for finer dissection of the neural circuit, similar to what is afforded with optogenetics. Finally, since calcium imaging preserves both spatial and genetic information, there is the potential to register functional activity with histology in postmortem analysis [8].

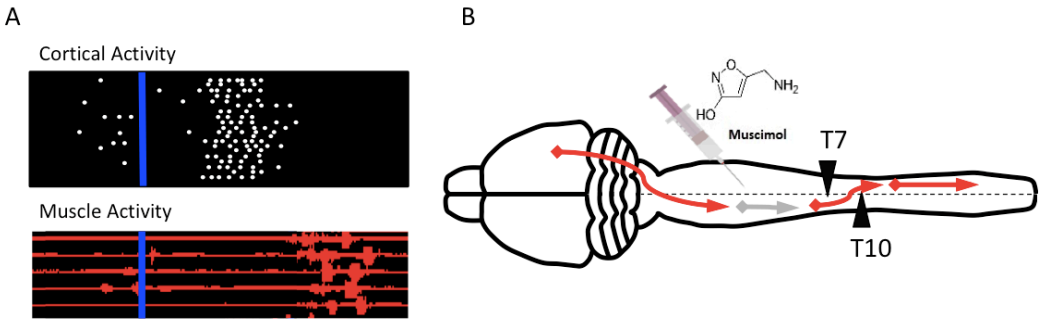

Figure 5.2: A) Cartoon data demonstrating an raster plot for comparing cortical activity with EMG activity during the beep-kick task. Each white dot represents the occurrence of an action potential, an each row corresponds to an individual beep-kick trial. B) Schematic of the multisynaptic daisy chain from the cortex to the spinal circuitry, and the potential for inactivating neurons with an injection of muscimol.

5.2.3 – Cortical Inactivation

A neural inhibitor, such as muscimol, can be injected into specific cortical areas to silence neural activity. If this prevents the animal from performing the beep-kick task, then the brain area is both necessary and sufficient for voluntary movement.

Inactivation studies can also be performed using optogenetic tools, such as halorhodopsin [9]. This is a light sensitive protein that when exposed to yellow light (570 nm) inhibits neural activity. In addition to genetic targeting, halorhodopsin enables precise temporal control. Pharmacological agents such as muscimol inactivate neural tissue for extended periods of time, often several hours, during which the brain may compensate for the lost neural function. Halorhodopsin will inhibit neural activity only when illuminated with yellow light. This enables precise perturbation of the neural circuit that can be performed in real-time during the beep-kick task. Halorhodopsin may cause a different behavioral effect than the pharmacological agents, which may provide insight into the functional properties of the cortical circuit.

5.2.3 – Spinal Inactivation

Since recovery occurs too quickly for the long-range monosynaptic connections to regrow, it is likely that the recovered pathway involves a multisynaptic daisy chain of neurons down the spinal cord. Muscimol can be injected between the vertebra at various spinal levels above, below, and between the injury [**Figure 5.2b**]. Since muscimol targets GABAa receptors, which are located primarily between the dendrites and the cell body, this drug will inactivate neurons populated at the injection site while sparing the axons that pass through. If the inactivation of a specific spinal level causes a loss in behavior, it would suggest that neurons located at that spinal level are part of the recovered pathway. This would lead to targeted histological analysis and therapeutic intervention.

5.2.4 – *Histological Tracing*

Once the cortical area has been located, tracer studies can label neurons along the recovered pathway from the cortex to the spinal circuitry. Anterograde tracers can be injected into the identified cortical region, which will label downstream neurons [10]. The inverse process can be performed in the spinal cord using retrograde

tracers, such as the pseudo rabies virus (PRV), which will propagate upstream towards the cortex [11].

Once these tracers label neurons along the recovered pathway, the tissue must be processed using histological techniques. This could be accomplished with the standard tissue slicing and slide mounting process, or the new histological technique of CLARITY [12,13]. This technique removes lipids from the tissue, rendering it transparent [**Figure 5.3a**]. The transparent tissue can then be imaged without needing to slice and slide mount, which preserves the 3D connections of the neurons and presents a more complete picture of how the tissue is organized. In either case (standard histology or CLARITY) the labeled neurons can then be imaged using immunofluorescence [**Figure 5.3b**]. This process can be used to identify the genetic subtype and spatial location of neurons along the recovered pathway.

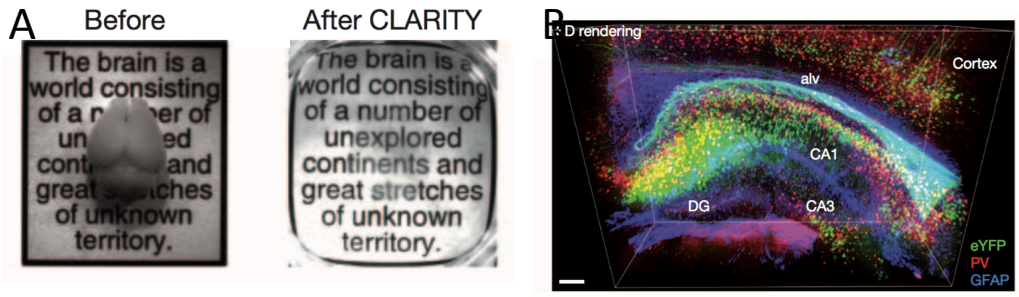

Figure 5.3: A) An example of the CLARITY technique. The tissue is opaque before treatment, but is transparent after treatment. [13] B) Example of 3D imaging of CLARITY tissue after it has been stained with immunofluorescence [12]

5.2.5 – *Modulating the Type of Spinal Injury*

To ensure that the results of the anatomical and functional mapping are not unique to a specific type of injury, we can repeat this mapping process for different spinal injury models. We can flip the sides of the hemisections (from left T7/right T10 to right T7/left T10). We can shift the spinal levels of the injury sites (from T7/T10 to

T6/T9 and so on). We can change injury method from hemisections to contusion models, or even study the effect of destroying individual neural pathways. The functional and anatomical mapping can be repeated to see if there is a characteristic response to a spinal injury, and to identify a consistent set of neurons involved in recovery.

5.2.6 – Optimizing the Stimulation Pattern

The optimal stimulation pattern for recovering voluntary movement is unknown. To improve this recovery, we need to understand how the brain responds to spinal stimulation. The standard 40 Hz stimulation pattern applies a pulse of current to the spinal cord every 25 milliseconds. An electrode can stimulate the cortex at various time points within this 25-millisecond interval, and the resulting EMG activity can be recorded. Studying the strength of the resulting EMG activity will suggest whether there is an ideal time for the cortex to activate the spinal circuitry in response to spinal stimulation. Cortical recordings can then study if the neurons take advantage of this ideal communication time, by calculating the probability of a spike occurring at various intervals between stimulation pulses. These cortical recordings could be performed both in the resting state and during the beep-kick task, to see if behavioral context is important. The stimulation pattern can then be optimized, such as changing the frequency/intensity or adjusting the electrode placements, to increase this communication window.

5.2.7 – *Paired-Pulse Facilitation*

Hebbian learning is thought to be the main mechanism for adjusting synaptic connections between neurons. This mechanism changes synaptic strength based on the relative timing between the firing of upstream and downstream neurons. If the upstream neuron fires before the downstream neuron, the synaptic connection is strengthened. If the downstream neuron fires before the upstream neuron, then the synaptic connection is weakened. We could use this Hebbian learning mechanism to strengthen the recovered pathway after a spinal injury. Motor cortex could be

stimulated, either with cortical electrodes or through noninvasive means such as transcranial magnetic stimulation (TMS) [14], then a few milliseconds later the lumbosacral enlargement can be stimulated. By staggering the timing between cortical stimulation and spinal stimulation we can attempt to strengthen the descending synaptic pathway. This method is referred to as paired-pulse facilitation [15]. The effect of this paired stimulation can be graded based on changes in the recovered EMG power, response latency, and muscle correlation.

5.3 – Spinal Influence on Cortical Encoding

5.3.1 – Cortical Encoding of Movement

The recovery of voluntary movement after a spinal cord injury is a unique opportunity to study how cortical neurons encode movement. There is growing debate about how the firing patterns of cortical neurons translate into movement [16]. Traditionally, cortical activity is modeled in a representational framework, where cortical firing (r) is related to a desired movement parameter (θ), such as force or velocity [17].

$$r = f(\theta).$$

While this has led to early success, it remains unclear which movement parameters are encoded (low-level muscle activity vs. high-level kinematics) [18], or why a significant fraction of neurons show no encoding at all [19]. An emerging argument claims that the representational framework is overly focused on the output of the cortical area, and ignores local connections [20]. To incorporate local processes, cortical activity should instead be modeled as a dynamical system [**Figure 5.4**].

$$\dot{r} = Ar + B\theta.$$

This expands the framework of cortical firing to include not only movement parameters, but also the activity of other neurons in the cortical circuit. Therefore, the local synaptic connections (A) shape the dynamics of the cortical activity, and the desired movement (θ) can influence the cortical circuit by adjusting the firing patterns of the cortical circuit (B).

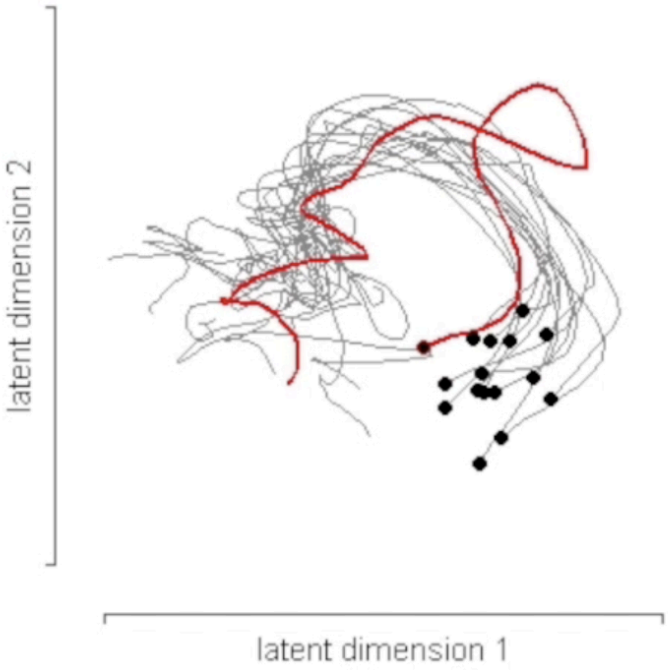

Figure 5.4: Example of dynamical framework. The two main principle components of neural activity recorded from motor cortex of a nonhuman are displayed during a reaching task. Each trace represent a reach performed by the animal, with the black dot representing the state of the cortex at the end of the reach. Each trace follows a similar arc, suggesting there is structure in the dynamics of the cortical activity. The red trace highlights a trial in which the animal had a delayed response. The extended arch of this reach suggests the dynamical framework can captures subtle details about movement. [20]

The recovery of voluntary movement presents a new paradigm for studying the dynamics of cortical activity. A neural population can be recorded before and after injury, and also with and without spinal stimulation. The dynamics can then be compared across conditions to see what aspects are consistent and what changes after injury. This may provide insight into the underlying dynamics necessary for generating voluntary movement. The first region to study is motor cortex, but the analysis can be repeated for different neural structures along the motor control pathway, such as parietal cortex. Do these areas undergo similar reorganization, or does motor cortex act as a firewall, reorganizing internally while presenting the same interface for upstream neural structures?

Also, neural prosthetics research is conducted in intact animals, but translated into injured humans. Cortical activity in the spinalized animal will be more representative of the brain activity of patients suffering from tetraplegia. By studying the injured animal, we may be able to build more clinically relevant models of neural activity, and thus lead to more effective neural prosthetics.

5.3.1 – Modeling of Motor Control

Despite its obvious role in movement, the spinal circuitry is ignored when modeling cortical activity for neural prosthetics. Both the dynamical and representational frameworks assume the spinal cord acts as a passive translator – converting cortical activity into muscle activity. This ignores the complex dynamics contained in the lumbosacral enlargement. Spinal circuits can generate walking patterns, without input from the brain, which is a remarkably complex behavior. In robotics, walking requires sophisticated control systems designed around nonlinear dynamics using advanced mathematical techniques like limit cycles and Poincare maps [21,22,23,24]. The fact that the spinalized animals can produce this behavior implies that the spinal circuitry has complex internal dynamics.

These dynamics in the spinal cord can transform a simple cortical input into a complex motor response. For example, a cortical neuron could trigger the activation of a motor neuron, producing a muscle twitch. This muscle twitch would activate both Renshaw cells [25] and muscle spindles [26], which would feed back into the spinal cord. This motor feedback would be integrated into the spinal circuitry, which could reactivate motor neurons, generating new muscle activity. This would in turn generate a new sensory response, which would again feedback into the spinal cord, and the process would repeat. To further complicate things, the muscle response from a cortical input may depend on its timing in the gait cycle. Therefore, cortical neurons must either have a mechanism for shutting off the spinal circuitry (which is unlikely) or they must account for these spinal dynamics.

This further expands the modeling of cortical activity to include the state of the spinal circuitry (s) [**Figure 5.5a**]:

$$\dot{r} = Ar + B\theta + Cs.$$

In this case, ascending synaptic projections (C) from the spinal cord allow spinal activity (s) to influence cortical activity.

Movement could therefore be seen as the product of a series of coupled dynamical systems. The output of the cortex is incorporated into the internal dynamics of the spinal circuitry, along with state information about the body (x) [**Figure 5.5b**]:

$$\dot{s} = A_2 s + B_2 r + C_2 x.$$

In this case, A_2 is the synaptic wiring of the spinal circuitry, B_2 are the descending projection from the cortex, and C_2 is sensory feedback from the body. The spinal circuitry then generates muscle activity that applies a force on the body, which itself is governed by the dynamics of gravity acting on its limbs: [**Figure 5.5c**]

$$\dot{x} = A_3 x + B_3 s.$$

In this case, A_3 captures the physics of gravity acting on the body and B_3 captures the forces generated by the spinal circuitry contracting the muscles.

Conceptually, this can be viewed as hierarchical motor control. The body naturally wants to obey the force of gravity [**Figure 5.5f]**, but the spinal circuitry stabilizes movement by applying a first level of control, such as a limit cycle for walking [**Figure 5.5e]**. The cortex can then control movement by influencing the state of the spinal circuitry, such as adjusting the shape of the limit cycle [**Figure 5.5d]**. In this configuration, the cortex can focus on higher-level motor commands, and relegate the lower-level muscle coordination to the spinal circuits.

This modeling is important because neural prosthetics is in effect an attempt to emulate the spinal circuitry. These devices take in cortical activity and produce movement, which is exactly the task of the spinal circuits. Understanding how the spinal circuitry accomplishes this task will improve the design of these devices,

hopefully one day making them a practical treatment for paralyzed patients. For this to be successful, new methods are needed to record from large-scale neural populations in the spinal cord. This has proven difficult because the spinal cord is encased in bone and flexes during movement, making it infeasible to insert rigid electrodes.

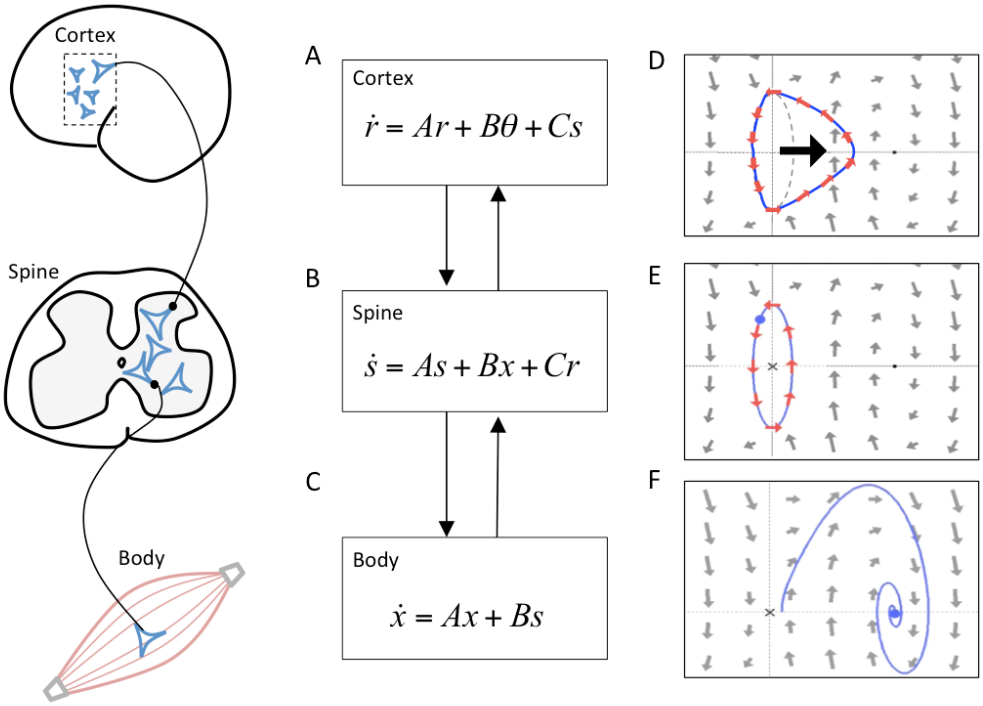

Figure 5.5: Motor Control As A Series of Coupled Dynamical Systems. A) Cortical activity incorporates the desired action (theta) with the state of the spinal cord (s) into its internal dynamics. B) The spinal circuitry incorporates the cortical activity (r) and the state of the body (x) into its dynamics. C) The body then moves according the dynamics of gravity and the muscle activity generated by the spinal circuitry. D,E,F) The visualization of these dynamical systems as an inverted pendulum moving through state-space [Tedrake]. F) The body wants to naturally follow the force of gravity. E) The spinal cord applies the first level of control by implementing a limit cycle. D) The cortex can control movement by adjusting the shape this limit cycle.

5.4 – Therapeutic Experiments

Mobility is only one concern for patients suffering from spinal injury. Paraplegics also rank sexual function, bladder/bowel control, heart rate, blood pressure, and chronic pain as critical factors in their quality of life [27] (**Figure 5.6**). Despite

being specifically designed to assist mobility, spinal stimulation helps with these issues [1]. To improve these therapeutic side effects, new experimental paradigms must be created.

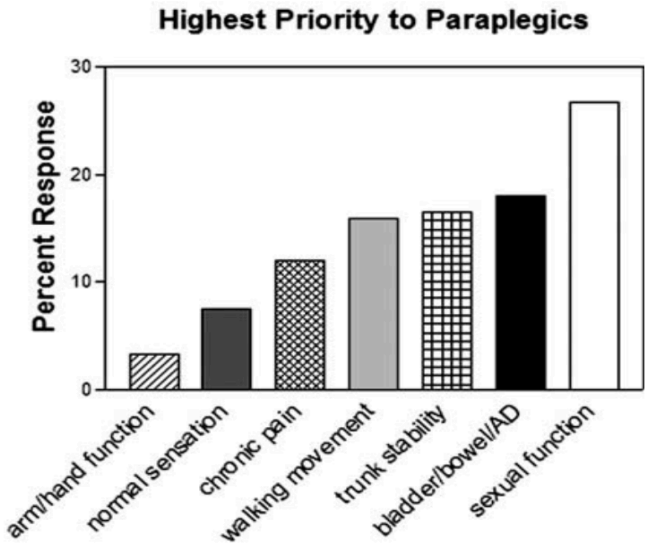

Figure 5.6: Survey response from paraplegic patients ranking priorities in quality of life. [27]

5.4.1 – Bladder Control Studies

Prior to 1970, bladder and kidney problems were responsible for 75% of deaths of patients suffering from spinal cord injury [28]. While there has been significant improvement in the treatment of the urinary system, bladder issues still affect a large majority of paraplegic and quadriplegic patients [29]. Current work is focused on the effect of spinal stimulation on the bladder [30,31]. Since spinal stimulation enables the voluntary control of the legs, it is likely that this stimulation can also improve voluntary control of the bladder. To study voluntary bladder control we need to develop new animal models to tease apart the neural circuit and to optimize the treatment.

An example experiment would be training rodents to voluntarily void their bladders. The animal's bladder could be filled using a catheter, and then a cue to

urinate could be issued. If the rodent successfully urinates they would be given a reward, and the process would be repeated. During this task, the catheter could monitor bladder pressure and EMG electrodes could record the activity of the urethral sphincter. After the animal learns to urinate on cue, a spinal injury could be induced. The animal could then be treated with spinal stimulation and rerun through the voluntary urination task. The bladder pressure and EMG activity can be compared before and after injury.

The treatment can then be optimized by adjusting the electrode placements, altering the stimulation patterns, or administering different drugs. The contribution of supraspinal input can be explored using the same methods described for mapping out the recovery of voluntary movement.

5.5 – Computational Problem

In addition to being an important biological discovery, the recovery of voluntary movement is fascinating from a computational perspective. The connection between the brain and the spinal circuitry is destroyed after injury. For a new pathway to form, the brain and spinal circuitry must test different descending and ascending connections. The success of these connections depends on the spinal circuitry and the brain listening to the same pathway concurrently. This must occur in a decentralized manner (i.e. without the brain or the spinal circuitry knowing what the other is attempting), and using neurons as the fundamental units of communication. The brain and the spinal circuitry will not know where the new pathway will occur or how to use it. There must be some decentralized rule followed by both the brain and the spinal circuitry that does not rely on a clear feedback mechanism. In effect, the recovery of voluntary movement is a biological example of a neural network performing unsupervised learning [33,34]. Understanding how the nervous system solves this problem could have important implications in the field of artificial intelligence for understanding the formation of neural networks.

5.6 – Conclusion

We live at an exciting time in the history of neuroscience. Advances in technology allow us to observe and interact with the nervous system in real-time. Results from this work are providing deep insights into the inner workings of our nervous system and has potential to profoundly impact the lives of people suffering from spinal injury in the very near term. This work lies at an incredible intersection between biology, mathematics, engineering, and medicine and is a rare opportunity to progress in lock step towards greater scientific knowledge and a humanitarian good.

5.7 – CITATIONS

[1] Harkema, Susan, et al. "Effect of epidural stimulation of the lumbosacral spinal cord on voluntary movement, standing, and assisted stepping after motor complete paraplegia: a case study." *The Lancet* 377.9781 (2011): 1938-1947.

[2] Neafsey, E. J., et al. "The organization of the rat motor cortex: a microstimulation mapping study." *Brain research reviews*11.1 (1986): 77-96.

[3] Sanes, Jerome N., et al. "Rapid reorganization of adult rat motor cortex somatic representation patterns after motor nerve injury." *Proceedings of the National Academy of Sciences* 85.6 (1988): 2003-2007.

[4] Nagel, Georg, et al. "Channelrhodopsin-2, a directly light-gated cation-selective membrane channel." *Proceedings of the National Academy of Sciences* 100.24 (2003): 13940-13945.

[5] Zhang, Feng, et al. "Channelrhodopsin-2 and optical control of excitable cells." *Nature methods* 3.10 (2006): 785.

[6] Histed, Mark H., Vincent Bonin, and R. Clay Reid. "Direct activation of sparse, distributed populations of cortical neurons by electrical microstimulation." *Neuron* 63.4 (2009): 508-522.

[7] Tian, Lin, et al. "Imaging neural activity in worms, flies and mice with improved GCaMP calcium indicators." *Nature methods* 6.12 (2009): 875.

[8] O'shea, Daniel J., et al. "The need for calcium imaging in nonhuman primates: New motor neuroscience and brain-machine interfaces." *Experimental neurology* 287 (2017): 437-451.

[9] Gradinaru, Viviana, Kimberly R. Thompson, and Karl Deisseroth. "eNpHR: a Natronomonas halorhodopsin enhanced for optogenetic applications." *Brain cell biology*36.1-4 (2008): 129-139.

[10] Veenman, C. Leonardus, Anton Reiner, and Marcia G. Honig. "Biotinylated dextran amine as an anterograde tracer for single-and double-labeling studies." *Journal of neuroscience methods* 41.3 (1992): 239-254.

[11] Strack, A. M., et al. "CNS cell groups regulating the sympathetic outflow to adrenal gland as revealed by transneuronal cell body labelling with pseudorabies virus." *Brain research* 491.2 (1989): 274-296.

[12] Chung, Kwanghun, and Karl Deisseroth. "CLARITY for mapping the nervous system." *Nature methods* 10.6 (2013): 508.

[13] Chung, Kwanghun, et al. "Structural and molecular interrogation of intact biological systems." *Nature* 497.7449 (2013): 332.

[14] Nakamura, Hiroshi, et al. "Intracortical facilitation and inhibition after transcranial magnetic stimulation in conscious humans." *The Journal of physiology* 498.3 (1997): 817-823.

[15] Manabe, T. O. S. H. I. Y. A., et al. "Modulation of synaptic transmission and long-term potentiation: effects on paired pulse facilitation and EPSC variance in the CA1 region of the hippocampus." *Journal of neurophysiology* 70.4 (1993): 1451-1459.

[16] Shenoy, Krishna V., Maneesh Sahani, and Mark M. Churchland. "Cortical control of arm movements: a dynamical systems perspective." *Annual review of neuroscience* 36 (2013).

[17] Georgopoulos, Apostolos P., et al. "On the relations between the direction of two-dimensional arm movements and cell discharge in primate motor cortex." *Journal of Neuroscience*2.11 (1982): 1527-1537.

[18] Kalaska, John F. "From intention to action: motor cortex and the control of reaching movements." *Progress in Motor Control*. Springer, Boston, MA, 2009. 139-178.

[19] Evarts, EDWAHD V. "Pyramidal tract activity associated with a conditioned hand movement in the monkey." *Journal of Neurophysiology* 29.6 (1966): 1011-1027.

[20] Churchland, Mark M., et al. "Neural population dynamics during reaching." *Nature* 487.7405 (2012): 51.

[21] Garcia, Mariano, et al. "The simplest walking model: stability, complexity, and scaling." *Journal of biomechanical engineering* 120.2 (1998): 281-288.

[22] Russ Tedrake. Underactuated Robotics: Algorithms for Walking, Running, Swimming, Flying, and Manipulation (Course Notes for MIT 6.832).

[23] McGeer, Tad. "Passive dynamic walking." *I. J. Robotic Res.*9.2 (1990): 62-82.

[24] Grizzle, Jessy W., Gabriel Abba, and Franck Plestan. "Asymptotically stable walking for biped robots: Analysis via systems with impulse effects." *IEEE Transactions on automatic control* 46.1 (2001): 51-64.

[25] Thomas, R. C., and V. J. Wilson. "Precise localization of Renshaw cells with a new marking technique." *Nature*206.4980 (1965): 211.

[26] Matthews, P. B. C. "Muscle spindles and their motor control." *Physiological Reviews* 44.2 (1964): 219-288.

[27] Anderson, Kim D. "Targeting recovery: priorities of the spinal cord-injured population." *Journal of neurotrauma* 21.10 (2004): 1371-1383.

[28] Schurch, Brigitte, Cécile Tawadros, and Stefano Carda. "Dysfunction of lower urinary tract in patients with spinal cord injury." *Handbook of clinical neurology*. Vol. 130. Elsevier, 2015. 247-267.

[29] Schurch, Brigitte, Cécile Tawadros, and Stefano Carda. "Dysfunction of lower urinary tract in patients with spinal cord injury." *Handbook of clinical neurology*. Vol. 130. Elsevier, 2015. 247-267.

[30] Gad, Parag N., et al. "Neuromodulation of the neural circuits controlling the lower urinary tract." *Experimental neurology*285 (2016): 182-189.

[31] Gad, Parag N., et al. "Initiation of bladder voiding with epidural stimulation in paralyzed, step trained rats." *PloS one* 9.9 (2014): e108184.

[32] Harkema, Susan, et al. "Effect of epidural stimulation of the lumbosacral spinal cord on voluntary movement, standing, and assisted stepping after motor complete paraplegia: a case study." *The Lancet* 377.9781 (2011): 1938-1947.

[33] Hertz, John, Anders Krogh, and Richard G. Palmer. *Introduction to the theory of neural computation*. Addison-Wesley/Addison Wesley Longman, 1991.

[34] Hastie, Trevor, Robert Tibshirani, and Jerome Friedman. "Unsupervised learning." *The elements of statistical learning*. Springer, New York, NY, 2009. 485-585.

[35] Desmurget, Michel, and Scott Grafton. "Forward modeling allows feedback control for fast reaching movements." *Trends in cognitive sciences* 4.11 (2000): 423-431.

Appendix A: Brain-Machine Interface

A.1 – Model Reduction

To simplify the telegraphers equations used for modeling deep brain recordings, the size of the inductance, resistance, conductance, and capacitance terms were calculated:

Inductance

$L_m = \mu_0 \pi r^2 = 10^{-7} \pi (10^{-4})^2 = \pi * 10^{-15}.$

$L_m = 0.$

Resistance

$R_m = \frac{\rho_w}{\pi r^2} = \frac{10^{-7}}{\pi (10^{-4})^2} = \frac{1}{\pi} * 10.$

$R_m \neq 0.$

Conductance

$G_i = \frac{2\pi}{\rho_i \ln \alpha} = \frac{2\pi}{10^{16} \cdot 10^{-2}} = 2\pi\ 10^{-14}.$

$G_i = 0.$

Capacitance

$C_i = \frac{2\pi\ \varepsilon_0 k_i}{\ln \alpha} = \frac{10^{-11} \cdot 1 \cdot 10}{10^{-2}} = 10^{-8} = 10pF.$

$C_i \neq 0.$

The size of these values suggests we can ignore the inductance and conductance terms.

A.2 – Stimulation Derivation

The effect of capacitive coupling during deep brain stimulation was derived by convolving the insulation filter with various stimulation waveforms. The first step was to simply the calculation.

Filter Form:

$$H = A(r) \cdot \frac{j\omega}{B + j\omega}.$$

$$h = A(r) \cdot \left(\delta(t) - Be^{-Bt} \cdot u(t)\right).$$

Voltage Definition:

$$v_{tissue} = h * v_{stim} = \int_{-\infty}^{+\infty} h(t-\tau) \cdot v_{stim}(\tau)\, d\tau.$$

$$v_{tissue} = A(r) \cdot \left[v_{stim} - B \int_{-\infty}^{+\infty} e^{-B(t-\tau)} \cdot u(t-\tau) \cdot v_{stim}(\tau)\, d\tau\right]$$

$$= A(r) \cdot \left[v_{stim} - Be^{-Bt} \int_{-\infty}^{t} e^{B\tau} \cdot v_{stim}(\tau)\, d\tau\right]$$

$$= A(r) \cdot [v_{stim} - v^*_{stim}].$$

$$v^*_{stim} = Be^{-Bt} \int_{-\infty}^{t} e^{B\tau} \cdot v_{stim}(\tau)\, d\tau.$$

Next, the voltage in the tissue was calculated for either a rectangular wave of a decaying exponential:

Rectangular Wave

$$v_{stim} = C \cdot [\, u(t+D) - u(t-D)].$$

$$v^*_{stim} = Be^{-Bt} \int_{-\infty}^{t} e^{B\tau} \cdot C \cdot [\, u(\tau+D) - u(\tau-D)]\, d\tau$$

$$CBe^{-Bt} \cdot \left[\int_{-D}^{t} e^{B\tau} d\tau \cdot u(t+D) - \int_{D}^{t} e^{B\tau}\, d\tau \cdot\ u(t-D)\right]$$

$$CBe^{-Bt} \cdot \frac{1}{B}([e^{Bt} - e^{-BD}] \cdot u(t+D) - [e^{Bt} - e^{BD}] \cdot u(t-D))$$

$$C \cdot ([1 - e^{-B(t+D)}] \cdot u(t+D) - [1 - e^{-B(t-D)}] \cdot u(t-D))$$

$$C \cdot \big(u(t+D) - u(t-D)\big) - C \cdot \big[e^{-B(t+D)} \cdot u(t+D) - e^{-B(t-D)} \cdot u(t-D)\big].$$

$$v_{stim}^{*} = v_{stim} - C \cdot \big[e^{-B(t+D)} \cdot u(t+D) - e^{-B(t-D)} \cdot u(t-D)\big] \ .$$

$$v_{tissue} = A(r) \cdot \Big[v_{stim} - \Big[v_{stim} - C \cdot \Big(e^{-B(t+D)} \cdot u(t+D) - e^{-B(t-D)} \cdot u(t-D)\Big)\Big]\Big].$$

$$v_{tissue} = A(r)C \cdot \Big(e^{-B(t+D)} \cdot u(t+D) - e^{-B(t-D)} \cdot u(t-D)\Big).$$

Decaying Exponential

$$v_{stim} = Ce^{-Dt} \cdot u(t).$$

$$v_{stim}^{*} = Be^{-Bt} \int_{-\infty}^{t} e^{B\tau} \cdot Ce^{-D\tau} \cdot u(\tau)\, d\tau$$

$$= CBe^{-Bt} \int_{0}^{t} e^{(B-D)\cdot\tau}\, d\tau \ \cdot u(t)$$

$$= CBe^{-Bt} \cdot \frac{1}{B-D}\big(e^{(B-D)t} - 1\big) \cdot u(t)$$

$$= \frac{B}{B-D}(Ce^{-Dt} - Ce^{-Bt}) \cdot u(t).$$

$$v_{stim}^{*} = \frac{B}{B-D} \cdot \big(v_{stim} - Ce^{-Bt} \cdot u(t)\big).$$

$$v_{tissue} = A(r) \cdot \Big[v_{stim} - \frac{B}{B-D} \cdot \big(v_{stim} - Ce^{-Bt} \cdot u(t)\big)\Big].$$

$$v_{tissue} = \frac{A(r)}{B-D} \cdot \big[(B-D)v_{stim} - B \cdot \big(v_{stim} - Ce^{-Bt} \cdot u(t)\big)\big].$$

$$v_{tissue} = \frac{A(r)C}{B-D} \cdot [B\, e^{-Bt} - De^{-Dt}] \cdot u(t).$$

Since D << 1

$$v_{tissue} = A(r)C\, e^{-Bt} \cdot u(t).$$

.

Appendix B: Neural Prosthetics

B.1 – Surgery

All surgical and animal care procedures were done in accordance with the National Institutes of Health Guide for the Care and Use of Laboratory Animals and were approved by the California Institute of Technology Institutional Animal Care and Use Committee. Monkey M and monkey R underwent two surgical procedures, a) head-post implantation and b) array implantation. Both procedures were performed using aseptic techniques and with the animal under anesthesia. A dedicated surgical technician continuously monitored the animal's vital signs (such as heart rate, body temperature) and adjusted the level of anesthesia accordingly. Following the procedures the animals were placed under observation to ensure proper recovery and to look for signs of distress. The animals were administered painkillers and antibiotics for the week following both procedure. The head-post implantation occurred a few months before the array implantation. Surgical procedures were similar for both monkey M and monkey R, so only the surgery for monkey M will be discussed.

B1.1 – Head-post Implantation

To protect the connections to the neural amplifiers and to restrict the animal's head movement, a head-post was fixed to the top of the animal's cranium. This procedure was performed by trained scientists and lab members. An incision was made on the top of the head, and the skull was exposed. A series of bone screws were embedded around the skull such that they were rigidly fixed into the bone but did not penetrate into the brain. Bone screws were not placed onto the portion of the skull that would be later removed during the array implantation. A mixture of dental acrylic was applied, and a head-post mount was pushed into the mixture. The mixture hardened around the heads of the bone screws and the base of the head-post, forming a rigid structure on the skull of the animal. The hardening of acrylic is an exothermic reaction, so the temperature of the skull was monitored and cooled to

protect the animal. After the surgery, the animal received weekly cleaning of the margin between the skin and the dental acrylic to prevent infection and to look for signs of damage.

B1.2 – Array Implantation

To record neural activity, two high-density electrode arrays were implanted onto the surface of the animal's cortex (one in area 5d of the parietal cortex and one in motor cortex). Prior to the array implantation, the animal underwent an anatomical MRI scan. This scan identified the stereotaxic positions of the desired array locations. Area 5d was defined as medial to the postcentral dimple, abutting the intraparietal sulcus. Motor cortex was defined as medial to the spur of the arcuate sulcus, abutting the central sulcus. The array implantation was performed by a team of neurosurgeons from USC and UCLA, as practice for human implantation. The animal was placed in a stereotaxic mount using eye-bars and ear-bars. The dental acrylic covering the desired portion of the skull was removed, and the border of a craniotomy was drawn encompassing the stereotaxic positions of area 5d and motor cortex. A craniotomy was performed and the portion of the skull was set aside. The Dura was cut along three of the four sides of the craniotomy and was peeled back.

At this stage, the locations of area 5d and motor cortex were visually identified, and the electrode arrays were positioned accordingly. Positioning was a complex process of ensuring the arrays sat flush to the cortex and the wire bundle leading from the array to the percutaneous connector was unkinked. Once positioned, the arrays were inserted using a stereotaxically-mounted impactor. The impactor was a piston that applied a brief but controlled force onto the surface of the array. This caused the tips of the electrode arrays to pierce through the arachnoid layer and enter into the neural tissue. The wire bundle was fixed onto the skull using a series of dog-bone mounts. After both the parietal and motor arrays were inserted, the Dura was sutured back into place. The portion of skull removed during the craniotomy was replaced and secured in place. To protect the wire bundles, the

portion of skull was shaved around the areas were the wire bundles transitioned from the cortex onto the skull.

The percutaneous connectors were fixed onto the acrylic surface on the opposite side of the skull using an additional layer of dental acrylic. Care was taken to ensure the two connectors were positioned far enough apart that connecting cables could fit onto both connectors simultaneously. The craniotomy was then covered in dental acrylic to protect the brain area and to embed the wire bundles.

B.2 – Experimental Equipment

B.2.1 – Neural Recordings

Neural activity was recorded simultaneously from the electrode arrays (Utah) using neural signal processors (Blackrock Microsystems). These processors recorded three versions of the neural activity: spikes, local field potentials, and wideband. The spike signal was a collection of waveforms recorded every time the high-pass filtered versions of neural activity (> 1KHz) crossed a threshold. The local field potential was a low-passed version of the neural activity containing all the frequencies below 100 Hz (this signal was never used). The wideband signal was the raw neural activity sampled at the full 40 kHz, and was recorded in case the spike signal was corrupted and needed to be recomputed.

Since a single electrode can record from multiple neurons simultaneously, the waveforms in the spike signal are generated from an unknown number of neurons. Often times this raw collection is used directly as a neural signal, but this will contain a lot of noise and may not be adequate for analysis. Since a neuron produces a consistent and unique waveform every time it fires, the waveforms can be grouped into clusters according to their shape. This was accomplished using an offline spike sorter (Plexon), which clustered the waveforms according to their three main principle components. [**Fig B.1**] The shapes of these clusters were set to

follow a T-distribution, which has a sharper fall off than the traditional Gaussian distribution. The number of clusters was computed using an expectation-maximization algorithm, which balances the goodness-of-fit of the clustering against how many clusters it includes. This spike sorting processes was executed in an unsupervised manner to avoid injecting bias into the data.

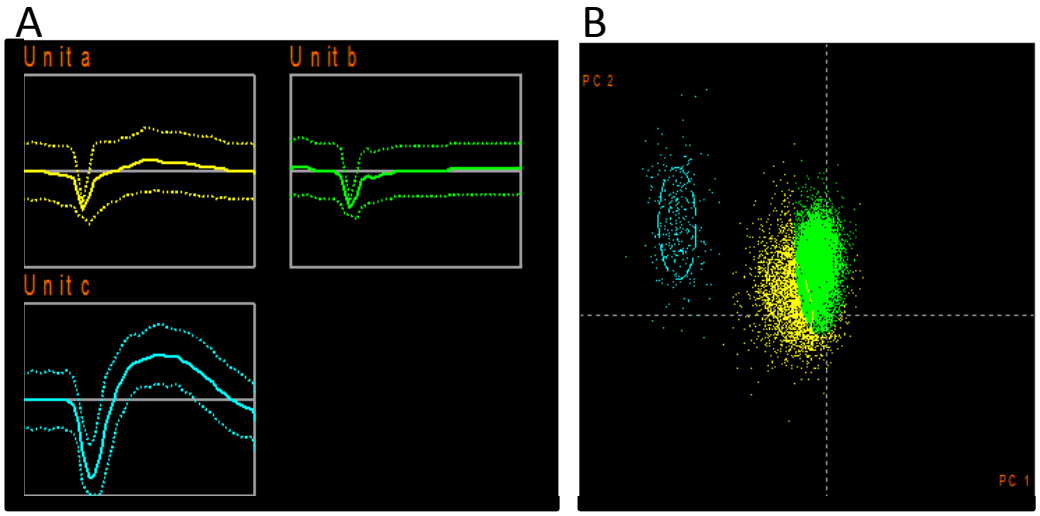

Figure B.1: A) Example neural units recorded from a single electrode (Plexon Offline Sorter). B) Clusters of waveforms plotted along the first two principle component axis.

B.2.2 – Experimental Rig

A custom experimental rig was built for each nonhuman primate [**Fig B.2**], but these systems were similar enough that only the rig for monkey M will be discussed. The main component of this rig was a computer running the MATLAB XPC real-time operating system. Traditional operating systems (such as Windows, OS X, and most forms of Linux) use scheduling software, which introduces a random delay between the time a command is issued and when it is executed. These random delays must be avoided because the experiments rely on the precise timing of images on a monitor and on the alignment of neural activity with the hand position. The XPC operating system avoids these delays by loading a Simulink model and executing it precisely every millisecond. This model ran the task logic, recorded the hand position, decided which images to display, issued rewards,

measured system latency, and emitted a timing signal to align neural activity. A control computer interfaced with this Simulink model to update task parameters, such as the size of the objects, the position of the obstacle, and the timing of the task.

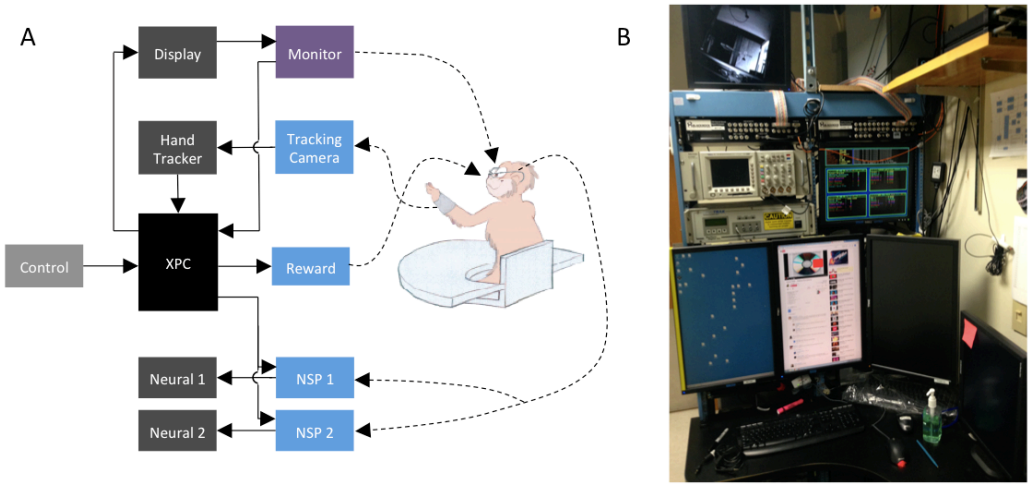

Figure B.2: A) Experimental system for the nonhuman primates [block diagram] B) Experimental system for the nonhuman primate [photograph]

The visual computer was in charge of displaying all of the objects to the animal. This computer ran custom MATLAB software, using the Psychophysics Toolbox. This toolbox is specifically designed for extremely precise control of the computer display. This computer received the object locations and their sizes from the XPC computer, and would update the display within the next frame refresh. The display for the animal was custom built using a high-performance gaming monitor (BenQ). This gaming monitor is specifically designed to have low latency between issuing a display command and the pixels changing on the screen. The monitor was removed from its casing and placed in a custom mount that would lock horizontally into the chair the animal sat in [**Fig B.3**]. This monitor laid flat on the mount, such that the animal would look down on it. The mount was elevated from the chair using a set of bolts, which made a space for the animals to perform their reaches underneath.

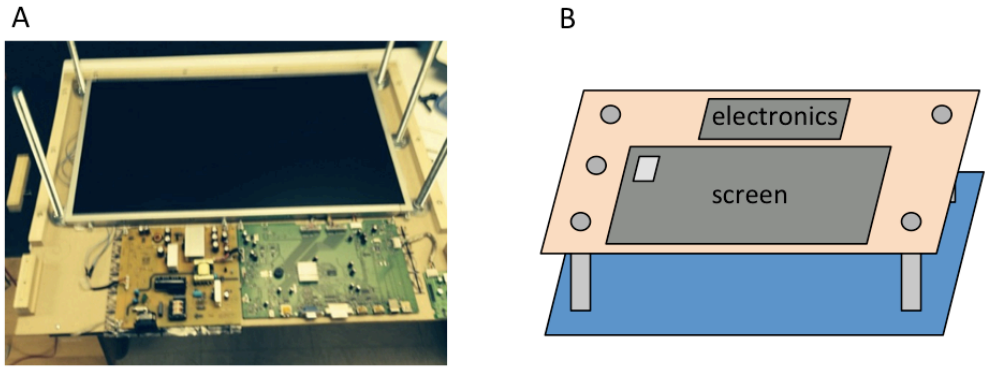

Figure B.3 A): Visual display without Plexiglas cover [photograph] B): Visual display [3D schematic]

The latency of the entire system was monitored using a custom-built photodetector [**Fig B.4a,b**]. The detector was positioned over an illuminated square in the top corner of the animal's monitor. The XPC system sent a command to the visual computer to toggle the color of this square between black and white. The XPC system also recorded the voltage from the photodetector. The latency of the system was measured by comparing the time between issuing the toggle command and the change in the photodetector voltage. With the use of the BenQ gaming monitor, the system latency was measured to be 17ms.

The 3D position of the hand was captured using a bank of cameras (Optotrak). These cameras imaged an LED on a bracelet, which was temporarily fastened to the animal's wrist. [**Fig B.4c,d**]. The hand-tracking computer extracted the 3D position of the LED from these images, and transmitted its location to the XPC computer. The position of the tracking bracelet was updated every 5 milliseconds.

Rewards were issued using custom circuitry connected to a beaker of fruit-juice. The XPC computer would issue a reward signal that opened a solenoid valve, allowing the liquid to flow. Rewards could also be issued manually with the press of a button. Liquid rewards were preferred to food rewards because muscle activity from chewing interferes with the electrode arrays.

Two neural signal processors (Blackrock Microsystem) recorded neural activity from the electrode arrays (Utah). These signal processors also recorded the timing signal from the XPC computer, which was later used to align the neural activity with the animal's behavior. Each neural signal processor had a dedicated computer, which saved the neural activity to its hard drive.

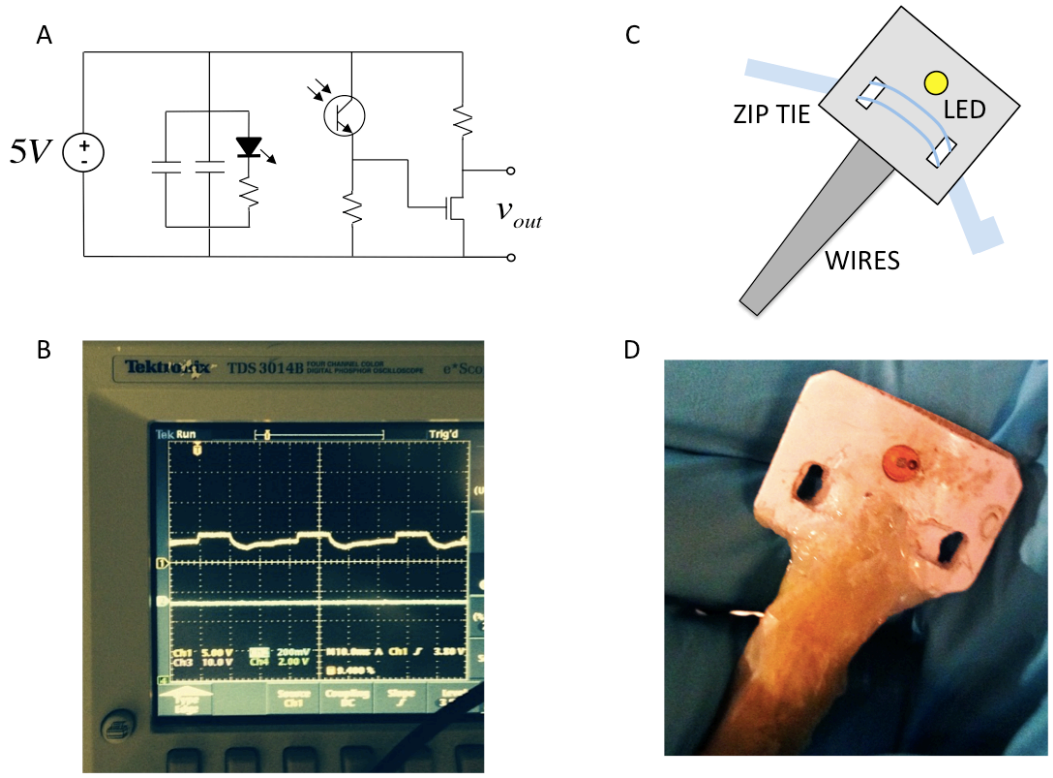

Figure B.4: A) Electrical circuit diagram for photodiode. B) Oscilloscope displaying timing signal [photograph] C) Tracking bracelet [schematic] D) Tracking bracelet (after some wear) [photograph]

B.2.3 – Analysis Computer

Data analysis was performed on a custom built computer running the 64-bit version of the Windows 10 operating system. The computer was installed with 24 gigabytes of RAM and two Intel® Xeon® X5680 processors. Each processor contained 6 cores, resulting in a total of 12 available processing cores. Data analysis code was written in the MATLAB programming language using the Parallel Computing

Toolbox. Data files from the Blackrock and Plexon systems were imported into MATLAB using the software development kits (SDK) provided by each company. The data recorded during experimental sessions and the data produced by the analysis were saved to a 20-terabyte network drive, configured in a RAID array.

Appendix C: Spinal Stimulation

C.1 – Surgery

All surgical and animal care procedures were done in accordance with the National Institutes of Health Guide for the Care and Use of Laboratory Animals and were approved by the University of California Los Angeles Institutional Animal Care and Use Committee. Rodents underwent two surgical procedures; an implantation, followed a month later with a spinalization. Trained surgical staff performed both surgical procedures using isoflurane anesthesia (1-2.5% via facemask) and aseptic techniques. The level of anesthesia was continuously monitored during both procedures. After each procedure, the animal was placed under observation and was administered fluids, painkillers (bupernex / carprofen), and antibiotics (baytril).

C.1.1 – Implant Surgery

The electrode implantation has been described previously. The implant consisted of insulated stainless steel wires (AS632, Cooner Wire) soldered into a percutaneous head-plug connector. Under aseptic conditions and isoflurane anesthesia (1-2.5% via facemask), incisions were made on top of the skull and over the desired muscle groups. The wires were fed under the skin from the skull to the desired muscle. A small notch was cut into the insulation of each wire to expose the underlying metal, which formed the electrode site.

All six of the treated rodents had bipolar intramuscular EMG electrodes embedded into soleous (Sol), tibalis anterior (TA), vastus lateralis (VL), and sartorius (ST) muscles of the right (trained) hindlimb. Four of these rodents had an additional EMG electrode embedded into the tibalis anterior (TA-L) of the left (untrained) hindlimb. The control and sham rodents had electrodes embedded only in the tibalis anertior of the right (trained) hindlimb. EMG wires were threaded through each muscle using a cannula. The wire was adjusted to embed the electrode site in the

belly of the muscle [**Fig C.1a**], and secured with a knot of suture at its entry and exit point.

The stimulating electrodes were embedded by first performing a partial laminectomy over the L2 and the S1 spinal levels. The stimulating electrodes were passed under the spinous process, and sutured to the midline of the Dura above and below the electrode site [**Fig C.1b**]. A set of common ground wires was inserted subcutaneously in the mid-back region. The percutaneous head-plug was fixed to the skull using bone-screws and dental cement.

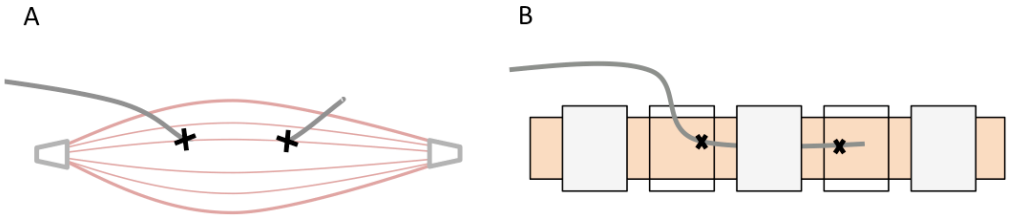

Figure C.1: A) EMG implant [schematic] B) Epidural implant [schematic]

C.1.2 – Spinalization Surgery

A laminectomy was performed at spinal levels T7 and T10 by incising the skin and separating the musculature over ~T6-T11. A small incision was made in the Dura just left of the midline of the spinal cord at spinal level T7, and a left over-hemisection was performed via aspiration. The same technique was used on the opposite side of the spinal cord to create the right hemisection at spinal level T10. The muscle and skin was then sutured closed with 4-0 Vicryl and Ethilon respectively. The bladder was manually expressed three times a day for two weeks, until reflex voiding was established.

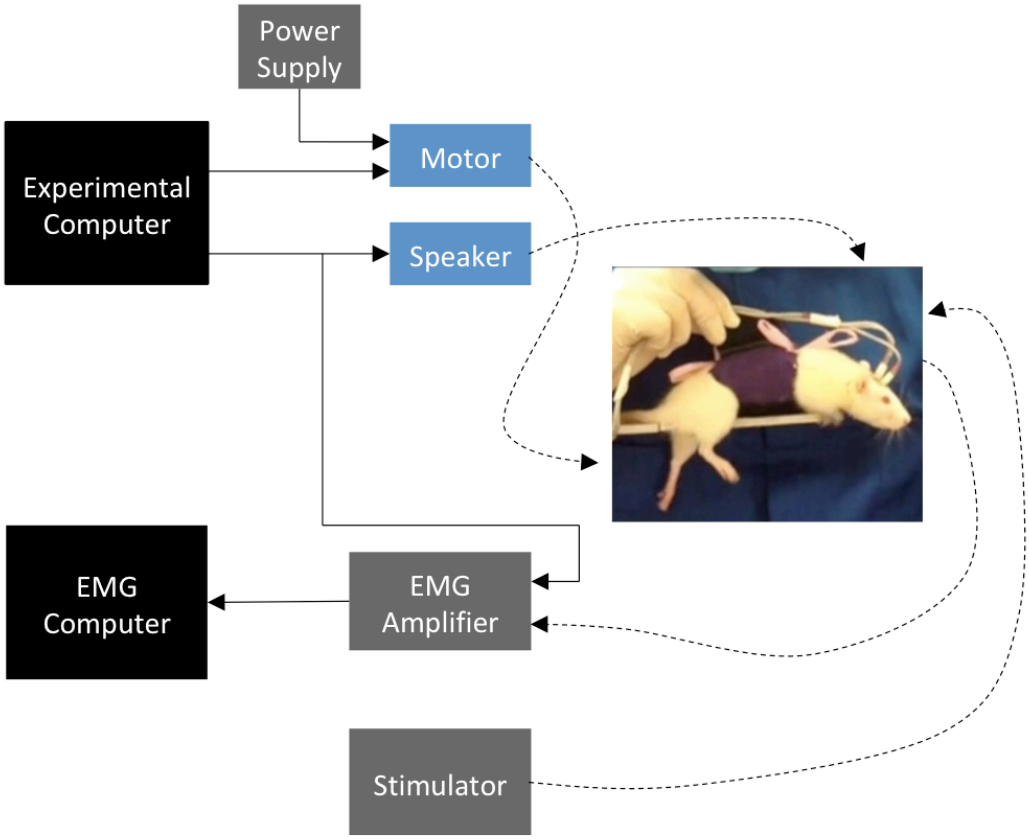

Figure C.2: A block diagram of the experimental system for rodents

C.2 – Equipment

C.2.1 – Experimental Setup

Experiments were conducted using a computer running custom MATLAB software. [**Fig C.2**] This software would play a sound through a speaker at a random interval. The experimenter could control the number of trials per minute by adjusting the range of this interval. For the beep-kick task, the sound was a pure 3kHz tone. For the startle task, the sound was white noise, and for the novel task, the sound was a chirp. The sound card of the computer was connected to a Y-splitter, which routed to the speaker and to the recording computer. The MATLAB software also controlled the vibrating motor used during training. A few hundred milliseconds after the sound played, the software toggled on and off a port on a data

acquisition card [NI USB-6281]. Custom circuitry used this port to drive the vibrating motor. Adjusting the voltage of the power supply to the circuit controlled the intensity of the vibration. [**Fig C.3**]

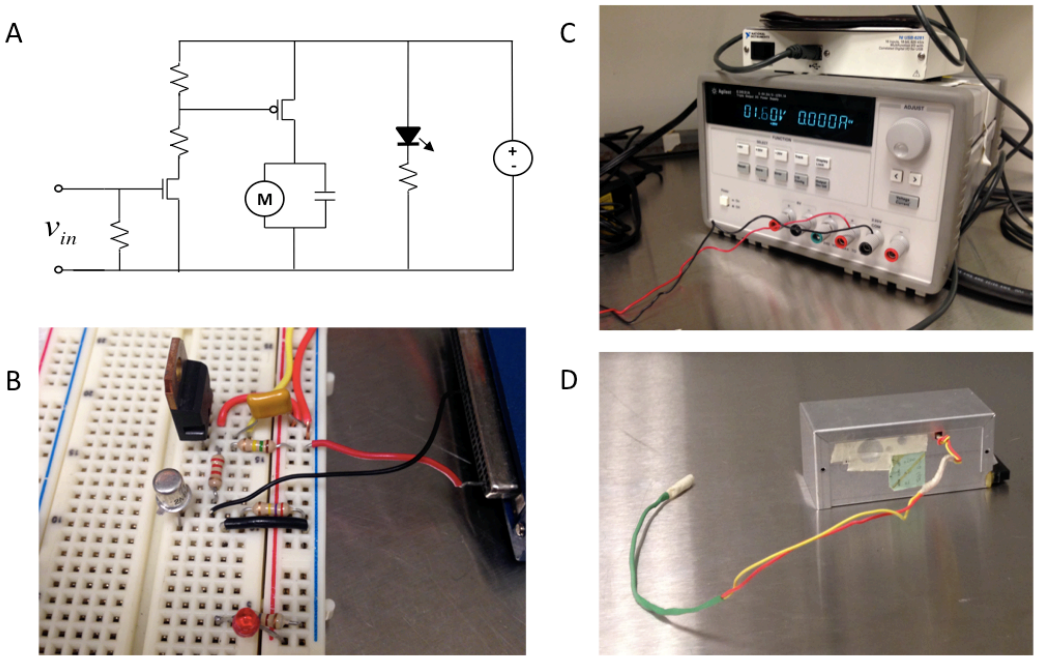

Figure C.3: A) Circuit diagram for driving the vibrating motor B) Prototype used to drive the vibrating motor [photograph] C) Variable power supply used to adjust intensity of vibration [photograph] D) Vibrating motor and the enclosed electrical circuit [photograph]

C.2.2 – Harness and Mount

During the beep-kick task, rodents were secured in place using a cloth harness. The harness was a strip of cotton that was secured around the waist of the animal using Velcro and a set of drawstrings [**Fig C.4a**]. On the belly of the harness was another piece of Velcro that coupled to the experimental mount. The mount was a flat metal rod that was approximately the width of the animal. Notches were cut into the sides of the mount to allow the animal's legs to hang free [**Fig C.4b**]. The mount was clamped to the side of a desk, and the experimenter sat such that the animal was suspended over their lap. To acclimatize the rodents to the harness and the mount, a

series of exposure sessions were conducted where the rodent was secured in the harness and placed on the mount multiple times [**Fig C.4c**].

Figure C.4: A) Inside of the jacket worn by the rodents [photograph] B) Diagram of mount. C) Example of rodent experimental setup

C.2.3 – Epidural Stimulator

The electrical stimulator was a stand-alone system [Grass] that was independent of the task parameters, and connected to the percutaneous head-plug containing the epidural electrodes. The stimulator was set to voltage-controlled stimulation, such that the L2 spinal level was positive and the S1 spinal level was negative. The stimulation pattern was a 40 Hz train of monophasic square pulses that were 200 microseconds in duration. The experimenter could adjust the amplitude of this

stimulation pattern. An output port of this system was routed to the recording computer.

C.2.4 – EMG Amplifier

Muscle activity was recorded using an amplifier system [AM-Systems]. A long cable connected the percutaneous head-plug containing the EMG wires to the input of the amplifier, which band-pass filtered the muscle activity (.1 Hz < 10 kHz). A dedicated computer recorded the output of the amplifier using a data acquisition card [NI BNC-2115] and custom LabView software. In addition to muscle activity, this computer also recorded the sound played by the speaker, the voltage of the vibrating motor, and the stimulation applied to the epidural electrodes. The sound played by the speaker was used to align the muscle activity with the task. The voltage of the motor was used to differentiate training sessions from test sessions (the motor was off during test sessions). The stimulation was used to tell when the stimulator was turned on and off, and to aligned evoked potentials (evoked potential data was not use).

C.2.5 – Reward System

Rewards were administered manually, using a wooden stick and a jar of chocolate spread (Nutella).

C.3 – Histology

Spinal tissue was stained using either standard immunofluorescence or tyramide signal amplification (TSA). Both processes label a targeted protein using a two-stage staining process. A primary antibody is bound to the desired protein, and then a fluorescent secondary antibody is bound to the primary antibody. The tissue is imaged using a fluorescent microscope. This microscope shines a specific color of light onto the tissue, which is absorbed and reflected by the secondary antibody. Multiple proteins can be separately stained and imaged in the same tissue by carefully selecting the antibodies. As long as the primary antibodies come from

separate animal strains, they can be selectively targeted by different secondary antibodies. The colors of these secondary antibodies were selected such that the fluorescent microscope can image each one with a unique color of light without interfering with the others.

In both the immunofluorescence and TSA approaches, staining begins by washing the tissue in a buffer solution. A detergent is then used to open the cell membranes, enabling better penetration of the antigens. The tissue is soaked in a blocking solution that binds to endogenous binding sites for the secondary antibody. This blocking step reduces background noise by preventing the fluorescent secondary antibody from binding to naturally occurring sites that are not connected to the primary antibody. The tissue is then left in a primary antibody solution over a period of days. The tissue is washed again, to remove any unbound primary antibody, and then immersed in the secondary antibody. After a period of time, the tissue is washed in buffer to remove any unbound secondary antibody, and then stained with a Hoechst dye to label cell nuclei. To further reduce background noise, the tissue was stained with a TrueBlack solution. The tissue is washed a final time using deionized water and then cover slipped using a fluorogel-mounting medium.

The TSA method has an intermediate step between the primary and secondary stages. A tree-like structure is bound to the primary antibody, providing multiple binding sites for the fluorescent secondary antibody. This enables a brighter fluorescence for weakly expressed proteins. Tissue could be stained using both the TSA method and standard immunofluorescence.

C.3.1 Immunofluorescence Procedure

	Immunofluorescence	**Tyramide Signal Amplification**
Wash	Tris-BSA	Tris-HCl (TNT)
Detergent	Tris-BSA + 4% Triton-X	1% H202+0.1% NaN2 in TNT
Block	Tris-BSA + 0.1% Triton-X +5% Normal Donkey Serum	Tris-NaCl (TNB)
Primary	Block + Primary antibody	Block + Primary antibody
Secondary	Block + Secondary	Block + Secondary

Primary Concentrations:

Standard Immunohistochemistry

Mouse anti-NeuN(1:1k)

Goat anti-ChAT(1:250)

Rabbit anti-cFos(1:1k)

TSA Concentrations:

Mouse anti-GaD67(1:2k)

Session 1:

	Immunofluorescence	**Tyramide Signal Amplification**
	Wash (x3) 10 min	Wash (x1) 10 min
	Detergent (x1) 15 min	Detergent (x1) 30min
	Block (x1) 1 hour	Wash (x3) 5 min
	Primary	Block (x1) 1.5 hour
		Avidin (1:1 TNT) 15min
		Wash (x3) 5 min
		Biotin (1:1 TNT) 15 min
		Primary

Primary was left for one day at room temperature and one day in the cold room (4C)

Session 2:

	Immunofluorescence	**Tyramide Signal Amplification**
	Wash (x4) – 10 min	Wash (x4) – 10 min
	Secondary – 1 hour	Bridge IgG – 1 hour
	Wash (x4) – 10 min	Wash (x4) – 10 min
	Hoescht(1:500 ddH20) – 5 min	SA-HRP – 1 hour
	Block + Secondary	Wash (x4) – 10 min
	Wash (x1) – 10 min	Secondary – 6.5 min
	True Black – 1 min	Wash (x1) – 15 min
	Wash (x1) – 1 min	
	ddH20 (x1) – 1 min	
	Cover Slip	

C.4 – Rat Robot

A previous graduate student built a robotic system to control the stance of a rodent. Four robotic linkages controlled the position (x, y, and z) and orientation (pitch, roll, yaw) of a small platform (**Fig C.5**). A rodent was meant to be suspended over this robotic platform, such that its bodyweight was supported by its hindlimbs. The platform could be moved, and the animal's muscle response could be measured. The intention was to study the response of the central pattern generator in the lumbosacral enlargement to disturbances in an animal's stance.

The device had fallen into disrepair. A number of the mechanical couplings were broken, the wiring for the motor encoders was incorrect, and all of the controlling software was lost. The CAD modeling was also missing, so exact dimensions of the

components were unknown. The kinematic derivation translating motor position to platform orientation was also unknown.

The linkages were repaired, encoders were rewired, and measurements of the components were taken. A summer student mounted a frame with a rubber gasket to collect any urine or fecal matter produced by the animal during experiments. New software was written to interface the MATLAB programming environment with a Galil controlling board (DMC-18x6), which operated the motors of the robotic platform. The inverse kinematics were rederived and implemented in MATLAB (**Fig C.5**). A GUI interface was created to assist researchers in generating basic movements of the platform. The researcher could select a degree of freedom (x, y, z, pitch, roll, yaw) and the platform would begin to oscillate around that dimension. The researcher could control the amplitude and speed of these oscillations. If desired, the researchers could also access custom MATLAB functions to program arbitrary motion patterns.

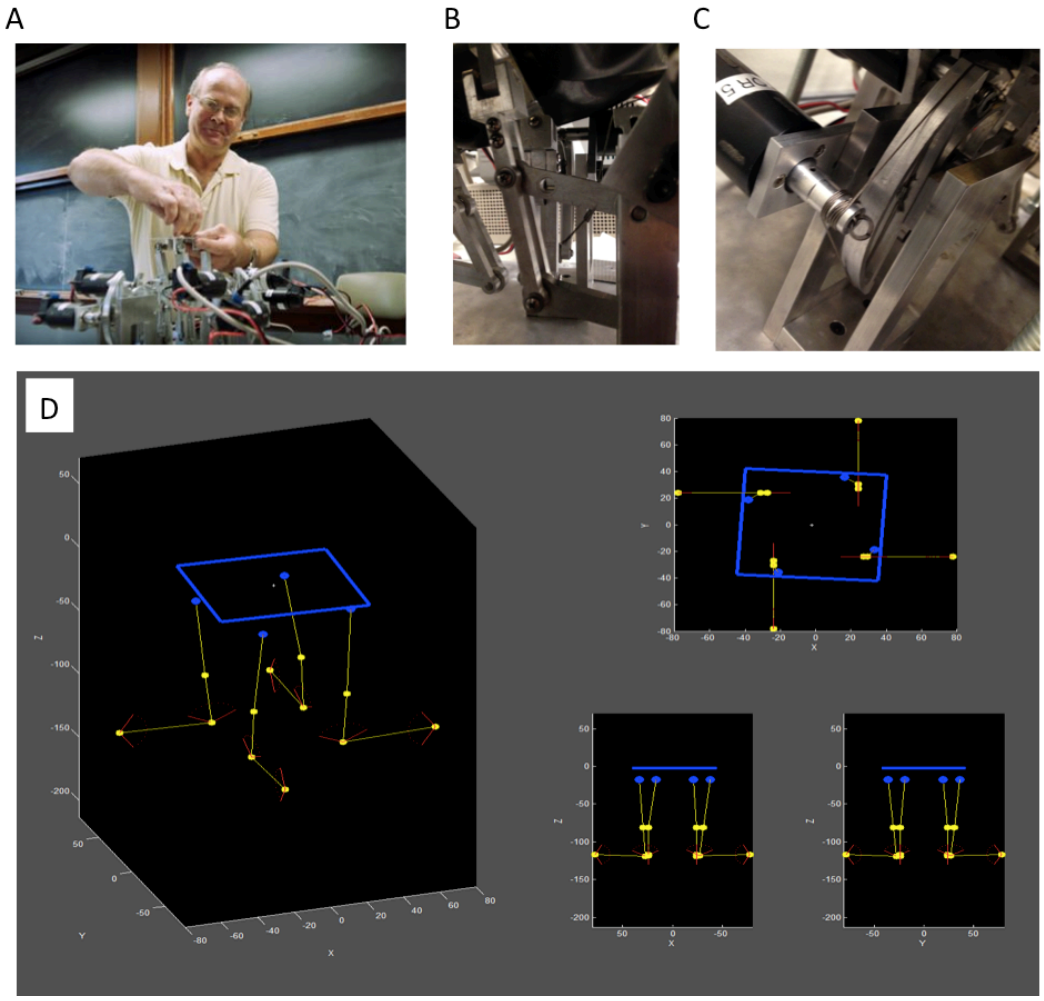

Figure C.5: A) Professor Joel Burdick with the rat robot B) Linkage mechanism C) Slip-less gear system D) GUI displaying rat-robot kinematics